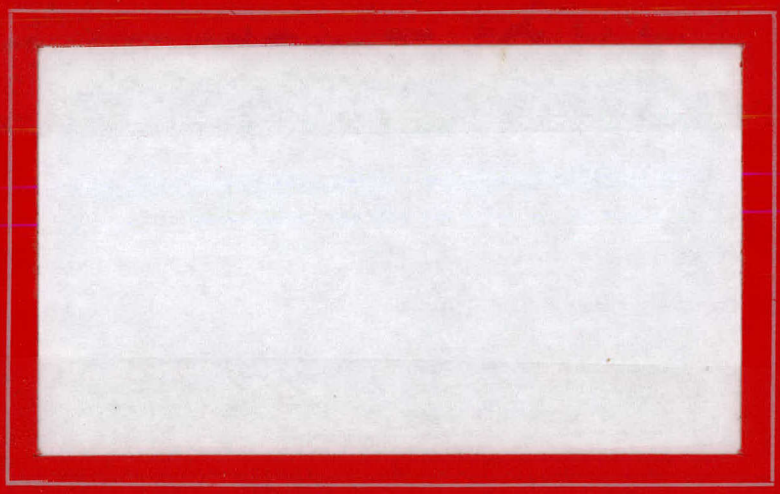

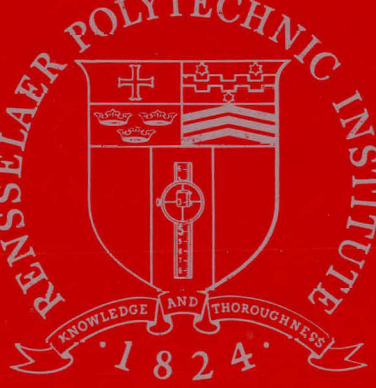

Rensselaer Polytechnic Institute

Troy, New York

DISCLAIMER

COO-3058-1

RECEIVED BY DTIE JAN 19 1972

LINEAR ACCELERATOR PROJECT

AEC Contract No. AT(30-1)-328

ANNUAL TECHNICAL REPORT

for

October 1, 1970 - September 30, 1971

LINEAR ACCELERATOR PROJECT

Rensselaer Polytechnic Institute
Troy, New York

E. R. Gaerttner

Erwin R. Gaerttner
Project Director

In this contract year, October 1, 1970 - September 30, 1971, the major effort at the Rensselaer LINAC was in two areas: (1) measurement and analysis of neutron cross sections necessary for the design of the LMFBR and (2) measurement, analysis and theory of fast neutron spectra in large homogeneous systems consisting of materials of interest in LMFBR.

Neutron capture and total cross sections were carried out in the Kev range for the isotopes of $^{50,52,53,54}Cr$, $^{54,58}Fe$ and $^{61,64}Ni$. From these measurements, S-wave and P-wave cross sections and the usual level parameters were determined. The P-wave strength function near mass 50 was found to be very small $\sim 5 \times 10^{-6}$ and a correlation between neutron and radiation widths of S-wave resonances was observed. The ^{240}Pu capture fission and total cross section measurements were completed; the average radiation width from 20-500 eV was measured to be 30 meV. High resolution total cross-section measurements were completed for gaseous hydrogen and deuterium, ^{60}Ni and ^{7}Li. The hydrogen cross section was measured to a fraction of one percent accuracy (from 0.5 to 20 MeV). A resonance-interference filtered beam experiment was carried out with iron. Doppler and resonance self-protection measurements were made for Ta over a wide range of temperature.

Analyses of the fast neutron spectra measurements in large assemblies of iron and depleted uranium have been performed and a comprehensive paper has been written on iron for publication in Nuclear Science and Engineering early in 1972; a paper for depleted uranium is in preparation. Similar measurements have also been made for a large aluminum assembly. Preliminary directional flux measurements were made in a two-region system near the interface between Al and Fe; analysis using one and two-dimensional transport codes is in process. A major effort has been directed toward directional flux measurements in a large metallic sodium assembly; some preliminary measurements have been made.

Several contributions to analytic capability include: the RPI version of SUPERTOG which is believed to be the most sophisticated

anisotropic treatment available; the completion of a set of in-house programs (RPI package) for generating group constants from non-ENDF data; improved difference approximation and anisotropic scattering treatment in DTF-IV and improved interpolation treatment in SUPERTOG. Analytic capability has also been in progress for analyzing and interpreting differential cross sections; included are: improved experimental resolution corrections, fitting and prediction capabilities of energy averaged cross sections, and modification of JUPITØR to calculate S and P-wave cross-section parameters.

TABLE OF CONTENTS

NEUTRON CROSS SECTIONS

NEUTRON CROSS-SECTION PROGRAM

The 250-meter MeV total cross-section sprectrometer became fully operational at the end of last year and its performance this year was excellent. The equipment operated extremely reliably and precision measurements were completed upon gaseous samples of hydrogen and deuterium and upon separated samples of ^{60}Ni and ^{7}Li. In particular, the hydrogen total cross section has now been measured to the fraction of one percent accuracy required for a standard neutron cross section.

The keV capture and total cross-section experiments this year concentrated upon separated isotopes of the reactor structural materials -- the isotopes of chromium, iron and nickel. These experiments provided a wealth of information on capture cross sections (s-wave and p-wave), resonance parameters, strength functions, average level spacings and the distributions of neutron widths and nearest-neighbor level spacings. Two interesting effects turned up -- the very low p-wave strength function near mass 50 and the large correlation between the neutron and radiation widths of the s-wave resonances. The low strength function is being interpreted by the optical model to imply a narrow, strongly peaked imaginary potential. The large correlations suggest a simple capture mechanism before the formation of the compound nucleus; experiments are planned for next year to look at these resonances with a Ge(Li) crystal to observe the strengths of individual gamma rays.

The ^{240}Pu capture, fission and total cross-section experiments were completed this year. By measuring all three cross sections at this laboratory, we were able to eliminate the need for intercalibration with other laboratories. Our capture and total cross-section measurements in the 20 to 500 eV region showed that the average ^{240}Pu radiation width was about 30 meV. This value of the radiation width plus the generally accepted values of the average

neutron width and the average level spacing predict a capture cross section in the keV region in excellent agreement with our own high-bias low-bias measurements.

A resonance-interference filtered beam experiment was conducted to see if this technique was applicable to time-of-flight spectrometers. A 14-inch iron filtered beam was employed and the results were very impressive -- a signal-to-background ratio of 500:1 was obtained near the 24 keV iron cross-section minimum. A transmission experiment was carried out with this filtered beam for a sample of iron and the results (which emphasize the iron minimum cross sections) were compared to ENDF/B-2. The comparison showed that the iron cross-section minima are significantly larger than listed in ENDF/B-2.

Transmission and self-indication experiments were carried out upon thick samples of Ta at 78°K, 300°K and 1200°K to study resonance self-protection and Doppler broadening in the unresolved resonance region. The results were interpreted by stochastically generating chains of pseudo-resonances from the known distribution laws and the low-energy average parameters. The unresolved resonance region results could be fitted with the low-energy average parameters within the error bars quoted for those parameters. Measurements have also commenced this year upon samples of depleted uranium.

We were fortunate this year to replace the old wooden 25-meter detector station with a modern metallic station with about three times greater floor area. This has relieved the congestion which we were forced to endure in the older station, and experimental apparatus may now be permanently set in position and adequately shielded to reduce cross-talk between the experiments. This new facility has greatly helped the keV angular distribution experiment which can now be permanently set up without disrupting other experiments.

NEUTRON CAPTURE AND TOTAL CROSS SECTIONS OF ^{240}PU

R. W. Hockenbury, W. R. Moyer and R. C. Block

The present status of the ^{240}Pu capture and transmission measurements[1] is as follows. Resonance parameters have been obtained from 20 eV to 500 eV and published.[2] The s-wave neutron strength function determined from these parameters and the level spacing is $(1.10 \pm 0.27) \times 10^{-4}$, in good agreement with previous transmission measurements.[3] The average radiation width from our data ($\overline{\Gamma}_\gamma = 0.0295 \pm 0.0015$ eV) is about 25% larger than that reported by Weigmann.[4] The present results are summarized in Table 1.

The keV capture cross section results have been sent to the National Neutron Cross Section Center. Using the theory of Lane and Lynn,[5] the keV capture cross section has been calculated and is compared to the measured values in Fig. 1. The RPI average resonance parameters for s-wave neutrons (Table 1) and the p-wave parameters of Ref. 6 have been used. The importance of the p-wave contribution in the keV region is evident in Fig. 1. Calculations to obtain a best fit to the measurements are still in progress.

REFERENCES:

1. Linear Accelerator Project Progress Report, April - June 1971, and previous reports.
2. R. W. Hockenbury, J. D. Boice, W. R. Moyer and R. C. Block, Proc. Third Conf. Neutron Cross Sections and Technology, Vol. 2, 721 (1971).
3. W. Kolar and K. H. Bockhoff, J. Nucl. Energy, 22, 299 (1968).
4. H. Weigmann and H. Schmid, J. Nucl. Energy, 22, 317 (1968).
5. A. M. Lane and J. E. Lynn, Proc. Phys. Soc. LXX, 557 (1957).
6. S. Yiftah, J. J. Schmidt, M. Caner and M. Segev, Fast Reactor Physics I, 123, IAEA, Vienna (1968).

FIGURE CAPTION

Fig. 1 Measured and Calculated Capture Cross Section for ^{240}Pu.

Table 1

^{240}Pu Average Resonance Parameters below 500 eV

$$D_{J=\frac{1}{2}}^{\ell=0} = 13.7 \text{ eV}$$

$$\langle \Gamma_n^o \rangle_{J=\frac{1}{2}}^{\ell=0} = 1.508 \text{ meV}$$

$$S_o = (1.10 \pm 0.27)10^{-4}$$

$$\langle \Gamma_\gamma \rangle_{J=\frac{1}{2}}^{\ell=0} = 0.0295 \pm 0.0015 \text{ eV}$$

Figure 1

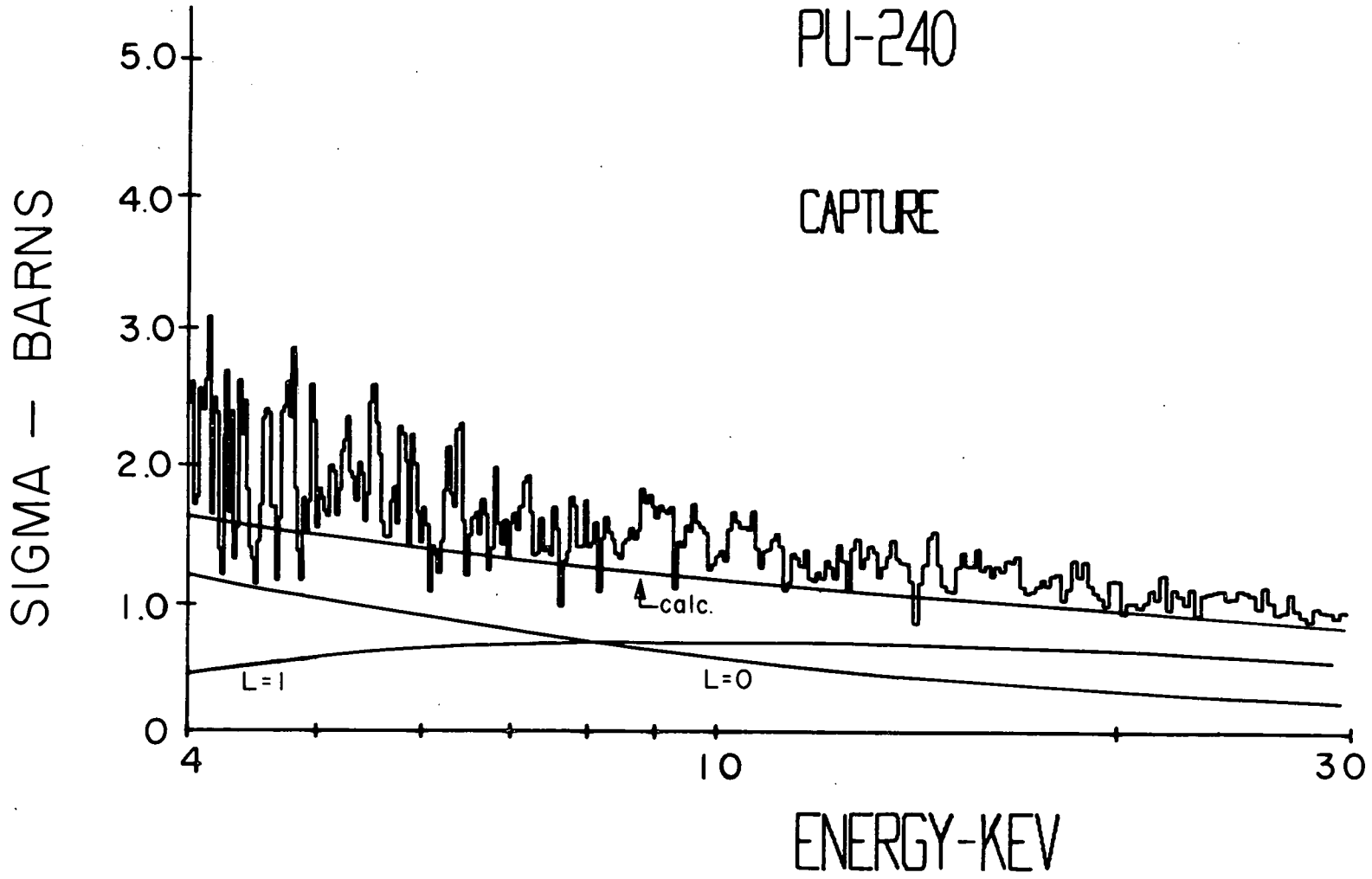
PU-240
CAPTURE
SIGMA — BARNS
5.0
4.0
3.0
2.0
1.0
0
calc.
L=1
L=0
4
10
30
ENERGY-KEV

NEUTRON CAPTURE MEASUREMENTS ON ^{54}FE, ^{58}FE, ^{61}NI AND ^{64}NI

R. W. Hockenbury, N. N. Kaushal, B. Ward* and R. C. Block

Capture measurements have been made on enriched samples of ^{54}Fe and ^{58}Fe from 20 eV to about 300 keV using the 1.25-meter scintillation detector. The experimental conditions are given in Table 1. Part of the raw** data for ^{54}Fe is shown in Figs. 1 and 2. These Figures exhibit many p-wave resonances and a few s-wave resonances, as has been observed[1,2] in measurements of other Fe and Ni isotopes. This sample will also be measured at a higher resolution from 35 keV to about 400 keV.

The capture samples were cycled (to provide normalization of data) under computer control using a new PDP-7 on-line data acquisition code (described elsewhere[3] in this report).

The samples of ^{61}Ni and ^{64}Ni are being packed for capture measurements to be carried out in the next quarter.

**"Raw" data are the unprocessed counting rate data.

REFERENCES:

1. R. W. Hockenbury, Z. M. Bartolome, J. R. Tatarczuk, W. R. Moyer and R. C. Block, Phys. Rev., 178, 1746 (1969).
2. R. G. Stieglitz, R. W. Hockenbury and R. C. Block, Nucl. Phys., A163, 592 (1971).
3. N. N. Kaushal, "A New Time-of-Flight Data Acquisition Code for PDP-7," this report, p. 40.

*Based in part on the Master's Engineering Project of B. Ward.

FIGURE CAPTIONS

Fig. 1 Capture Counting Rate for ^{54}Fe from 6-20 keV.
Fig. 2 Capture Counting Rate for ^{54}Fe from 25-250 keV.

Table 1

Experimental Parameters

Linac Pulse Width = 0.050 μsec

Flight Path = 25.7 m

TOF Channel No.	Width (μsec)
1-2000	0.03125
2001-4000	0.0625
4001-6000	0.1250

Figure 1

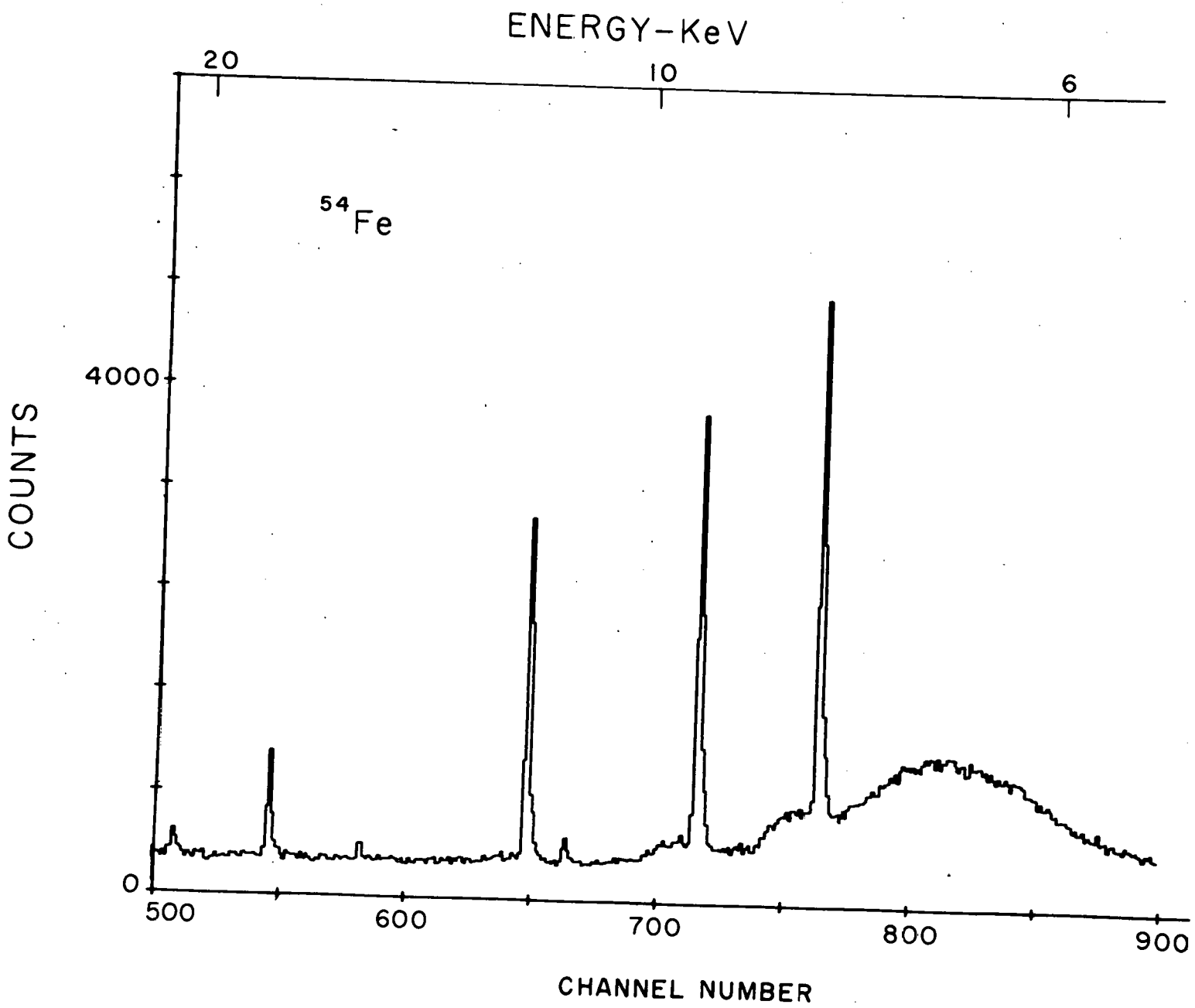
ENERGY-KeV
20
10
6
^{54}Fe
4000
0
COUNTS
500
600
700
800
900
CHANNEL NUMBER

Figure 2

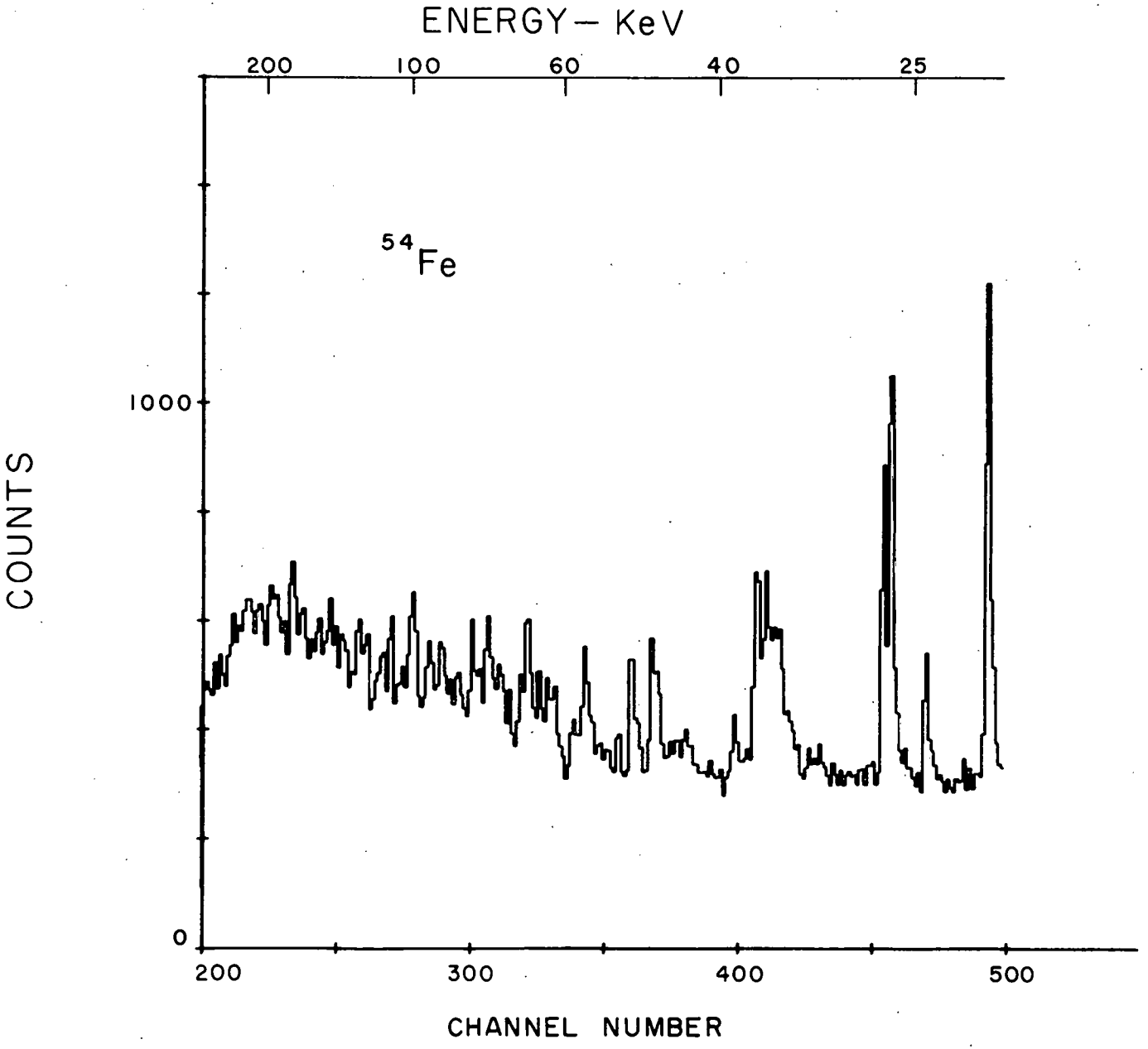
ENERGY — KeV
200
100
60
40
25
^{54}Fe
1000
0
COUNTS
200
300
400
500
CHANNEL NUMBER

TOTAL NEUTRON CROSS SECTIONS ON ^{7}LI FROM 1.0 TO 25 MEV

C. A. Goulding, P. Stoler and J. M. Clement

The measurement of the total neutron cross section on ^{7}Li has been completed. With an electron beam energy of 68 MeV, the measured cross section ranges from 1.0 to 25 MeV neutron energy. Since the neutron burst width was 20 nsec, we chose the time-of-flight channel width to be 16.7 nsec, giving a resolution of 0.13 nsec/meter. The data was accumulated in two separate runs, each of 48 hours of linac time. For the purpose of adding the data, the resolution was averaged to 0.26 nsec/meter.

As in previous experiments,[1] layers of lead and Cd were used to filter out gamma flash and low energy neutrons. A 3/4-inch diameter collimator was used before, and a 1-inch collimator after, the sample.

The sample consisted of metallic ^{7}Li encapsulated in Al cans. The sample thickness was 0.3187 atoms/barn, which gave a transmission of about 58%. Since the Li sample was enriched, no corrections for sample contamination were necessary.

The cross section obtained, shows the broad peak at 4.6 MeV neutron energy ($\Gamma\sim$1.0 MeV) but the narrow peak ($\Gamma\sim$0.08 MeV) at 5.1 MeV indicated by Foster and Glasgow[2] is not apparent. Also, the narrow alpha emitting state in ^{8}Li at 6.53 MeV excitation energy ($\Gamma\sim$.04 MeV) found by Watson and Ajzenberg-Selove[3] is not apparent in these total neutron cross-section data.

REFERENCES:

1. Linear Accelerator Project Annual Technical Report, October 1, 1969 - September 30, 1970, 24, RPI-328-200.
2. D. G. Foster, Jr. and D. W. Glasgow, Phys. Rev., C3, 578 (1971).
3. J. W. Watson and F. Ajzenberg-Selove, Phys. Letters, 18, 302 (1965).

FIGURE CAPTIONS

Fig. 1 ^{7}Li Total Neutron Cross Section from 1.0 to 5.0 MeV.

Fig. 2 ^{7}Li Total Neutron Cross Section from 5.0 to 15.0 MeV.

Fig. 3 ^{7}Li Total Neutron Cross Section from 15.0 to 25.0 MeV.

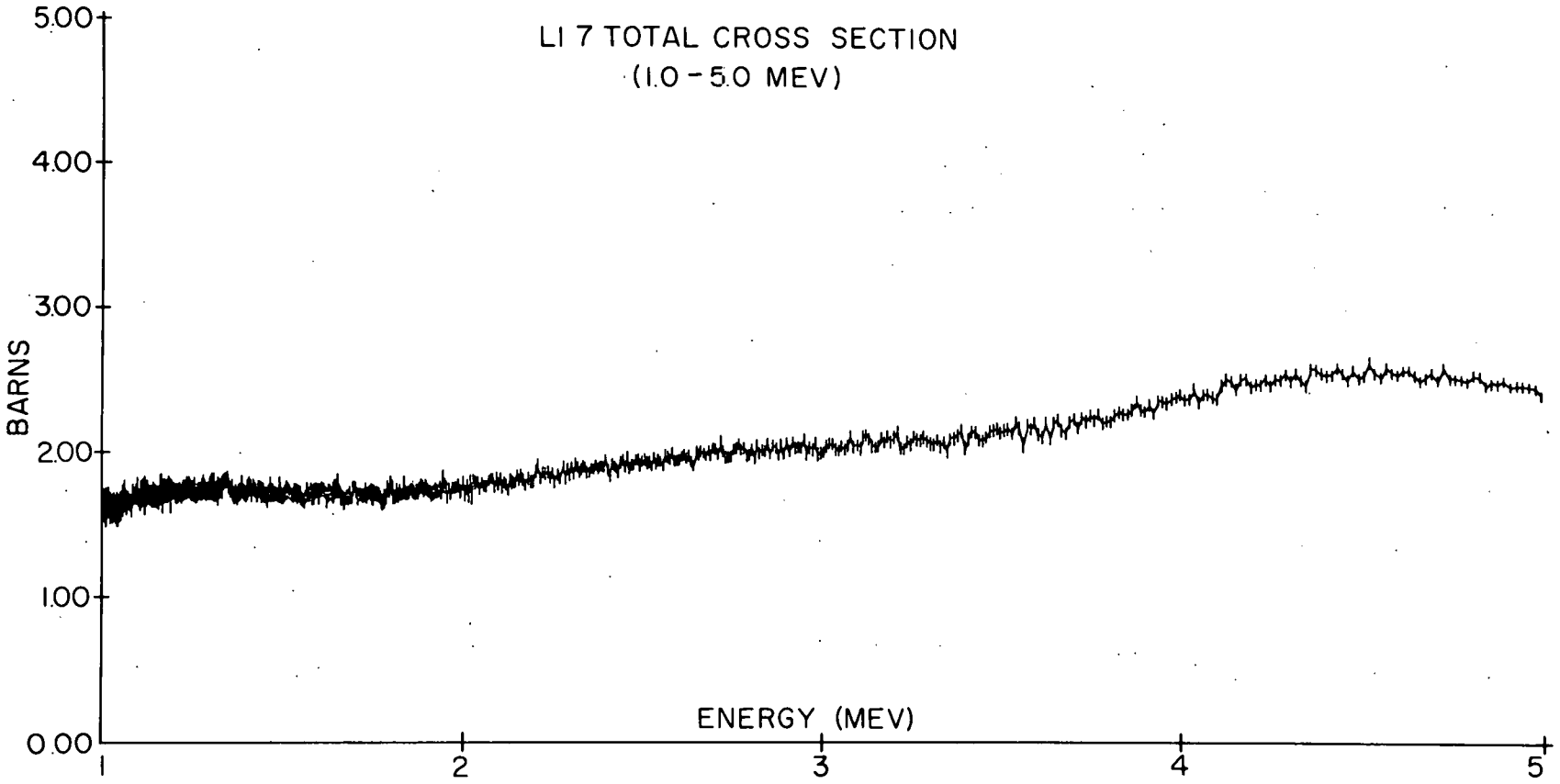
LI 7 TOTAL CROSS SECTION
(1.0 - 5.0 MEV)
5.00
4.00
3.00
2.00
1.00
0.00
BARNS
ENERGY (MEV)
1
2
3
4
5

Figure 1

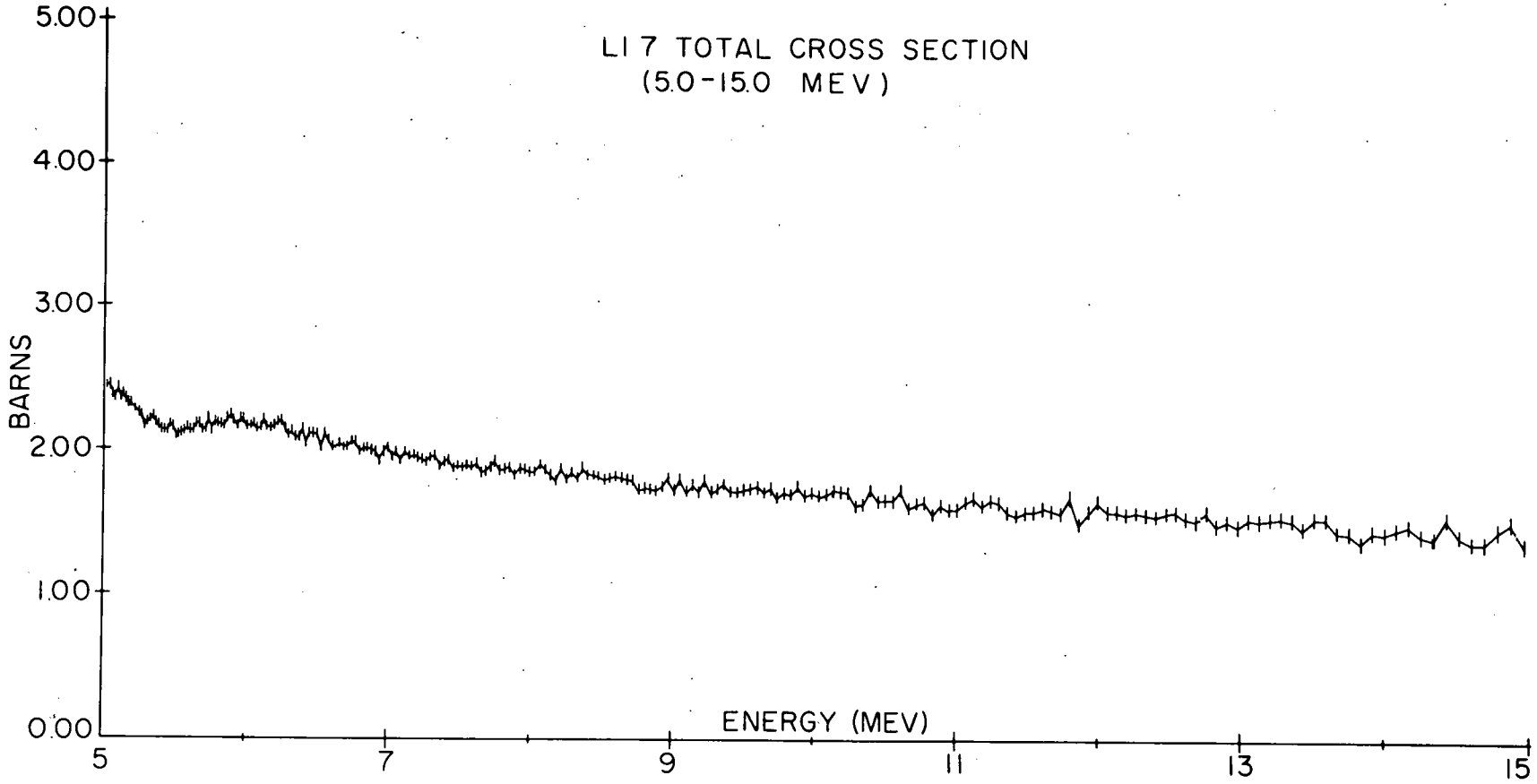
LI 7 TOTAL CROSS SECTION
(5.0-15.0 MEV)
5.00
4.00
3.00
2.00
1.00
0.00
BARNS
5
7
9
11
13
15
ENERGY (MEV)

Figure 2

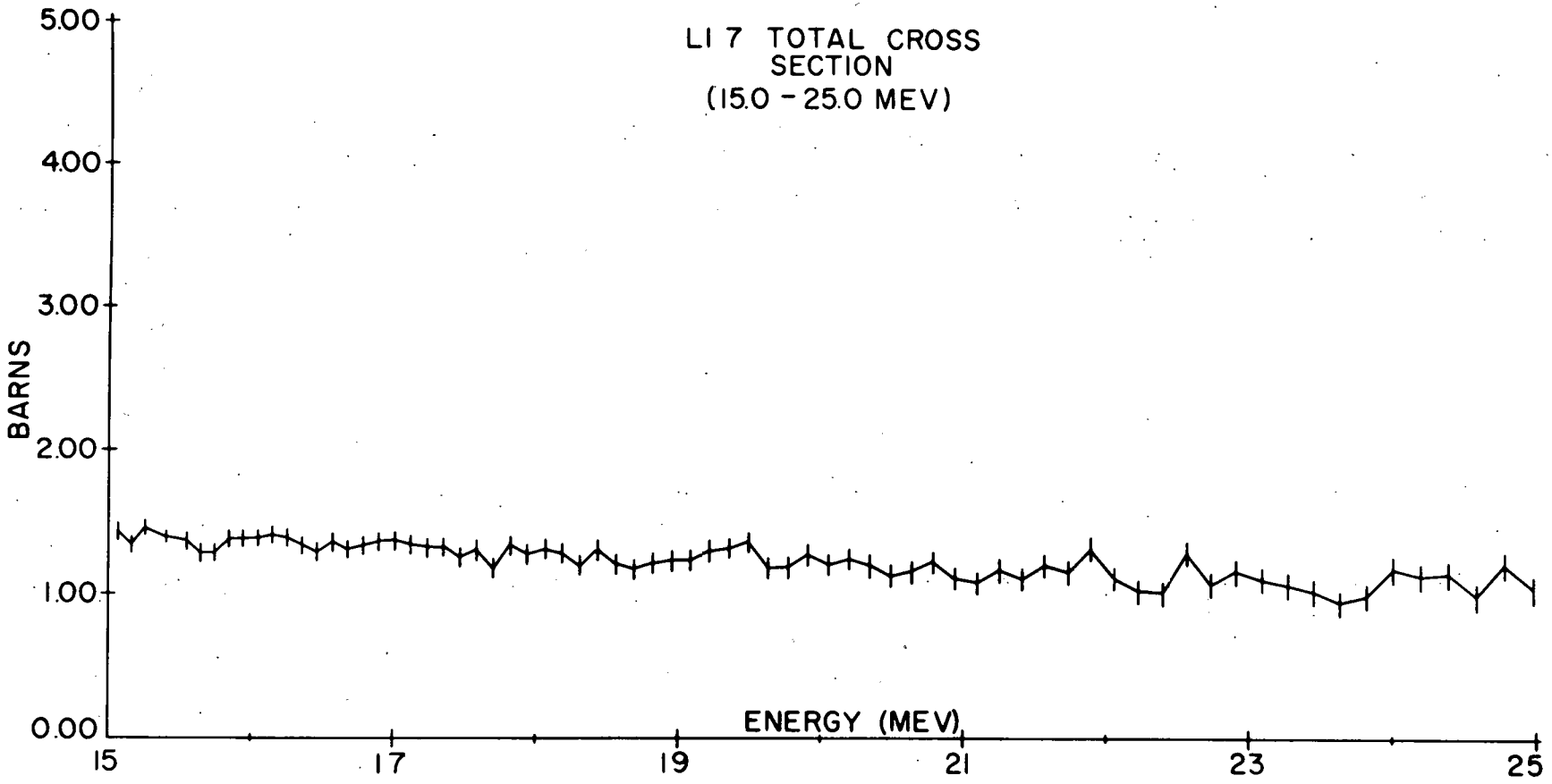
LI 7 TOTAL CROSS
SECTION
(15.0 - 25.0 MEV)
5.00
4.00
3.00
2.00
1.00
0.00
BARNS
ENERGY (MEV)
15
17
19
21
23
25

Figure 3

ELASTIC SCATTERING OF KEV NEUTRONS FROM NATURAL IRON

R. Zuhr* and K. Min

Previously we reported the differential elastic scattering cross sections of keV neutrons scattered from natural iron.[1] These results were cross section averaged over an energy interval approximately ±5% of the assigned neutron energy. Before proceeding to evaluate the cross sections in smaller energy intervals, the present data were averaged over a larger energy interval ($\Delta E_n = \pm 50$ keV) so that a direct comparison can be made with the previously published lower resolution data by Langsdorf, Lane and Monahan.[2] A Legendre polynomial fit of the form $\sigma(\theta) = \sum_{n=0}^{2} a_n P_n$ was made through the $\Delta E_n = \pm 50$ keV differential cross sections, and the total scattering cross section was determined by the coefficient $a_o (\sigma_s = 4\pi a_o^2)$. The results are compared in Fig. 1 with the Langsdorf, Lane and Monahan data and also with the evaluated total cross sections (ENDF/B MAT 1122). The present data yield the scattering cross-section values about 5% lower below 300 keV, but higher by about 10% over the 400 keV peak. However, it is to be noted that the present data are not corrected for multiple scattering.

Within the assigned errors, the two scattering cross-section values are consistent with each other. Over the energy range of the present measurement, the elastic scattering cross section approaches the total interaction cross section within about 10%.

REFERENCES:

1. Linear Accelerator Project Progress Report, April - June 1971, 35, RPI-328-226.
2. A. Langsdorf, R. O. Lane and J. E. Monahan, Phys. Rev., 107, 1077 (1957).

*Based in part on the Ph.D. Thesis of R. Zuhr.

FIGURE CAPTION

Fig. 1 Total Scattering Cross Section from Natural Iron. The present elastic scattering results are compared with the results of Ref. 2 and the total cross sections.

Figure 1

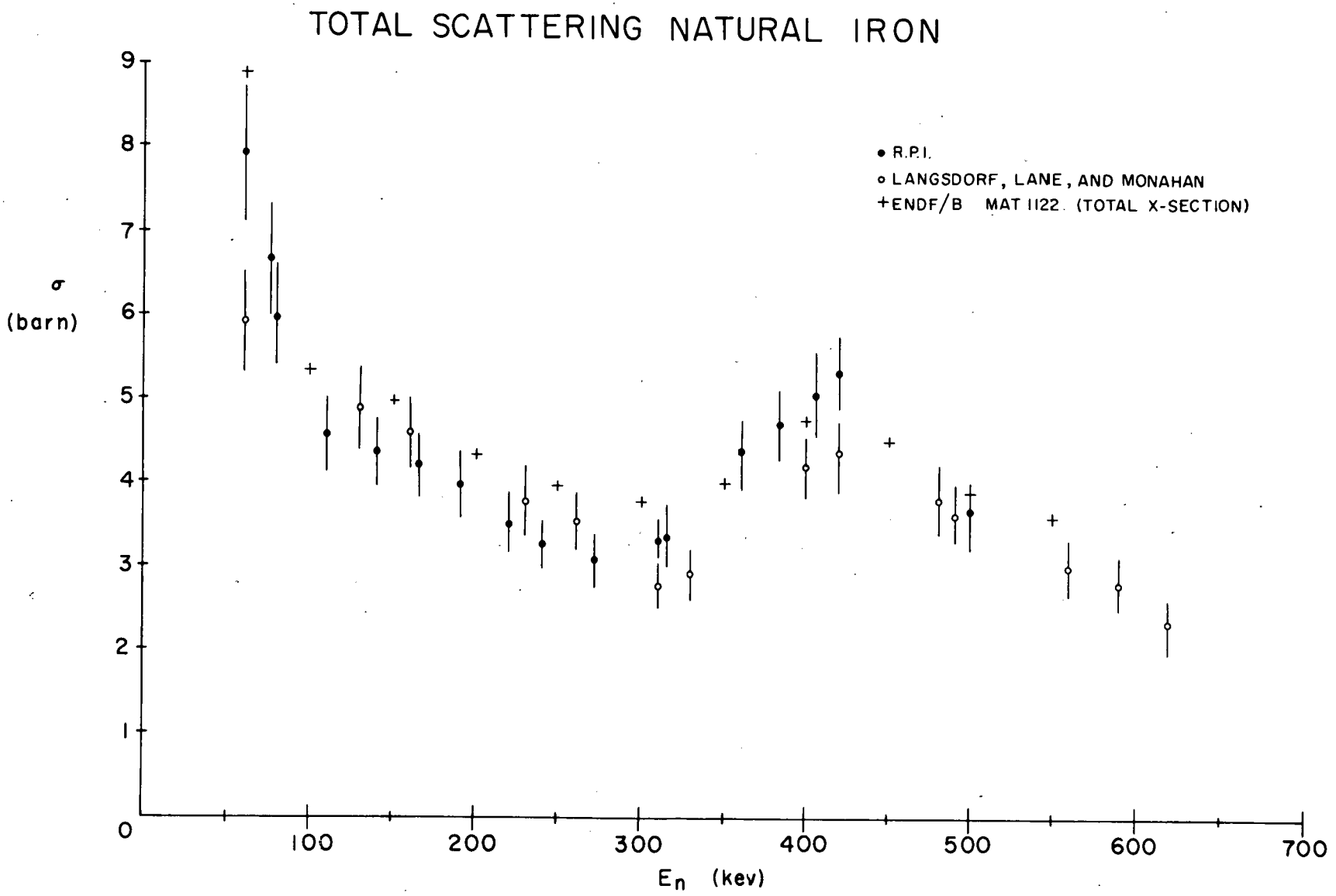
TOTAL SCATTERING NATURAL IRON
• R.P.I.
○ LANGSDORF, LANE, AND MONAHAN
+ENDF/B MAT 1122. (TOTAL X-SECTION)
σ
(barn)
0
1
2
3
4
5
6
7
8
9
100
200
300
400
500
600
700
E_n (kev)

AREA ANALYSIS OF NEUTRON TRANSMISSION THROUGH THICK IRON SAMPLES

K. Alfieri,* P. J. Turinsky and R. C. Block

The data from the experiment designed to test the feasibility of using resonance filters to obtain monochromatic neutron beams for time-of-flight experiments[1] has been, in addition, analyzed for a preliminary comparison with ENDF/B-II and other data files. Ultimately, the results of this experiment will be used to calculate the point total cross sections for natural iron in energy regions about the minima. To do this, one must know the experimental resolution function. However, in order to facilitate a cursory comparison with the other data, certain simplifying assumptions can be made so that one can dispense with the resolution corrections.

The number of counts for a given energy and sample thickness is

$$C(d,E) = \int_o^\infty R(E,E')e^{-\Sigma_t(E')d}dE' \tag{1}$$

where d is the sample thickness, $\Sigma_t(E')$ is the macroscopic total neutron cross section at the energy E', and R(E,E') is the experimental resolution function centered about energy E. If E_1 and E_2 are energies bracketing a minimum in the total cross section; i.e., a maxima in the transmission curve, the area under the transmission curve between E_1 and E_2 is given by

$$A(d,E_1,E_2) = \int_{E_1}^{E_2} C(d,E)dE = \int_o^\infty e^{-\Sigma_t(E')d}dE' \int_{E_1}^{E_2} R(E,E')dE \ . \tag{2}$$

Define

$$f(E',E_1,E_2) = \int_{E_1}^{E_2} R(E,E')dE \tag{3}$$

and assuming that R(E,E') is highly peaked and that its shape changes little with E', one obtains

$$f(E',E_1,E_2) = \begin{cases} g(E_1,E_2) \text{ if } E_1 < E' < E_2 \\ 0 \text{ for all other } E' \end{cases} . \tag{4}$$

*Based in part on the Master's Engineering Project of K. Alfieri.

Employing Eq. (4) in Eq. (3), this implies

$$A(d,E_1,E_2) = g(E_1,E_2) \int_{E_1}^{E_2} e^{-\Sigma_t(E')d} dE' \qquad (5)$$

provided E_1 and E_2 correspond to energies where the cross section is large.

By taking the ratio of areas for two different sample thicknesses, we obtain from Eq. (5)

$$R = \frac{\int_{E_1}^{E_2} e^{-\Sigma_t(E')d_1} dE'}{\int_{E_1}^{E_2} e^{-\Sigma_t(E')d_2} dE'}, \qquad (6)$$

an expression that is independent of any resolution corrections, (d_1 and d_2 equal 14 and 20 inches, respectively.) This ratio, obtained directly from the counts in the RPI experiment, was compared to the theoretical values derived from Eq. (6) by using the total iron cross-section files from ENDF/B-II (material number 1122), ORNL (material number 1124) and KAPL-Version 19[2].

Table 1 shows the percent standard deviation in the RPI area ratio. The maximum, mean and minimum percent errors indicating the discrepancy between the RPI ratio and the 1122, 1124 and Version 19 ratios for various minima in the cross section are also shown. These errors are calculated from

$$\epsilon_{mean} = \frac{R_{RPI} - R_T}{R_{RPI}} \times 100\% \text{ and } \Sigma_{\substack{max \\ min}} = \frac{R_{RPI} \pm \Delta R_{RPI} - R_T}{R_{RPI} \pm \Delta R_{RPI}} \times 100\% \qquad (7)$$

where R_{RPI} is the RPI ratio, ΔR_{RPI} is the experimental standard deviation in the RPI ratio, and R_T is the theoretical ratio from one of the data files.

If one now supposes there is a weighted average cross section $\overline{\Sigma}_t$ for the particular energy interval over which the integration is taken, then the ratios become

$$R_{RPI} = e^{+\overline{\Sigma}_t(d_2-d_1)} \tag{8}$$

and

$$R_T = e^{+(\overline{\Sigma}_t+\Delta\overline{\Sigma}_t)\ (d_2-d_1)} \tag{9}$$

where $\Delta\overline{\Sigma}_t$ is the deviation of the data file cross sections from those of RPI.

The percent error is then

$$\varepsilon = (1-e^{+\Delta\overline{\Sigma}_t(d_2-d_1)})\ x\ 100\% \ . \tag{10}$$

Hence, if $\varepsilon<0$, then $\Delta\overline{\Sigma}_t>0$ and the data file cross sections are larger than RPI's; whereas, when $\varepsilon>0$, $\Delta\overline{\Sigma}_t$ is negative and they are lower than RPI's. Table 1 also contains this information.

While it is not possible to draw any definite quantitative conclusions from this kind of analysis, it can be seen that Version 19 best agrees with the RPI cross sections; while 1124 is quite poor. Out of the nine energy ranges analyzed with Version 19 data where definite conclusion can be drawn, six of them show values that are too high. The opposite in trend is evident in the 1122 file; where the cross sections are underestimated in all but two energy ranges. Corrections are presently being conducted to determine if the trace impurities in the iron samples have significance on our results.

Presently, work is under way to incorporate the experimental resolution function for the determination of the iron point cross sections at the minima.

REFERENCES:

1. Linear Accelerator Project Progress Report, April - June 1971, 22, RPI-328-226.
2. C. Lubitz, private communication (1971).

TABLE 1

Energy Range (Kev)	Standard Deviation in RPI Ratio	Material 1122 Max Error	Material 1122 Mean Error	Material 1122 Min Error	Material 1122 Comparison with RPI's Cross Sections	Material 1124 Max Error	Material 1124 Mean Error	Material 1124 Min Error	Material 1124 Comparison with RPI's Cross Sections	Version 19* Max Error	Version 19* Mean Error	Version 19* Min Error	Version 19* Comparison with RPI's Cross Sections
781.8 to 1282.5	15%	2%	-13%	-34%	over	6%	- 8%	- 28%	over	-	-	-	-
576.6 to 781.8	7%	23%	17%	11%	under	13%	6%	- 7%	-	-	-	-	-
425.0 to 525.9	10%	18%	9%	- 2%	under	- 16%	- 29%	- 44%	over	-	-	-	-
326.2 to 392.6	5%	16%	12%	7%	under	5%	2%	5%	under	15%	10%	6%	under
284.5 to 326.2	4%	29%	26%	23%	under	- 85%	- 92%	-100%	over	29%	26%	23%	under
228.5 to 284.5	5%	6%	1%	- 4%	-	- 91%	-101%	-112%	over	3%	- 1%	- 7%	-
203.7 to 228.5	6%	-17%	-25%	-34%	over	- 19%	-208%	-231%	over	-13%	-21%	-30%	over
173.3 to 192.7	6%	16%	11%	6%	under	37%	33%	29%	under	4%	- 2%	- 8%	-
160.7 to 173.3	4%	8%	4%	- 1%	under	-112%	-121%	-132%	over	- 9%	-14%	-19%	over
132.9 to 142.4	3%	21%	19%	17%	under	- 46%	- 50%	- 54%	over	-33%	-37%	-41%	over
125.7 to 132.9	5%	40%	37%	34%	under	- 95%	-106%	-118%	over	- 1%	- 5%	-11%	over
116.6 to 145.8	4%	27%	25%	22%	under	- 41%	- 46%	- 52%	over	-27%	-32%	-37%	over
76.7 to 83.7	5%	17%	13%	8%	under	-176%	-189%	- 20%	over	- 6%	-11%	-17%	over
21.5 to 25.6	3%	12%	9%	6%	under	29%	27%	24%	under	11%	8%	5%	under

* No Version 19 data above 471 Kev available.

NEUTRON AVERAGE TRANSMISSION AND SELF-INDICATION RATIO MEASUREMENTS UPON DEPLETED URANIUM AT ROOM TEMPERATURE[#]

T. Y. Byoun[*] and R. C. Block

Neutron average transmission and self-indication measurements have been performed upon depleted uranium (containing about 0.21 percent ^{235}U) at room temperature from 350 eV to approximately 250 keV. The ^{10}B-NaI detector at 28 meters and the 1.25-meter diameter liquid scintillator detector at 25 meters were used respectively for the transmission and self-indication measurements. The data have been taken with 20 nsec (for transmission) and 100 nsec (for SIR) LINAC electron pulse widths. Four neutron filters (S, Al, Cu-Mn and Co) have been used for background determination. The sample thicknesses of 0.00758, 0.01552, 0.03155, 0.04670 and 0.06206 atom/barn were used for the transmission measurements. For the self-indication measurements the same five samples were used as shielding samples and a 0.00378 atom/barn self-indication sample was placed inside the scintillation detector.

The transmission data have been reduced to effective average cross sections[1,2] and plotted in Fig. 1. The effective average cross section is defined by

$$\langle\sigma\rangle_{TR}^{eff} = -\frac{1}{N} \ell n \langle TR \rangle \quad ,$$

where N is sample thickness (atom/barn) and <TR> is average transmission. The data have been grouped into 10% wide energy bins[3] and the statistical (standard deviation) accuracy of the transmission data is approximately 1% per bin. In Fig. 1, we can see the sample thickness dependency of the effective average cross section due to self-shielding effects in the neutron energy region below 50 keV. However, this effect becomes smaller at higher energies because of decreasing peak cross sections and the overlapping of resonances.

[#]Supported by NASA Grant NGR33-018-134.

[*]Based in part on the Ph.D. Thesis of T. Y. Byoun.

The self-indication data are being analyzed. The high temperature ($\sim$1073^{o}K) and the low temperature (78^{o}K) measurements will be performed next to determine the temperature dependence of depleted uranium (which is the main purpose of this series of measurements).

REFERENCES:

1. Linear Accelerator Project Progress Report, January - March 1970, 32, RPI-328-187.
2. T. Y. Byoun, R. C. Block and T. Semler, Conf.-710301 (March 1971), Vol. 2, 895, Proc. Third Conf. Neutron Cross Sections and Technology (1971).
3. Linear Accelerator Project Annual Technical Report, October 1, 1969 - September 30, 1970, 34, RPI-328-200.

FIGURE CAPTION

Fig. 1 Effective Average Cross Sections Calculated from the Average Transmission for Five Different Sample Thicknesses.

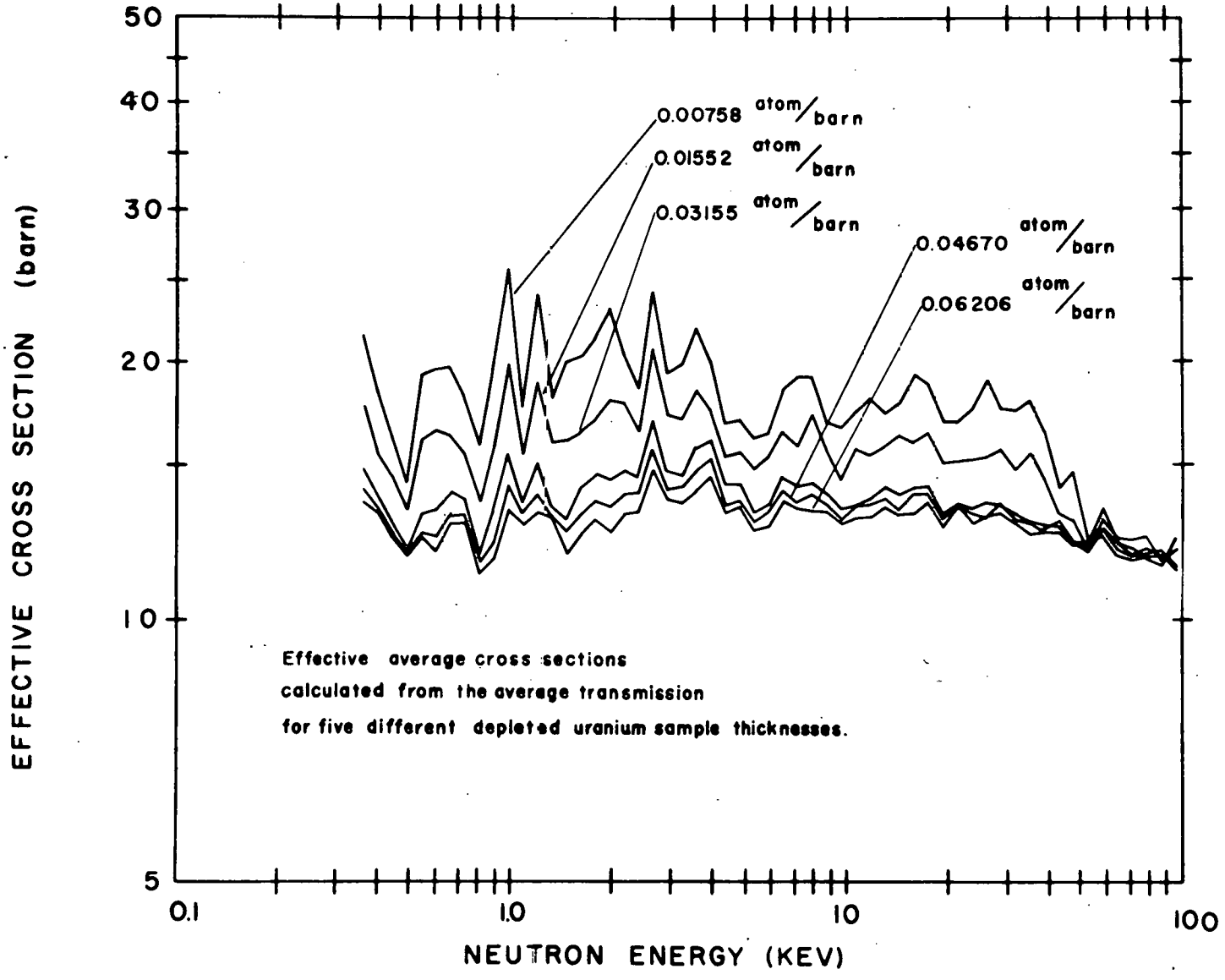
50
40
30
20
10
5
0.1
1.0
10
100
EFFECTIVE CROSS SECTION (barn)
NEUTRON ENERGY (KEV)
0.00758 atom/barn
0.01552 atom/barn
0.03155 atom/barn
0.04670 atom/barn
0.06206 atom/barn
Effective average cross sections
calculated from the average transmission
for five different depleted uranium sample thicknesses.

Figure 1

RESOLUTION STUDIES ON THE PROTON-RECOIL DETECTOR AT 250-METER STATION

R. Fairchild* and P. Stoler

I. Introduction

Much work has been done on the theoretical and experimental determination of the time resolution of scintillation counters.[1-6] Since the timing accuracy is one of the critical factors in the MeV neutron cross-section measurements at RPI, an attempt has been made to determine the actual resolution of the large proton-recoil detector system and to see if it compares favorably with other results.

Work pioneered by E. Gatti[1] and L. G. Hyman[2] on the theoretical considerations led to a series of experimental studies of the resolution of various scintillation systems.[3-6] Both theories approach the problem with similar statistical models. Both use an exponential illumination function, $\emptyset(t)$, with decay constant. The transit time fluctuation from photocathode to first dynode is described by a probability density function and the remainder of the photomultiplier (PM) tube is characterized by the single electron response function of the particular PM tube. For an ideal geometry, E. Gatti calculated that the best timing would be on the first photoelectron; whereas, L. G. Hyman determined that the best resolution occurred when the timing was set at about 2% of total charge collected. Several experiments performed indicate the minimum to be collected at about 15% of total charge. The results of McDonald et al.[6] indicate that the minimum resolution of the scintillation counter should be on the order of .30 to 3.0 ns., depending on the scintillant and geometry.

---

*Undergraduate Summer Research Participant.

II. Experiment and Results

The modular proton-recoil detector at the 250-meter flight station, described in detail elsewhere,[7] consists basically of seven detectors, each with four XP1040 PM tubes looking at a scintillation chamber (5" x 15" x 15") filled with toluene, p-terphenyl and POPOP. During actual experiments the PM tubes are used in fourfold coincidence with the timing set on the first tube that fires. Therefore, the timing uncertainty is entirely dependent on one photomultiplier tube.

Several methods were tried to determine the resolution of the scintillant-photomultiplier-electronics system. Following the work of M. Bonitz et al.[8] a light pulser was used to determine the response of the photomultiplier tubes and electronics. The pulser used is a mercury-wetted SPDT relay with a variable H. V. of 600-1700 V. applied to the moveable contact. A variable voltage 60hz A.C. signal is applied to the coil of the relay such that the swing of the contact can be adjusted for minimum 'bounce'. An electrical signal is derived across a resistor in the H. V. circuit. (see Fig. 1). This signal has a width of about 3 ns. on an oscilloscope, although this is near the resolving limit of the oscilloscope and, therefore, the pulse could be narrower. The light signal is fed to the seven modules through a nine-branch fiber optics light pipe. Using the electrical output of the pulser as a start for the TAC, the stop signal is formed by a cable-delayed signal from the PM electronics. The data was then fed into a 4096 channel ADC and then stored in a PDP-7 computer. (see Fig. 2B).

The experiment using the light pulser did not produce consistent results on the first attempts because of problems in transmitting the signals from the 250-meter station to the control room where the analyzer was located. This was solved by using the TAC and a portable multichannel analyzer at the 250-meter station. The data for one tube (Fig. 3) show a fwhm of 4 channels (2.5 ns.) for the high intensity light pulses for which every pulse was detected. The results for a low intensity

pulse -- one, two, or three photoelectrons for which only about 10% were detected -- shown in Fig. 4 gives a resolution of 11 channels (6.9 ns.). This is possibly due to the mapping out of the distribution of the photoelectrons as they undergo multiple reflections inside the module.

A second method used a Co^{60} source placed on line between the proton-recoil detector and a stilbene crystal-PM tube assembly. The pulse from the stilbene detector was used as a start for the TAC. The signal from the PM electronics was cable-delayed and fed into the stop of the TAC. The TAC signal was fed into the 4096 ADC and stored in the PDP-7 computer. (See Fig. 2A for a diagram of the layout). The second method produced no useful data because of difficulties in transmitting the signal to the control room and other problems related to the stilbene detector, such as the lack of knowledge regarding the intrinsic resolution.

The third method also used the Co^{60} source and other gamma sources of various energies. The start signal was derived from one of the PM tubes and the stop was a cable-delayed signal from another tube. The TAC signal was fed into a 1024 channel analyzer. Since four PM tubes observe the same event, various modes of coincidence were tried, including 1 vs 1, 1 vs 2, 1 vs 3, and 2 vs 2. Resolution measurements were made on one module using several different gamma sources. Figure 2C shows a diagram of this layout.

The best resolution obtained for a close gamma source is 2.3 ns. fwhm using module 6. A typical resolution curve is plotted in Fig. 5. The tabulated results for all modules appear in Tables 1-3.

Two other experiments were performed using the 1024 channel analyzer. A time spectrum was made looking after the main pulse for evidence of afterpulsing, which is suggested in several experiments.[9,11] The analyzer was also used as a pulse height analyzer to determine the distribution according to voltage of the background noise in the PM tubes and the pulse height spectrum for various energy gamma sources. These measurements can be

related to the neutron detection pulses since the efficiency ratio for gammas and neutrons is known.

In the other tests the time spectrum of the output of one tube is plotted in Fig. 6. This is a plot of pulses occurring after the main pulse. The peak at about 350 ns. indicates the presence of afterpulsing due to H_2 ions in the phototube. This characteristic was observed in all PM tubes. Also, Fig. 7 shows the pulse height spectrum for one PM tube using a ^{60}Co source. The background noise and net Co^{60} spectrum with background subtracted are shown. These indicate that most events produce signals of less than 6 volts. One can observe signals of 6 volts on an oscilloscope; however, these are few in number and probably correspond to cosmic ray events.

III. Discussion and Conclusion

The results of these tests indicate that the proton-recoil detector at the 250-meter station has a resolution of better than 3 ns. fwhm which is consistent with theory and other experiments. The main factor limiting the resolution of the detector is the relatively large volume-1125 cubic inches of scintillant. Most other experiments were performed with small volume scintillators; less than 10 cubic inches. However, in our experiments, the large volume of scintillator is necessary to get a reasonable efficiency for detecting neutrons.

These tests also show that the characteristic afterpulsing is present in our PM tubes although they present little concern for our fourfold coincidence detection requirement. Also the pulse height spectrum indicates that background and tube noise is less than one volt in amplitude and that cosmic events have a constant effect from tube noise to saturation. The 1.16 and 1.33 Mev energy from the Co^{60} correspond to about 6 Mev neutron, and therefore most information signals; i.e., neutrons from 1 Mev on up, fall above most of the tube noise signals. The fourfold coincidence requirement effectively eliminates the random tube noise problem for smaller voltages. The discrimination level is at 150 mv. such that events to 350 kev can be observed although

at that energy the detector is not very efficient.

At this time the resolution of the 250-meter proton-recoil detector is more than adequate for the experiments performed at the LINAC since the shortest electron pulse is still several times longer than the resolution. Only at such time that the LINAC is producing much narrower pulses, will there be any need to improve the resolution of the detector.

REFERENCES:

1. S. Donalti, E. Gatti, and V. Svelto, Nucl. Instr. and Meth. 77, 179-180 (1970).

2. L. G. Hyman, R. M. Schwarcz, and R. A. Schluter, Rev. Sci. Instr. 35, 393 (1964).

3. D. Porter, J. M. McDonald, and D. T. Stewart, Nucl. Instr. and Meth. 44, 309-313 (1966).

4. W. Bartl and P. Weinerl, Rev. Sci. Instr., 34, 252-255 (1963).

5. Yu. K. A. Kimov and S. V. Medved, Nucl. Instr. and Meth., 78, 151-153 (1970).

6. W. J. McDonald and D. A. Gedcke, Nucl. Instr. and Meth., 55, 1-14 (1967).

7. P. Stoler, P. F. Yergin, J. C. Clement, D. Mann, C. G. Goulding and R. Fairchild, Nucl. Instr. and Meth., 91, 541-545 (1971).

8. M. Bonitz, W. Meiling, and F. Stary, Nucl. Instr. and Meth., 29, 309-313 (1964).

9. R. A. Schrack, H. T. Heaton, II, and R. B. Schwartz, Nucl. Instr. and Meth., 77, 175-176 (1970).

10. Y. Shin, S. H. Ku, C. Glavina and J. A. Rawlins, Nucl. Instr. and Meth., 58, 353-355 (1968).

11. G. A. Morton, H. M. Smith, R. Wasserman, IEEE Trans. on Nucl. Sci., 433-438 (Feb. 1967).

FIGURE CAPTIONS

Fig. 1 Circuit Diagram of Light Pulser Assembly.

Fig. 2A Schematic of Stilbene Detector Measurement.

2B Schematic of Light Pulser Interconnections.

2C Schematic of Co^{60} Experiment Geometry.

Fig. 3 Resolution Curve for High Intensity Light Pulser Experiment.

Fig. 4 Resolution Curve for Low Intensity Light Pulser Experiment.

Fig. 5 Resolution Curve for Module 4 Using Co^{60} Source.

Fig. 6 Time Spectrum at PM Tube.

Fig. 7 Pulse Height Spectrum of PM Tube.

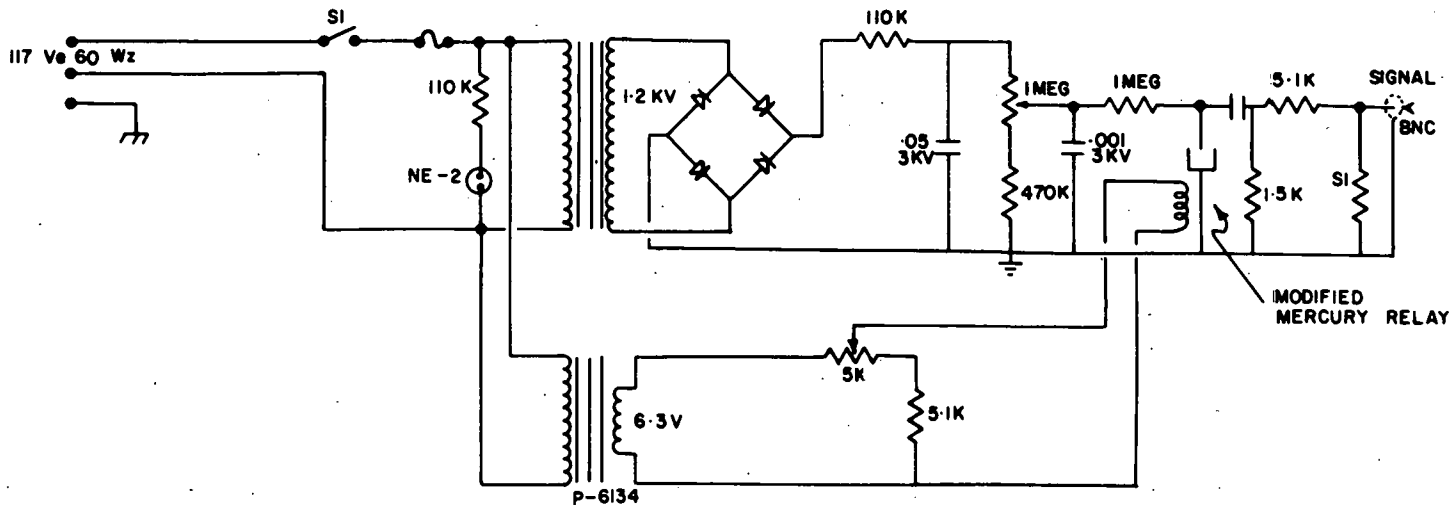

FIG·1

LIGHT PULSE GENERATOR
SCHEMATIC

FIG. 2A

STILBENE DETECTOR EXPERIMENT DIAGRAM

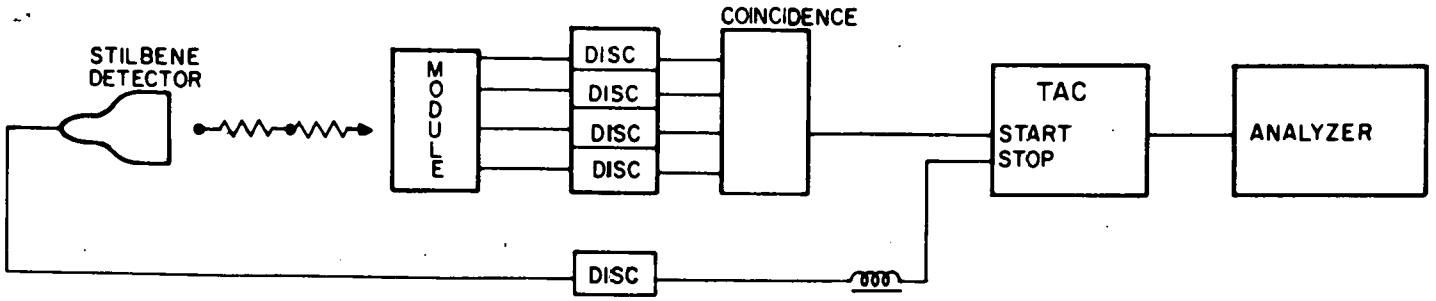

FIG. 2B

LIGHT PULSER EXPERIMENT DIAGRAM

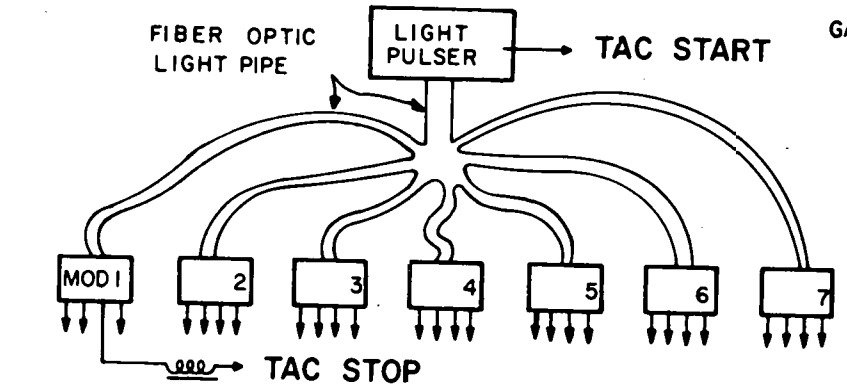

FIG. 2C

MODULE EXPERIMENT DIAGRAM

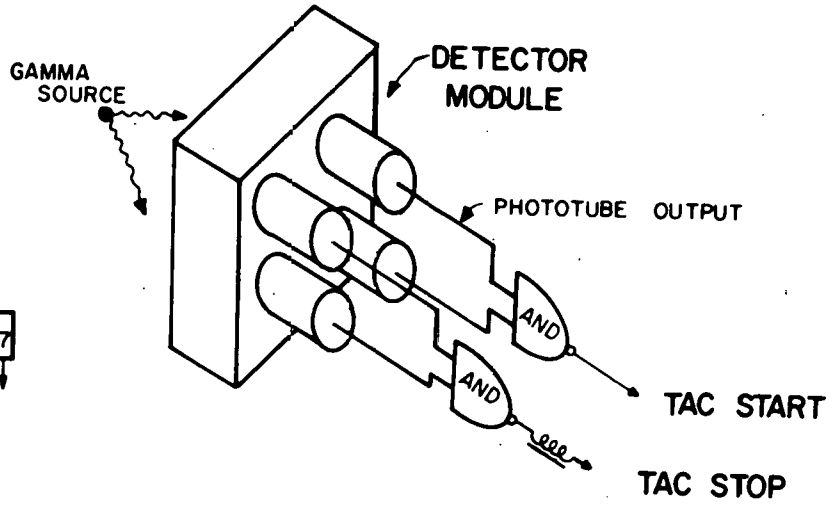

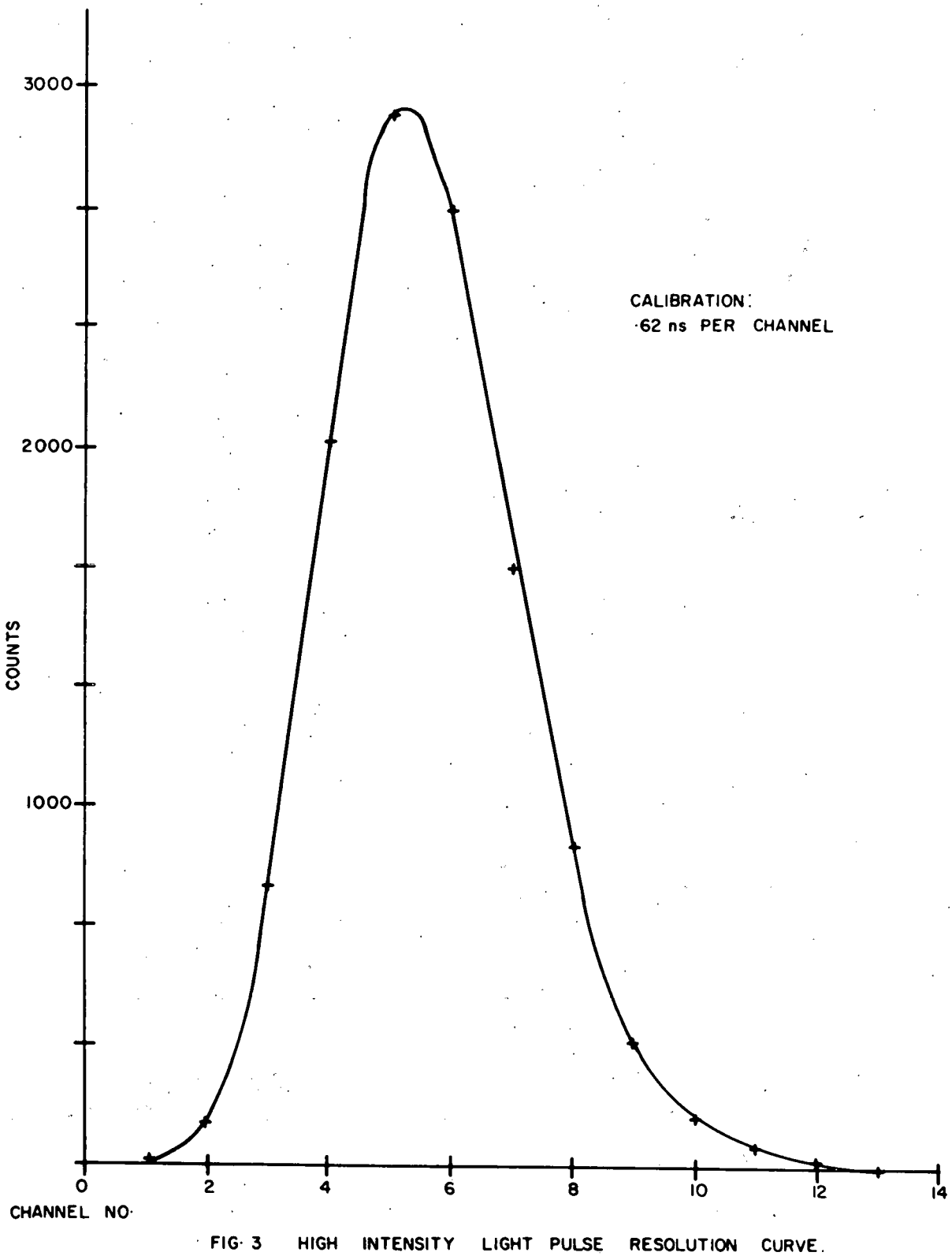

FIG. 3 HIGH INTENSITY LIGHT PULSE RESOLUTION CURVE.

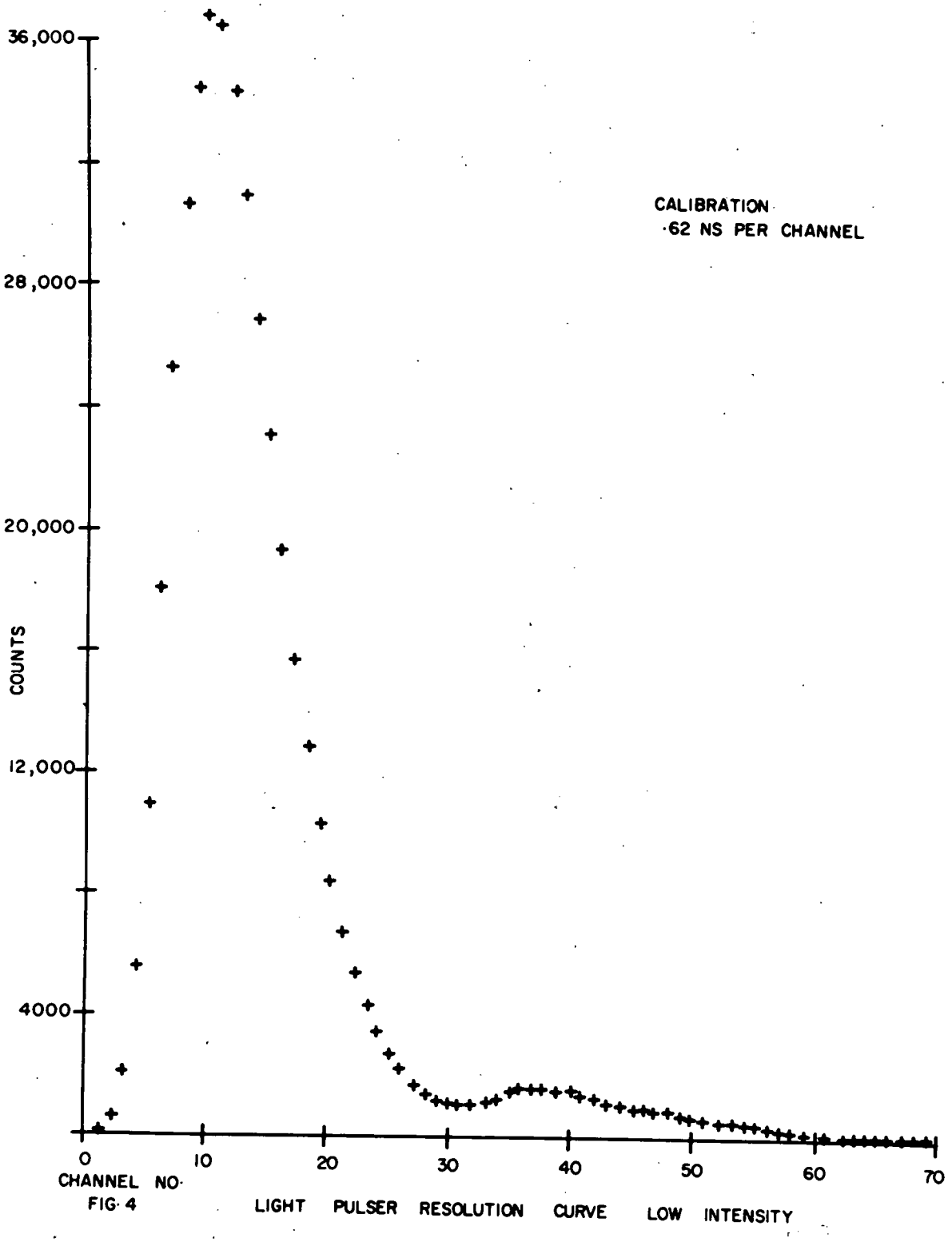

FIG. 4 LIGHT PULSER RESOLUTION CURVE LOW INTENSITY

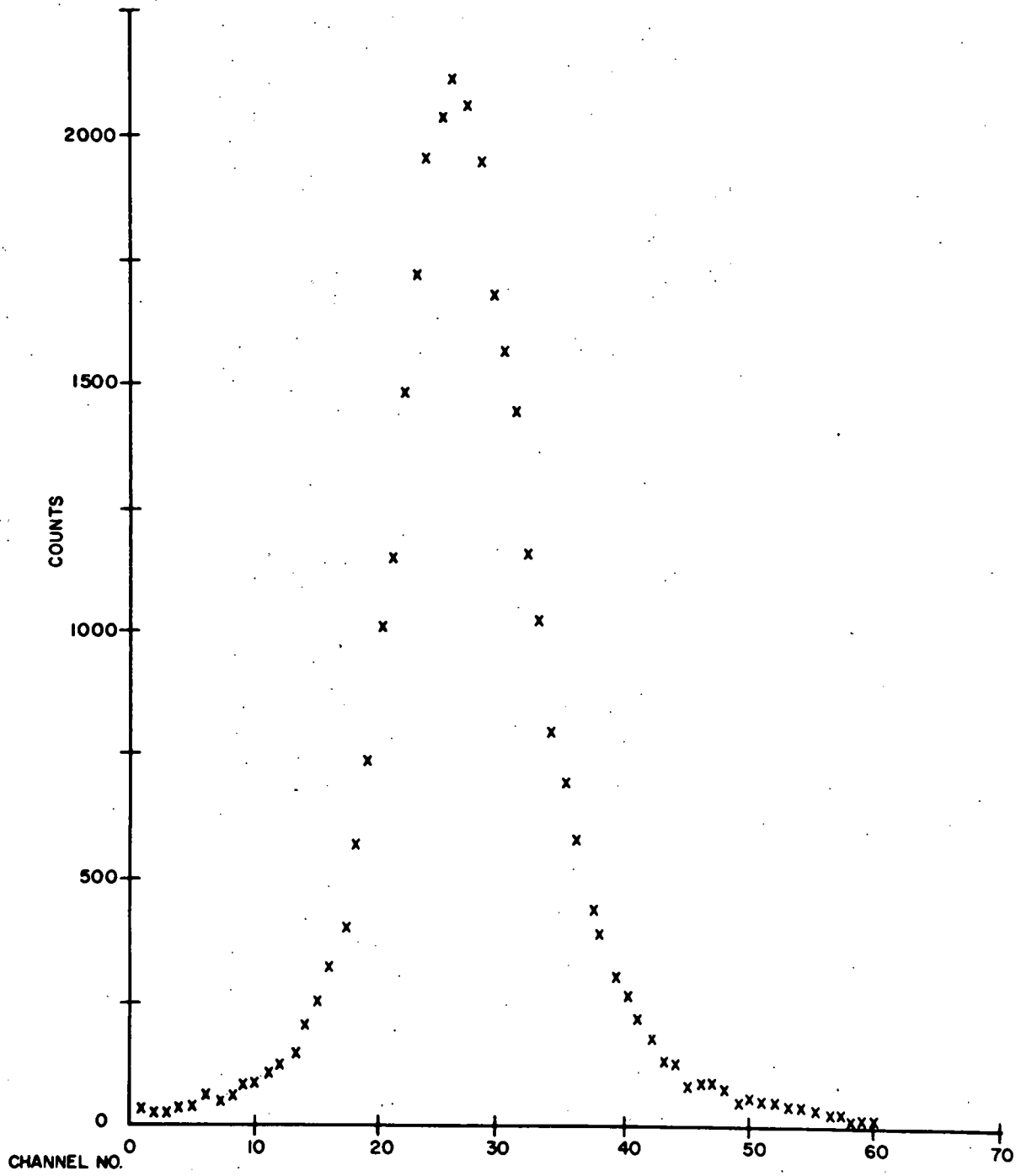

FIG. 5 MODULE RESOLUTION CURVE – I VS. 2

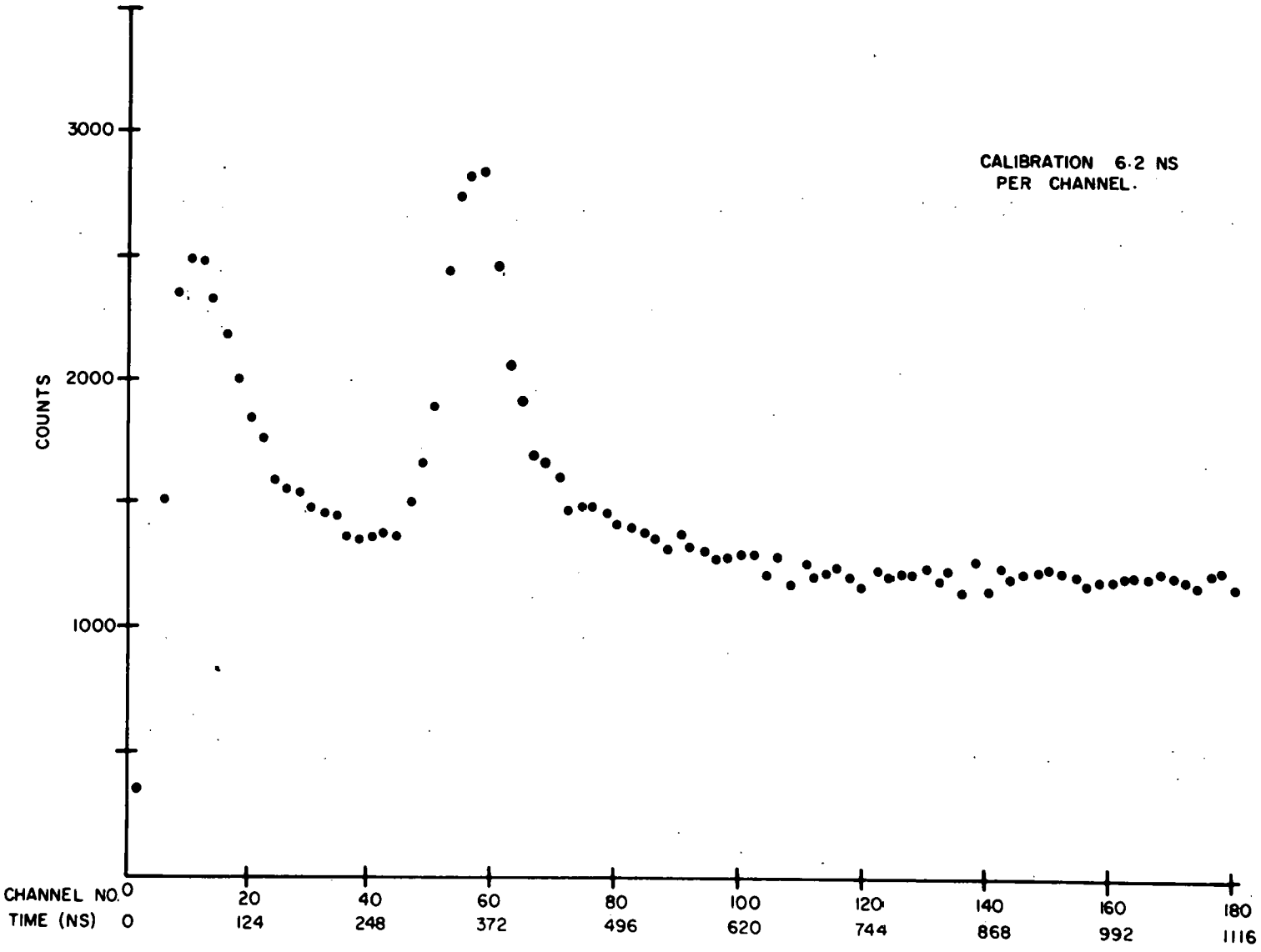

FIG 6 EXTENDED TIME SPECTRUM

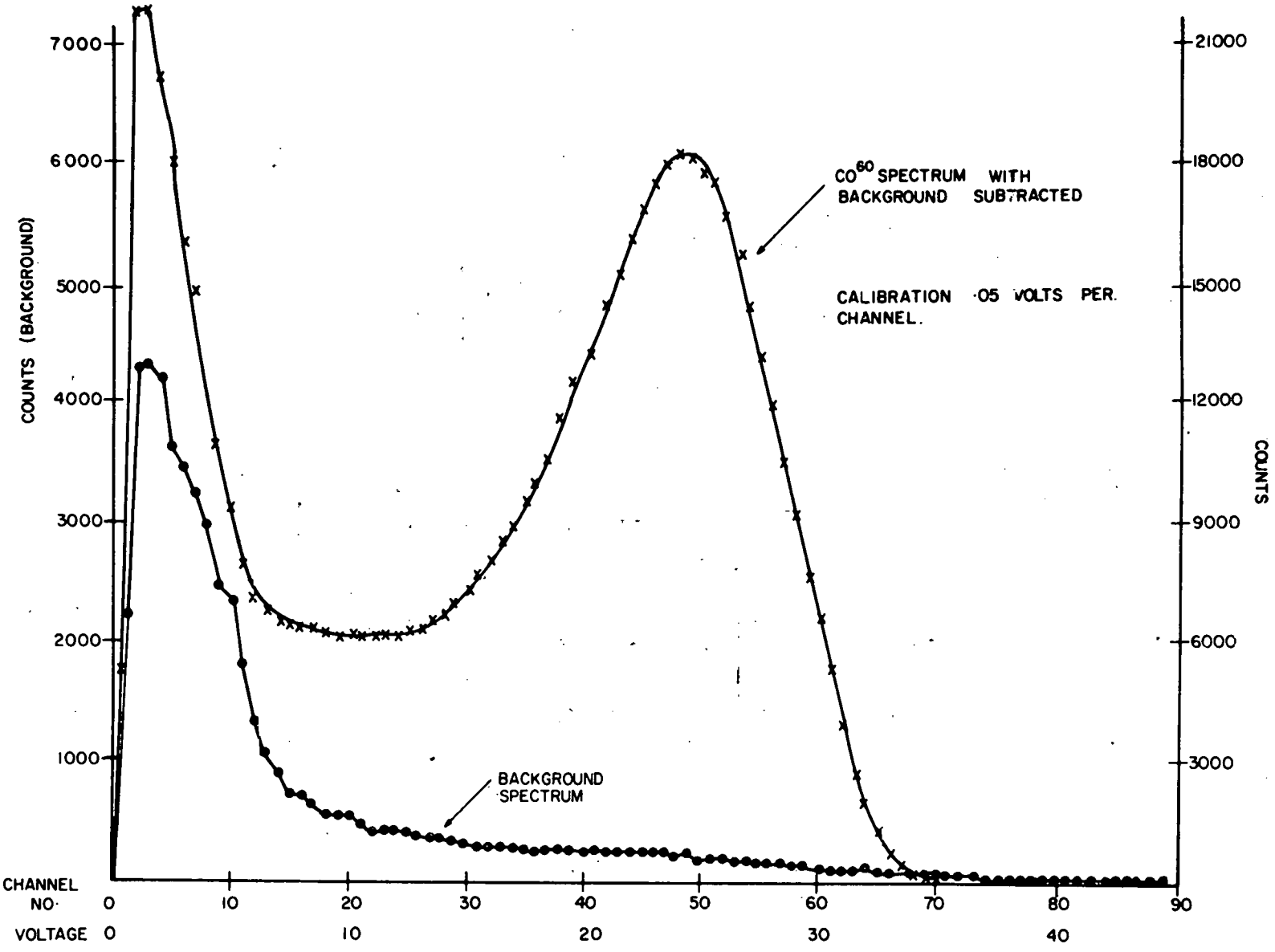

FIG·7 PULSE HEIGHT SPECTRUM–TUBE 18

Table 1

Co^{60} Source Coincidence 1 vs 2

Mod. No.	Near fwhm	Near $t_{\frac{1}{2}}$	Far fwhm	Far $t_{\frac{1}{2}}$	None fwhm	None $t_{\frac{1}{2}}$
2	30	3.81	37	4.80	36	4.60
4	22	2.81	29	3.71	30	3.81
5	20	2.55	26	3.32	28	3.57
6	18	2.30	26	3.32	25	3.19
7	32	4.11	35	4.45	37	4.79

Table 2

Module 4 Coincidence 1 vs 2

Source	Energy (Mev)	fwhm	$t_{\frac{1}{2}}$ (ns)
Cd^{109}	.087	24	3.06
Cs^{137}	.662	28	3.57
Co^{60}	1.33	22	2.81

Table 3

Module 4 Co^{60} Source

Coinc.	fwhm	$t_{\frac{1}{2}}$ (ns)
1 vs 1	28	5.57
1 vs 2	24	3.06
1 vs 3	23	2.93
2 vs 2	22	2.81

A NEW TIME-OF-FLIGHT DATA ACQUISITION CODE FOR PDP-7

N. N. Kaushal

A new code (TOFCOM) has been written and checked for taking time-of-flight data with sample cycling capability. The code operates as a "plug in" subroutine compatible with the general purpose supervisor code BOSS (Level 12)[1,2] and is capable of cycling up to 8 samples with 6144 channels of data for each sample. As each sample is brought into position, the data for that sample are read into core from tape. The sample is held in position for a preassigned number of LINAC triggers and at the end of this period (subcycle), the data from core are written on tape and the data for the next sample brought into core. This process is repeated for the desired number of samples and then the cycle is repeated.

The first 64 of the 6144 channels are reserved for storage of data other than time-of-flight. Such information as the run number, total number of samples, sample position, number of LINAC triggers per sub cycle, the cycle number etc. are stored in this region. The rest of the region is divided into four regions with assignable data compression factors and range. The information as to the range and the compression factors assigned to these regions is also stored in the first 64 channels. There is also a provision for reading a 100 MC decimal scaler at the end of each subcycle and adding this number to the data in preassigned channels in the first 64 channels. This feature is used for accumulating neutron monitor counts for the purpose of normalizing data for various samples.

The code performs some experiment monitoring functions also. Every time an undesirable situation is detected, a message is produced on the console teletype along with activating a warning light or buzzer. The time of occurrence of the situation is also recorded. The following situations are constantly monitored:

(a) Break in the incoming data caused by an interruption of LINAC operation or due to a break in the start/stop pulse train,

(b) Count rate too high to be handled by the program,

(c) Sample changer stopping in a position other than called for by the computer (due to a mechanical or electronic failure of the sample changer).

(d) Malfunction of the Dectape unit. In this case three tries are made to correct for the error and if the error persists, a warning message and alarm are generated.

LINAC operation is not interrupted during sample cycling operations, thus eliminating interference to any "piggyback" experiment that may be in progress.

The code has been tested and used for taking neutron capture data and has been found to be quite efficient. In most cases all sample cycling operations in the computer are completed well before the mechanical sample changer is ready for data-taking in the called-for position.

The code is expected to find use in a number of other experiments such as neutron scattering, self-indication experiments and total neutron cross-section measurements.

REFERENCES:

1. Linear Accelerator Project Annual Technical Report, October 1, 1968 - September 30, 1969, 143, RPI-328-171.

2. J. M. Clement, private communication.

ELECTRONIC IMPROVEMENTS FOR THE NUBAR EXPERIMENT

R. L. Reed,* G. Krycuk and R. C. Block

Figure 1 shows the basic equipment setup for the ^{233}U nubar measurement. The tank contains xylene with p-terphenyl as a scintillant. The scintillant also contains 0.5% by weight gadolinium, a low-energy neutron absorber. The scintillant is viewed by four 58 AVP photomultipliers with the photocathode faces immersed in the xylene for maximum detection efficiency. Output signals are taken from the anode and sent to a D.C. mixer, amplifiers, and discriminators to provide fission event and neutron capture event logic signals. Both neutron and fission signals are sent to the logic scaler. The fission signals are counted during auxiliary data-taking to determine the accidental coincidence rate. The fission signals are delayed, inverted and amplified and sent to the fast coincidence unit, an ORTEC 414A.

Two fission chambers are placed in the tank through-tube. The ^{252}Cf fission chamber is placed in the bottom of the through-tube, out of the beam line. The fission chamber is placed in the center of the tank. Pictured are the electronics for the ^{233}U chamber. If the ^{235}U chamber is used, the fast current amplifiers, pulse shapers and delay-inverter would be replaced by a preamplifier-amplifier, TSCA discriminator combination. The delays are necessary for coincidence. The OR unit is a diode OR that allows positive signals to pass only to the coincidence unit. The fast coincidence unit with an adjustable resolving time between 10 and 110 nsec will allow maximum fission detection efficiency with minimum accidental coincidences.

A fission event will be detected in the fission chamber and the tank. Through electronics a coincidence signal is generated and sent to start the logic unit. If it was a californium fission,

*Based in part on the Ph.D. Thesis of R. L. Reed.

a routing signal is also sent to the CF register. The start signal initiates a sequence that sets a "double fission" inhibit gate, clears the logic scaler and starts the scaler counting neutrons (i.e., Gd captures) for 32 μsec. After the scaler completes counting, all information is transferred to output buffers. These output buffers then transfer the data to the PDP-7 computer at the end of 120 μsec. However, if a second fission occurs during the 120 μsec, the "double fission" inhibit gate causes everything to stop and be cleared. One-hundred twenty μsec after the second fission, if no other fission event has been detected, the inhibit gate is cleared and the next fission event will be accepted. Thus, no fission may be detected within 120 μsec of another fission or data from both fissions are discarded.

In addition to the events due to fission neutrons from the initiating fission, the scaler counts may include cosmic ray events, scattered neutrons from the neutron beam, fission neutrons from undetected fissions and other background events. The background generator (BKG GEN) provides "false" starts to the logic unit which are accepted only if a fission event has not occurred in the previous 120 μsec. If a fission event is detected during the background counting, the count is inhibited and the fission event restarts the sequence. The fission neutron counts can thus be corrected for background events by those background data which correspond in time-of-flight to the fission neutron data.

It is desirable to reduce the effect of two corrections necessary to the nubar results. These are the accidental coincidence correction for alpha pileup in the fission chambers and the deadtime correction for the neutron counting. The use of the fast coincidence unit will allow a maximization of the fission detection efficiency with a minimization of the accidental coincidence rate.

The logic unit initially had a 10 megahertz scaler, but the signal from the phototubes and the discriminator characteristics made possible only a 6-7 megahertz rate. This made a 1% or so deadtime correction necessary to the data -- a correction comparable

to the variations expected in nubar. A 100 megahertz scaler has been incorporated into the logic unit. This scaler, utilizing Schottky TTL Integrated Circuit units from Texas Instruments was designed and built at this laboratory (Fig. 2). An inverting amplifier (Fig. 3) was also built to change the negative EG&G logic signals to positive 2-volt signals necessary for the TTL units.

The scintillant in the tank has a decay time constant of $\sim$ 4-5 nsec. Thus the light pulse associated with an event in the tank would have a time duration of several time constants about 15-20 nsec. Convoluting this pulse shape with the 58 AVP characteristics yields a signal on the anode of 15-25 nsec duration.

The phototube bases have been designed to yield an anode signal reproducing the light pulse shape. Ringing on the output signal has been eliminated by employing mylar capacitors, with leads as short as possible, as interdynode capacitors. Elimination of the ringing is also demonstrably helped by bringing the coaxial signal cable directly to the anode standoff capacitor (Fig. 4).

Some estimates of gain shifts were made using the approximate formula

$$\frac{\Delta G}{G} = \tau \cdot \frac{I_a max}{I_b} \cdot \frac{e^{-t/\tau} - e^{-t/RC_n}}{\tau - RC_n} \quad **$$

where

τ = time constant of the scintillator

$I_a max$ = peak anode current

RC_n = time constant of last dynode stage

I_b = voltage divider current

With τ = 5 nsec, $RC_n \approx 0.6$ msec, I_b = 6 ma for $\Delta G/G \approx 0.1$, I_a would need to be $\sim$ 1.6 A. For the normal anode currents $\simeq$ Ima, $\Delta G/G \simeq 10^{-5}$. Thus, only the target gamma flash or some very energetic cosmic rays should cause significant gain shifts. The time-dependent gain shift due to the target gamma flash can be corrected

**Amperex Data Handbook - Photomultiplier Tubes, p. 7, July 1968.

by recording T-O-F data for ^{252}Cf nubar taken simultaneously with the uranium data. This gain shift effect should be dissipated by the next machine burst. Any gain shift due to cosmic rays should be sufficiently random and infrequent to not cause any problems.

These phototubes will exhibit gain shifts due to excessive count rates. If 100 events were detected in a single time constant, RC_n, $\Delta G/G$ would approach 0.1%. This would be a rate of >100000/sec, possible only at very early times due to high energy neutrons scattered into the tank from the neutron beam. That resultant gain shift would be an addition upon that due to the gamma flash and corrected in the same manner. With photomultiplier signals of $\sim$ 20 nsec duration, the deadtimes will be 20-25 nsec as compared with 140 nsec previously. This will significantly decrease the amount of deadtime correction necessary.

FIGURE CAPTIONS

Fig. 1 Equipment Arrangement for the Nubar Experiment.

Fig. 2 100 Megahertz Scaler Using Schottky TTL Integrated Circuits.

Fig. 3 Inverting Amplifier to Change -.5 Volt Signals to +2 Volt Signals.

Fig. 4 Schematic of Phototube Base Used for the Nubar Experiment.

Figure 1

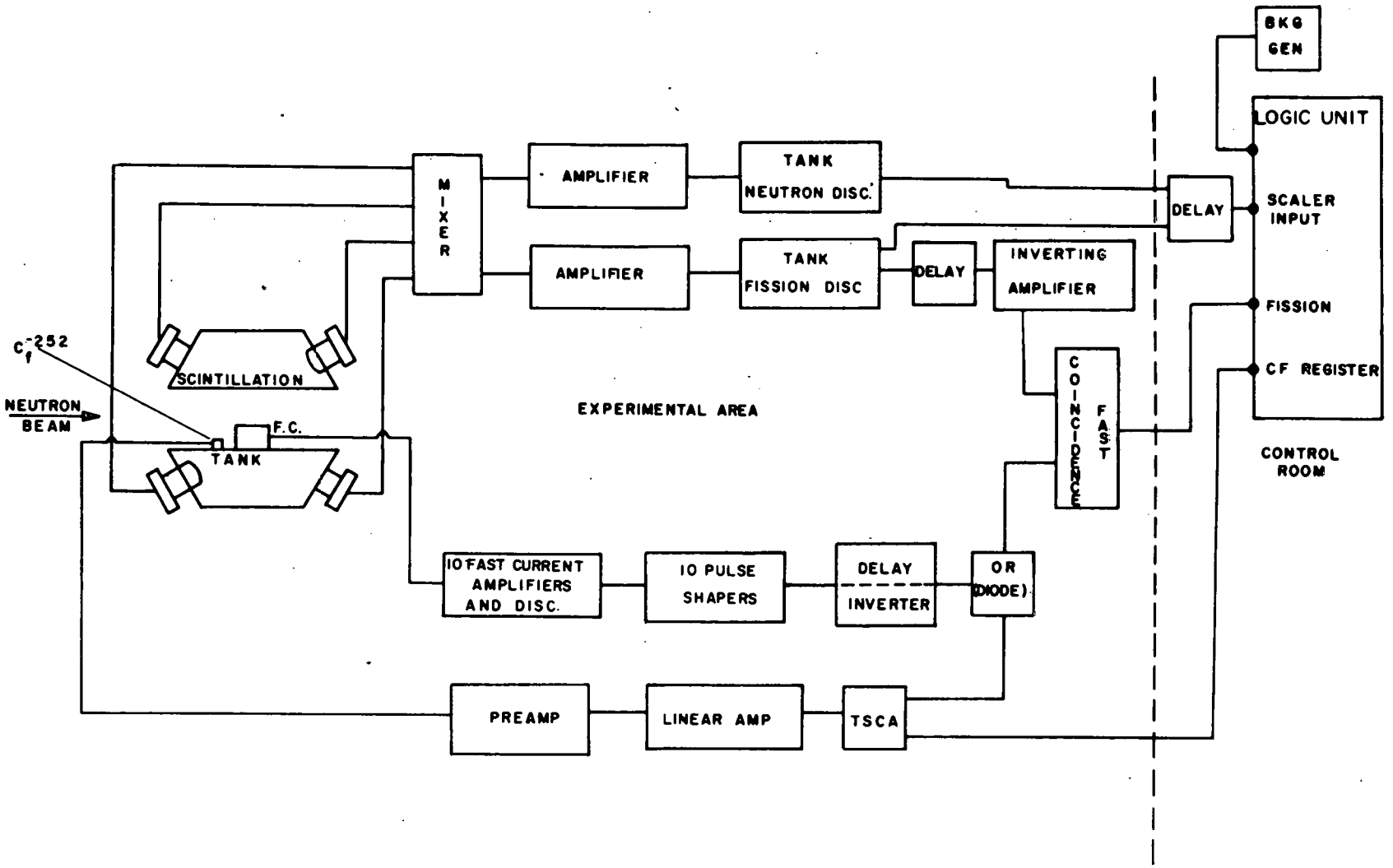

NUBAR EXPERIMENT EQUIPMENT

Figure 2

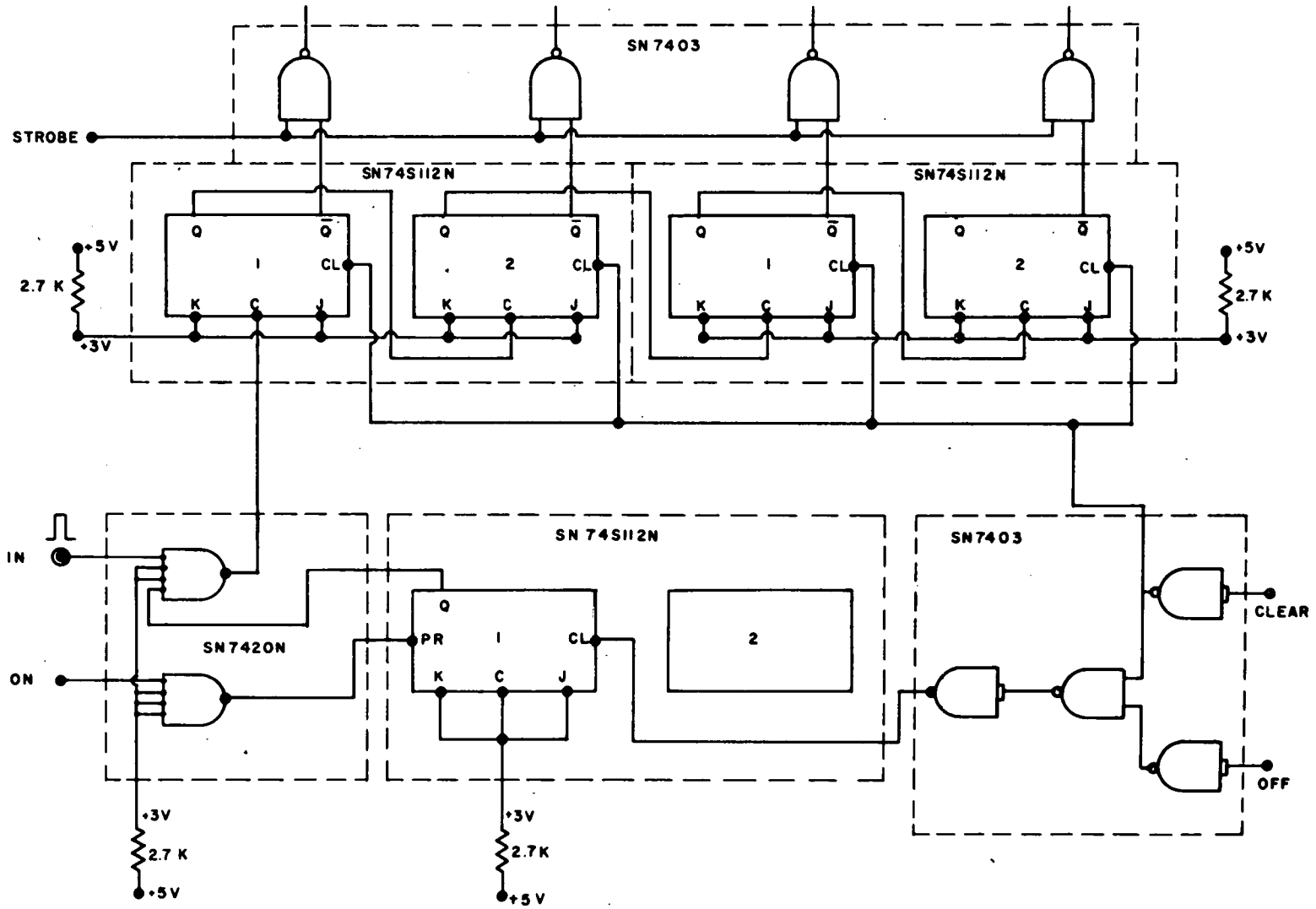

100 MHZ SCALER SCHEMATIC

Figure 3

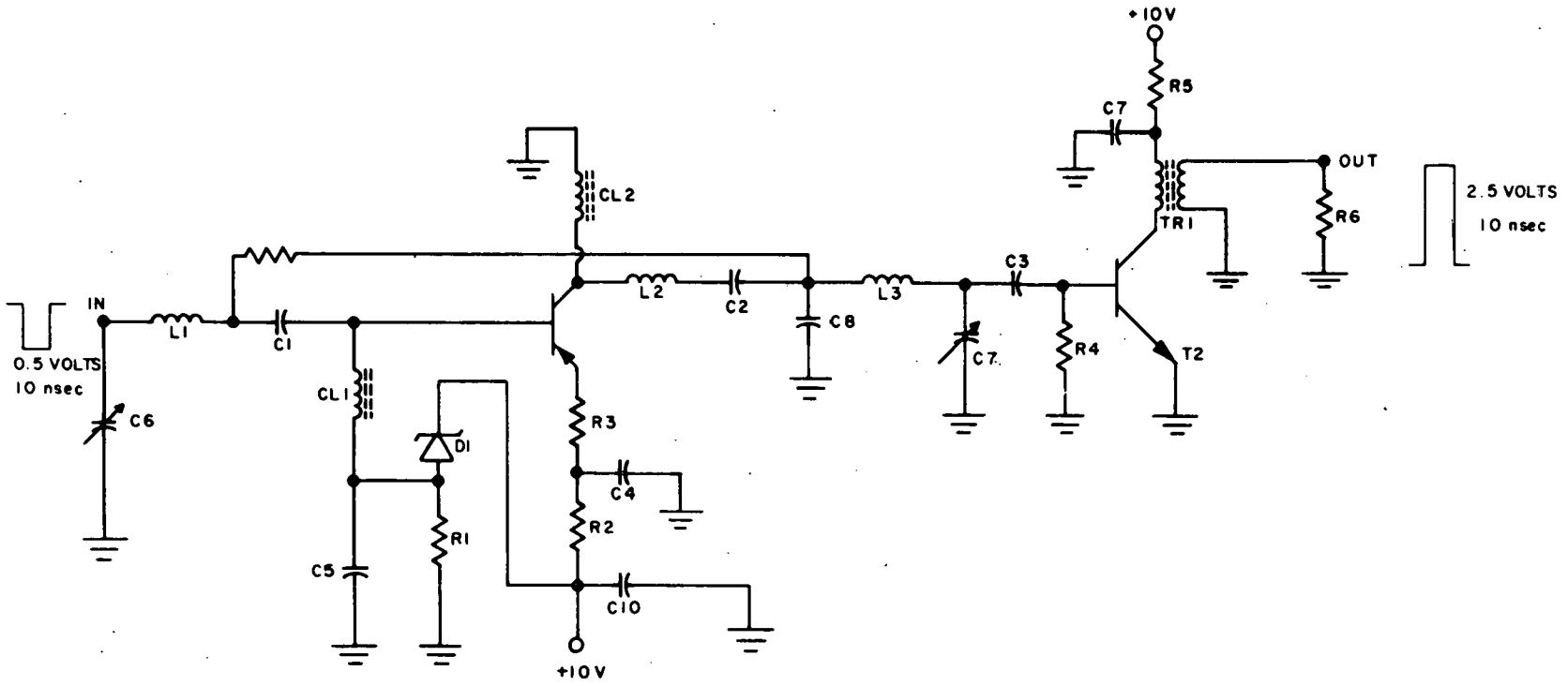

T1: 2N3639
T2: 2N3563
C1, C2, C3, C4, C5: .002 uf CERAMIC DISC CAPACITORS
D1: IN429
C10: 3.9uf ELECTROLYTIC
L1, L2, L3: 5 TURNS NO. 22 WIRE
C9: .22 uf
C8: 22 uf
C6, C7: 2-20uf ADJUSTABLE
R1: 1000Ω

R2: 270Ω
R3: 35.7Ω
R4: 5000Ω
R5, R6: 50 Ω
CL1, CL2: 15 TURNS NO. 28 WIRE ON 4C4 CORE FEROXCUBE
TR1: TRANSFORMER 10 TURNS NO. 28 WIRE 1:1 RATIO – ON CORE 891CT0503B7

FAST PULSE INVERTING AMPLIFIER

Figure 4

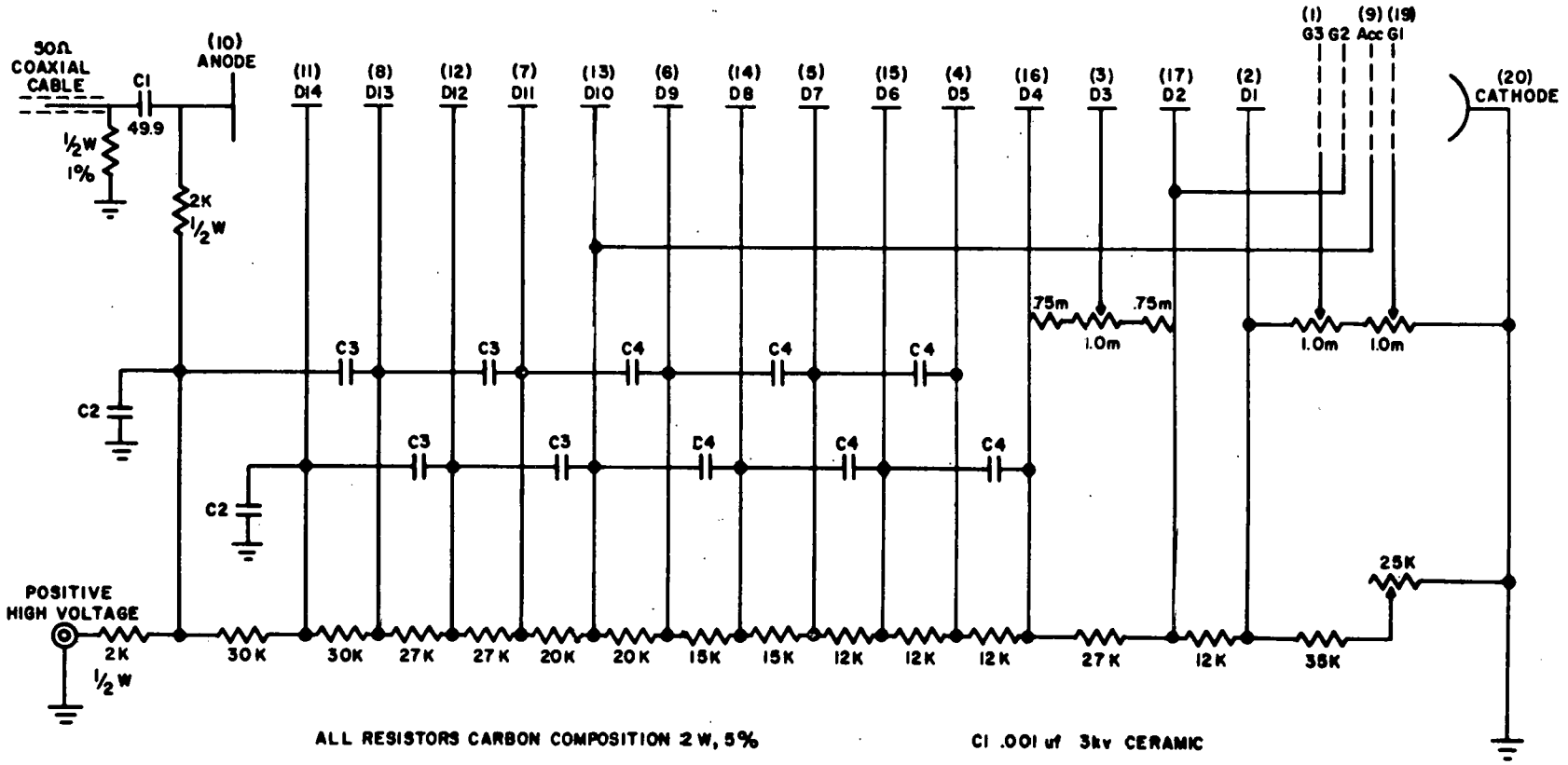

ALL RESISTORS CARBON COMPOSITION 2 W, 5%
UNLESS OTHERWISE INDICATED

PIN NUMBERS IN PARENTHESIS

C1 .001 uf 3kv CERAMIC
C2 .02 uf 3kv CERAMIC
C3 .022 uf 600 V MYLAR
C4 .0068 uf 400 V MYLAR

PHOTOTUBE BASE SCHEMATIC

REACTOR PHYSICS AND ENGINEERING - EXPERIMENTAL

REACTOR PHYSICS AND ENGINEERING - EXPERIMENTAL

During the current year, the principal activities under this program have been directed to four areas: the assessment of data files for materials (iron and depleted uranium) on which measurements were completed earlier; the measurement and analysis of position-dependent fast neutron spectra in aluminum; preliminary exploratory measurements on a two-region assembly and the development of analytical approaches for these studies; and finally, the construction and bringing into operation of a facility for the study of fast neutron spectra in metallic sodium in bulk. Concomitantly, supplemental activity in other areas has also continued.

The measurement and analysis of position-dependent fast neutron angular flux spectra in a large homogeneous assembly of iron have provided the basis for the evaluation of currently available cross-section data sets; the ENDF/B-I, ENDF/B-II and KEDAK (Karlsruhe, KFK-750) data files have been assessed, yielding important results and definitive conclusions with respect to these files; a check of the standard transport-theory codes has also been possible. A comprehensive paper entitled, "Experimental and Analytical Studies of Fast Neutron Transport in Iron," is to be published in Nuclear Science and Engineering. Similarly, measurement and analysis of fast neutron spectra in a depleted-uranium assembly have led to the assessment of data sets for ^{238}U: ENDF/B-I, ENDF/B-II and KEDAK files and an ANL multigroup set. A full paper on these results for depleted uranium is also being submitted to Nuclear Science and Engineering.

The measurements of fast neutron spectra in a large aluminum assembly have been completed and the analysis based on S_{16}, 49-group, Po (with transport approximation) calculation and ENDF/B (versions I and II) and KEDAK data files is under way. Preliminary conclusions regarding adjustment of aluminum cross-section data

for experiment-theory agreement of neutron spectra, were reported at the Winter ANS Meeting in Miami Beach in October, 1971.

Preliminary studies of fast neutron angular flux spectra in a two-region system have involved the measurement of neutron spectra in the vicinity of an interface between aluminum and iron regions, with a spherical source embedded in the aluminum region. These measurements are being analyzed, using one and two-dimensional transport codes, to investigate several aspects of cross-section data and calculational recipes. Detailed results are expected in FY 1972.

A major part of the effort in this program has been devoted to the preparatory work toward bringing into operation a sophisticated system appropriate to the study of detailed position-dependent fast neutron angular flux spectra in metallic sodium at room temperature. An integrated sodium facility consisting principally of a six-foot cuboidal steel container, filled with sodium (with a target-placement recess and re-entrant holes) and the associated safety and sodium-handling equipment, has been designed and constructed and is now operational. The entire system has been checked out at the experimental site in the LINAC target room. Some preliminary measurements of fast neutron spectra in the sodium assembly have been started. The actual detailed measurements will continue in FY 1972 and parallel analytical work will accompany the measurements.

Efforts were continued towards the development of calculational techniques for the analysis and interpretation of in-core time-dependent neutron spectra. Some off-line experimental tests were performed on a Li^6 solid-state neutron detector in order to assess its suitability for in-core spectrum measurements.

The results of the measurement and analysis of fast neutron spectra and the assessment of data files, as they are generated, are also being compiled in the format of a SPECTRUM Book and communicated to data evaluation groups.

STUDIES OF FAST NEUTRON TRANSPORT IN IRON WITH AN ASSESSMENT OF DATA FILES

B. K. Malaviya, N. N. Kaushal, M. Becker, E. T. Burns and E. R. Gaerttner

The assessment of currently available nuclear differential data files for iron, based on the measurement and analysis of position-dependent fast neutron angular flux spectra in a large homogeneous assembly, has been completed and a comprehensive paper[1] on this subject is to be published in Nuclear Science and Engineering. The salient features of this study and the major conclusions are summarized here.

The details of the measurements, experimental setup and techniques and the approaches and codes employed in the analysis have been discussed in previous Progress Reports.[2] Basically, time-of-flight measured fast neutron spectra, over the energy range 10 keV to 10 MeV, at several different positions in a large iron assembly have been analyzed using cross-section data libraries, the MC^2 code system and both multigroup transport calculations and continuous slowing down theory. The currently available data sets included in the analysis for evaluation are: ENDF/B-I (Material 1020)[3], KEDAK (KFK-750)[4] and ENDF/B-II (Material 1122)[5].

Examples of the ways in which data from these files differ from one another can be seen from Figs. 1 and 2 which show plots of the iron scattering cross section from ENDF/B-I, KEDAK and ENDF/B-II files. The ways in which these files differ provide insight into the uncertainty to be attached to the several types of cross sections in various energy ranges. There are three distinct areas of importance whose consequences we can investigate separately: (a) the high-energy cross-section data (500 keV to 10 MeV) with varying degrees of resolution; (b) the intermediate energies (30 keV to 500 keV) with substantial amplitude disparities; and (c) the s-wave scattering interference minimum at 25 keV. Con-

sidering first the Karlsruhe data versus the ENDF/B-I data (Fig. 1), the Karlsruhe data are more highly resolved with respect to the scattering resonances; in the energy range 30 keV-500 keV, ENDF/B-I data have consistently and significantly higher average values than Karlsruhe data; the dip in the cross-section minimum of the 28.5 keV resonance is much lower in ENDF/B-I data than in the Karlsruhe data; the difference in the location of the 25-keV dip is also noteworthy. The principal characteristics of the ENDF/B-II data for iron (Fig. 2 shows Σ_s vs E) are: (a) the cross-section amplitude in the 30-500 keV range is similar to Karlsruhe data; (b) the depth of the 25-keV minimum is much less than in ENDF/B-I and is comparable to that of Karlsruhe data; (c) the total cross section has a large number of very sharply resolved resonances at intermediate (hundreds of keV) energies with very deep minima; (d) the capture cross section is much more highly resolved over the entire energy range, and the average amplitude follows the Karlsruhe data more closely than ENDF/B-I data; (e) high-energy resolution is greater than in the other two files.

These and other features of the data files have been analyzed and evaluated by comparing experimentally determined space-dependent angular flux spectra with the results of calculations based on different approaches, using data from different files as input.

Detailed measurements of fast neutron angular flux spectra were made for a variety of positions in the iron assembly, corresponding to different values of the spatial variable and angle. In comparing measured and calculated spectra, variation with respect to both shape and normalized amplitude is pertinent. Figure 3 shows a typical result of the comparison of normalized spectra; the calculated and measured spectra are each entirely independently normalized with respect to a common source spectrum. The multigroup transport calculations here are based on ENDF/B-I data as input and involve 49 groups, S_{16} quadrature and Po scattering matrix with the transport approximation; the source representation in terms of a black absorber has been described earlier.

The overall agreement in the macroscopic as well as microscopic features of the spectrum is good; the amplitude agreement lends confidence to the experimental normalization techniques and indicates that the larger order-of-magnitude disagreements reported by other investigators[6] are probably due to procedural problems and not due to discrepant ENDF/B data. The particularly significant disagreements are at high (above a few MeV) and low (in the vicinity of the 25-keV minimum) energies. Detailed interpretation of high-energy disagreements is deferred until a complete anisotropic scattering analysis capability is available. The shape of the low-energy part of the spectrum is very sensitive to the dip of the 25-keV anti-resonance which is discrepant in ENDF/B-I data. The implications of these disagreements are examined in detail in later paragraphs.

Figure 4 shows comparisons similar to Fig. 3 except that Karlsruhe multigroup cross sections are utilized in the calculation. In the intermediate energy range, the ENDF/B-I data provide better agreement, because of better scattering cross section amplitudes in the 30-500 keV range than the Karlsruhe data. This conclusion is further examined in detail later. At higher energies it appears that both KEDAK and ENDF/B-I provide good slowing-down spectrum calculations despite the better resolution of the KEDAK file. However, at very high energies (MeV range) anisotropic scattering may cause the simple transport approximation to be of dubious value when compared with the experiment. Preliminary calculations using anisotropic scattering confirm the propriety of assessing low and intermediate-energy data with Po-transport-approximation calculations.

In view of the critical importance of the 25-keV scattering minimum for fast reactor applications and the large differences among alternative data files, the value and the effect of this minimum were investigated in detail. Figure 5 shows the comparison of experimentally measured spectrum with the calculated slowing down spectrum in iron in the vicinity of the major scattering reso-

nance at 28.5 keV, based on ENDF/B-I and KEDAK data as input. It is evident from this figure that the KEDAK data yield better agreement with experiment in the vicinity of the large 28.5 keV resonance than the ENDF/B-I data. These results indicate that the cross-section minimum at 25 keV is most appropriately taken at the KEDAK value of about 0.557 barns. This good representation of the major resonance by the KEDAK data seems to indicate that the ENDF/B-II value of 0.375 barns is about 30% too low, but is more realistic than the 0.15 barns listed in the ENDF/B-I file. These conclusions are in accord with the experimental value of 0.497 barns for the 25-keV dip, based on recent RPI measurements.[7] These results will also be discussed further in later paragraphs.

While some degree of interpretation of theory-experiment discrepancy is possible directly from multigroup transport calculations, in general, interpretation is greatly simplified by use of models providing better insight into detailed relationships among basic data, integral parameters and spectra. The age parameter $\tau(u)$ has been especially useful in assessing iron data files. Subtle differences in cross sections among different data sets lead to substantial differences in age and these large age differences lead -- because of the $(\text{age})^{-3/2}$ dependence -- to substantially different spectra. Thus by tracing age differences, it is possible to further evaluate ENDF/B-I, KEDAK and ENDF/B-II data. For example, the age as calculated from 10 MeV for these three standard data sets for iron, is shown in Fig. 6. Consider first the major discrepancy between the KEDAK and ENDF/B-I age calculations which occurs below the s-wave interference minimum at 25 keV; the age graphically illustrates the preponderant effect of that resonance on the diffusion of neutrons. The substantial increase in age as calculated with the ENDF/B-I data implies a large decrease in the number of neutrons which are scattered to below the dip at any given radius. Physically this indicates that neutrons are not easily transferred to energies below this minimum. The evaluation of the minimum based on comparison with experiment has already been discussed (Fig. 5).

Consider another very important discrepancy evident in Fig. 6. The age from KEDAK data is consistently higher than the age calculated from ENDF/B-I from the energy range 30 keV to 500 keV. This is a reflection of the systematically lower elastic scattering cross section for KEDAK data in this energy region (Fig. 1). The age parameter is very sensitive to such differences because in any given energy interval the increment in age depends essentially on the inverse square of the scattering cross section. The higher age implies a larger "attenuation" with energy at any given space point, the dominant term as predicted by age theory being $\tau^{-3/2}$. Thus, we expect the predicted spectrum from KEDAK at low energies to be substantially lower than the corresponding ENDF/B-I prediction, as shown in Fig. 8. Analogous results are obtained in multigroup transport calculations (compare, for example Figs. 3 and 4).

The reasons for the especially sharp increases in the age for ENDF/B-II data are also significant and instructive. As seen from Figs. 1 and 2, iron cross sections for ENDF/B-II appear to be similar to KEDAK data but are more highly resolved (based on an R-matrix calculation). However, the integral parameter, $\tau(u)$ pointedly demonstrates that there are again subtle differences among these files (Fig. 6). The reason for the large steps in the age are traced to the s-wave interference minima in the resonance region (100-500 keV). It appears that a number of these dips are too low as a result of coincident minima in the isotopes of iron.[8] The material of interest is natural iron (91.7% ^{56}Fe). The cross section of the ^{56}Fe isotope can go very nearly to zero in the large s-wave minima; however, the 8.3% of the other iron isotopes (^{54}Fe and ^{57}Fe) act as a background scatterer which maintains the microscopic cross section at a higher effective value. It does not seem reasonable to find cross-section minima at the same energies for more than one isotope of the same material for several resonances. In accordance with the earlier conclusions based on comparison with experiment, both ENDF/B-II age at the intermediate energies (100 to 500 keV) and the ENDF/B-I age at 25

keV suffer from this lack of accurate knowledge of the 'background' cross section in iron. The effect of using this ENDF/B-II iron data is evident -- it tends to favor diffusion and leakage over slowing down. Consequently, caution must be exercised in using these iron cross-section data. However, despite the apparent magnitude of the difference, the seriousness of this problem is greatly alleviated in the cores of typical fast reactors since scattering minima of individual materials may not always have a pronounced effect due to the large scattering background from other materials. If, however, there is a disproportionately large amount of localized iron, as in a pressure vessel wall or reflector, then this ENDF/B-II iron data may yield poor calculational results.

Another area of importance in the evaluation of ENDF/B-II data is the energy region 500 keV to 10 MeV, particularly with respect to the degree of resolution. Calculations of neutron age of spectra with the age model, indicate that age, and therefore spectra, while affected by differences in resolution are not very sensitive to such differences. The main consequence of inadequate resolution appears to be in deep penetration of a small fraction of source neutrons in their first flight. For slowing down spectra as a whole, however, resolution differences are not too important. Figure 7 indicates the insensitivity of age to high-energy resolution.

The capture cross section for ENDF/B-II file offers much greater resolution and a slight difference in overall amplitude. It does not appear to have a pronounced effect on the slowing down spectrum in a pure iron assembly, the ratio $\xi\Sigma_t/\Sigma_a$ being of the order of 23. However, our knowledge of the RPI experiments[9] on which the capture data are based, leads us to consider the new capture data to be appropriate.

An example of the manner in which age differences in cross-section data, are reflected in the differences in spectra, is seen from Fig. 8 which shows the space dependent continuous scalar flux $\emptyset$ (r,E), according to age theory, for the KEDAK and ENDF/B-I data for iron. This Figure brings out and reaffirms several of the

points discussed earlier. Figures 1, 6 and 8 viewed together bring out the sensitivity of cross sections to age and to spectra. Two aspects of the differences between KEDAK and ENDF/B-I data, viz, the dip at 25 keV and cross section amplitude disparities in the range 30-500 keV are very clearly seen in Fig. 8. In the energy range 30-500 keV, the spectra from Karlsruhe data attenuate more strongly with energy than do the spectra calculated from ENDF/B-I data (by either DTF-IV or age theory -- these two being in good agreement as seen later) or the experimental spectra. This reconfirms the earlier inference that the ENDF/B-I evaluation is to be preferred in the range 30-500 keV. However, this is not to say that ENDF/B-I data in this range are clearly satisfactory. We consider this energy range to be one of uncertainty that merits further measurement and evaluation. On balance, the ENDF/B-I data appear more nearly acceptable.

In view of the complementary use of continuous slowing down (age) and transport models, a brief aside on their correspondence is in order. Figure 9 shows age and transport scalar flux spectra at two locations. The correspondence is deemed to be acceptable, particularly for the qualitative tasks of interpretation for which the age model is used. It should be noted that there are several differences in physical model involved. First, the age model is an infinite-medium model, while the transport calculation is based on a finite radius. By most criteria, the experimental assembly is effectively infinite. However, the existence of a very deep interference minimum in a cross section can lead to a very high age at low energies, thereby bringing neutrons to the vicinity of the outer radius from which leakage can occur. Direct streaming from the minimum is also a possibility. The appearance of discrepancies between low energy attenuation (spatial or energy) in age and transport calculations serves as a signal to us to give closer attention to the influence of leakage.

The simple continuous flux $\emptyset$ (r,E) of age theory was also used to check the effect of the space dependence of weighting spectrum

for the generation of broad group constants for a multigroup calculation. Broad group elastic removal cross sections in iron were calculated for 49- and 13-group sets in the energy range 10 keV to 10 MeV, using three different spatial weighting functions, as derived from age theory (scalar fluxes at 6, 10 and 14 inches from a point source in an infinite medium, using ENDF/B-I data). While some slight variation with position was observed for the 49-group set (at high energies), the magnitude of the variation was not serious on either the group constants themselves or on calculated fluxes. Thus, the use of the 49-group structure seems appropriate. However, in view of the space-dependence of the 13-group sets, a significant reduction in number of groups without space-dependent weighting could lead to difficulty.

To summarize, the principal conclusions regarding the assessment of the ENDF/B-I, KEDAK (Karlsruhe, KFK-750) and ENDF/B-II (material 1122) data sets are as follows:

(1) The value of 0.15 barns in ENDF/B-I for the s-wave scattering cross-section interference minimum at 25 keV is much too low and causes unduly severe attenuation (in energy) in the spectrum at lower energies. A more appropriate value, 0.577 barns, is listed in the KEDAK (KFK-750) data file. ENDF/B-II also lists a substantially higher scattering cross section in this scattering window (0.375 barns, for material 1122); however, this is not as good as the KEDAK value. The value of 0.497 barns based on recent measurements seems to be reasonable enough to be adopted.

(2) The ENDF/B-I data yield slowing down spectra in better general agreement with experiment than do Karlsruhe data because of better cross-section amplitudes in the intermediate (30-500 keV) energy range. However, the ENDF/B-II data in this range are similar to Karlsruhe data.

(3) The ENDF/B Version II has a large number of s-wave scattering minima at intermediate (100-500 keV) energies which are unreasonably deep. This results in an inordinate jump in the integral parameter, the age τ, and consequently leads to large attenuation of the flux with energy. This is not supported by the experimental measurements and the minima appear to be too low. The background scattering from other isotopes of iron (^{54}Fe and ^{57}Fe) is important and must be incorporated in the evaluation.

(4) The ENDF/B-I set has insufficient resolution in most high-energy scattering resonances. Recently, the high-energy resolution has been greatly increased[10,11] and the ENDF/B Version II has a very substantial increase in high energy structure. At present basic parameters and the calculated slowing down spectrum do not appear to be overly sensitive to the degree of resolution. The increased structure may, however, be important in deep penetration problems.

(5) The capture cross section in ENDF/B-II is much more highly resolved over the entire energy range and the average amplitude follows the KEDAK data more closely than ENDF/B-I. However, experiment is not significantly sensitive to capture in iron (although very sensitive in some other materials).

(6) Current effort in measurement and evaluation of data may be placing excessive relative emphasis on resolution at high energies and in-

sufficient relative emphasis on large discrepancies in average values -- in the 30-500 keV range, for example.

Some of the conclusions, not relating specifically to data assessment can be stated as follows:

(1) Useful by-products of this investigation are the check and assessment of standard codes used in fast reactor analysis and the incorporation of improvements and removal of errors.
Improvements in both models and programming efficiency have been made in the MC^2, DTF-IV and SUPERTOG codes and have been made available by direct communication, or through Argonne and RSIC code centers.

(2) Use of the transport approximation alone may not be adequate in predicting neutron spectra at high energies and detailed anisotropic scattering effects should be incorporated into the analysis.

(3) Previously reported[6] order-of-magnitude discrepancies between theory and experiment, particularly regarding amplitude, appear to be due to procedural problems rather than to basic inadequacy of theory or data.

(4) The use of infinite-medium flux spectrum as the weighting function for multigroup constants can introduce large errors for iron if too few groups are used in a multigroup calculation, but errors are small for the group structure used in this paper.

Overall we do not consider the new ENDF/B-II data (revised version) for iron to be good enough to be adopted. For fast reactor applications, we consider ENDF/B-I to be preferable, subject to the limitations cited above. As an interim measure, ENDF/B-I could be modified with respect to the data used for the 28.5 keV resonance (using Karlsruhe data values).

REFERENCES:

1. B. K. Malaviya, N. N. Kaushal, M. Becker, E. T. Burns, A. Ginsburg and E. R. Gaerttner, "Experimental and Analytical Studies of Fast Neutron Transport in Iron," to be published in Nucl. Sci. Eng.
2. Linear Accelerator Project Annual Technical Report, October 1, 1969 - September 30, 1970, RPI-328-200.
3. H. C. Honeck, "ENDF/B, Specifications for an Evaluated Nuclear Data File for Reactor Applications," BNL-50066 (T-467) ENDF 102, Brookhaven National Laboratory (May 1966).
4. I. Langner, J. J. Schmidt and D. Wall, "Tables of Evaluated Nuclear Cross Sections for Reactor Materials," Karlsruhe Report, KFK-750, EUR 3715^{e} EANDC (E)-88 "U", (1968).
5. Marvin Drake, Brookhaven National Laboratory, private communication (1970).
6. R. J. Cerbone, "Neutron and Gamma-Ray Spectra in a Spherical Iron Assembly," Trans. Am. Nucl. Soc., 12, 401 (1969).
7. Nuclear Structure Group (R. W. Hockenbury), private communication (1971).
8. Marvin Drake, Brookhaven National Laboratory, private communication (1971)
9. R. W. Hockenbury et al., "Neutron Radiative Capture in Na, Ag, Fe and Ni from 1 to 200 keV," Phys. Rev., 178, 1746 (1969).
10. S. Cierjacks et al., "High Resolution Total Neutron Cross Sections between 0.5-30 MeV," KFK-1000, EUR 3963^{e} EANDC (E)-111 "U", Gesellshaft fur Kernforschung M.B.H. Karlsruhe (1968).
11. A. D. Carlson and R. J. Cerbone, "High Resolution Measurements of the Total Neutron Cross Section of Nitrogen and Iron," Nucl. Sci. Eng., 42, 28 (1970).

FIGURE CAPTIONS

Fig. 1 Elastic Scattering Cross Section for Iron; ENDF/B-I and KEDAK Data.

Fig. 2 Elastic Scattering Cross Section for Iron; ENDF/B-I and ENDF/B-II Data.

Fig. 3 Comparison of Source-normalized Measured and Calculated (DTF-IV; ENDF/B-I) Spectra in Iron Assembly: R = 10 inches, $\mu = \pm 0.8$.

Fig. 4 Comparison of Source-normalized Measured and Calculated (DTF-IV: KEDAK) Spectra in Iron Assembly: R = 10 inches, $\mu = \pm 0.8$.

Fig. 5 Slowing-down Spectrum in Iron in the Vicinity of the Major Scattering Resonance at 28.5 keV: Measurement and Calculation (DTF-IV; KEDAK and ENDF/B-I).

Fig. 6 Comparison of the Age in Iron for Three Standard Data Files.

Fig. 7 High-energy Age in Iron Using ENDF/B-II Data.

Fig. 8 Age-theory Flux in Iron: ENDF/B-I and KEDAK Data.

Fig. 9 Iron ENDF/B-I Scalar Flux from Age Theory and DTF-IV.

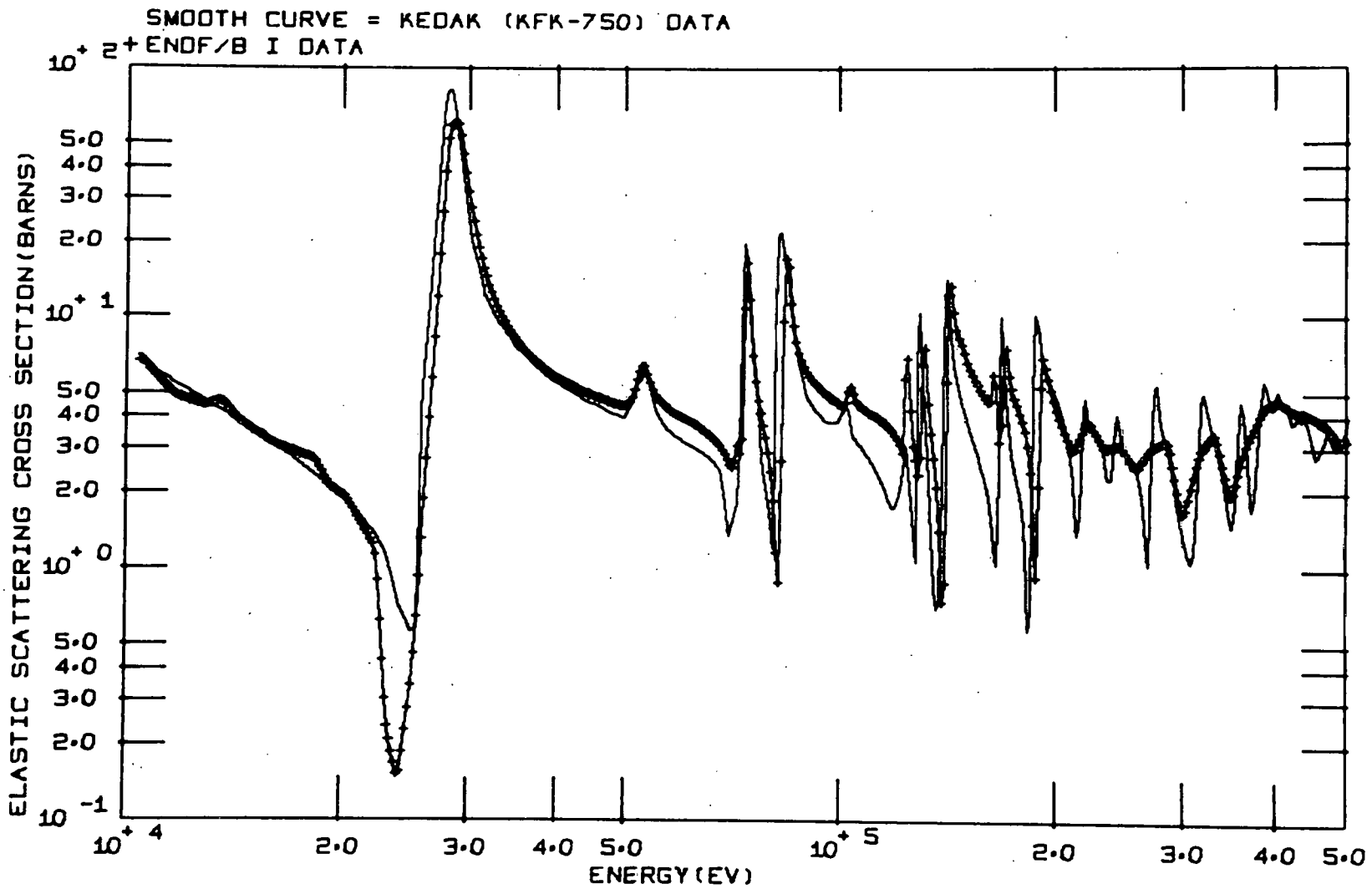
SMOOTH CURVE = KEDAK (KFK-750) DATA
ENDF/B I DATA
ELASTIC SCATTERING CROSS SECTION(BARNS)
ENERGY(EV)

Figure 1

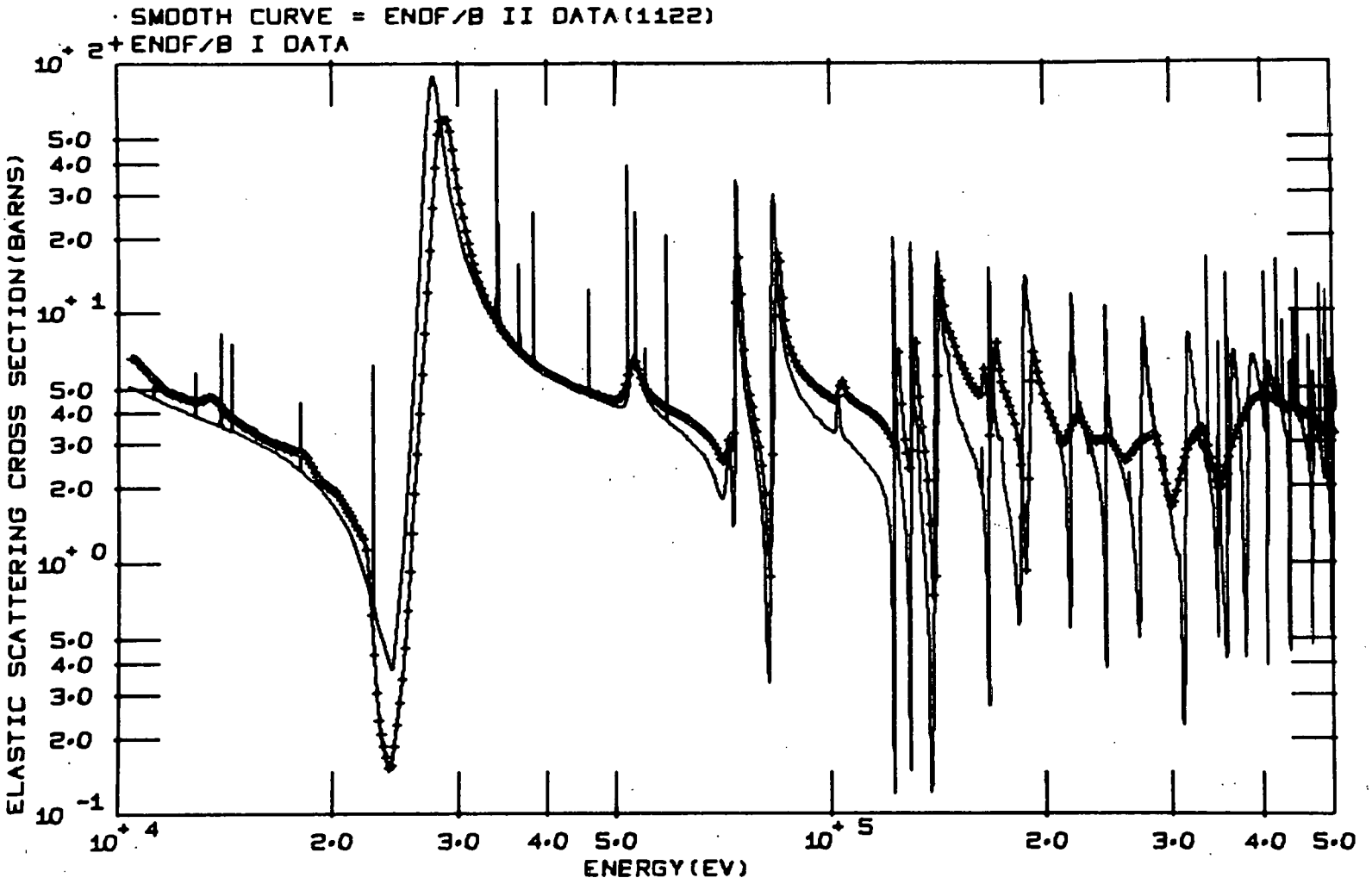
· SMOOTH CURVE = ENDF/B II DATA(1122)
+ ENDF/B I DATA
ELASTIC SCATTERING CROSS SECTION(BARNS)
ENERGY(EV)

Figure 2

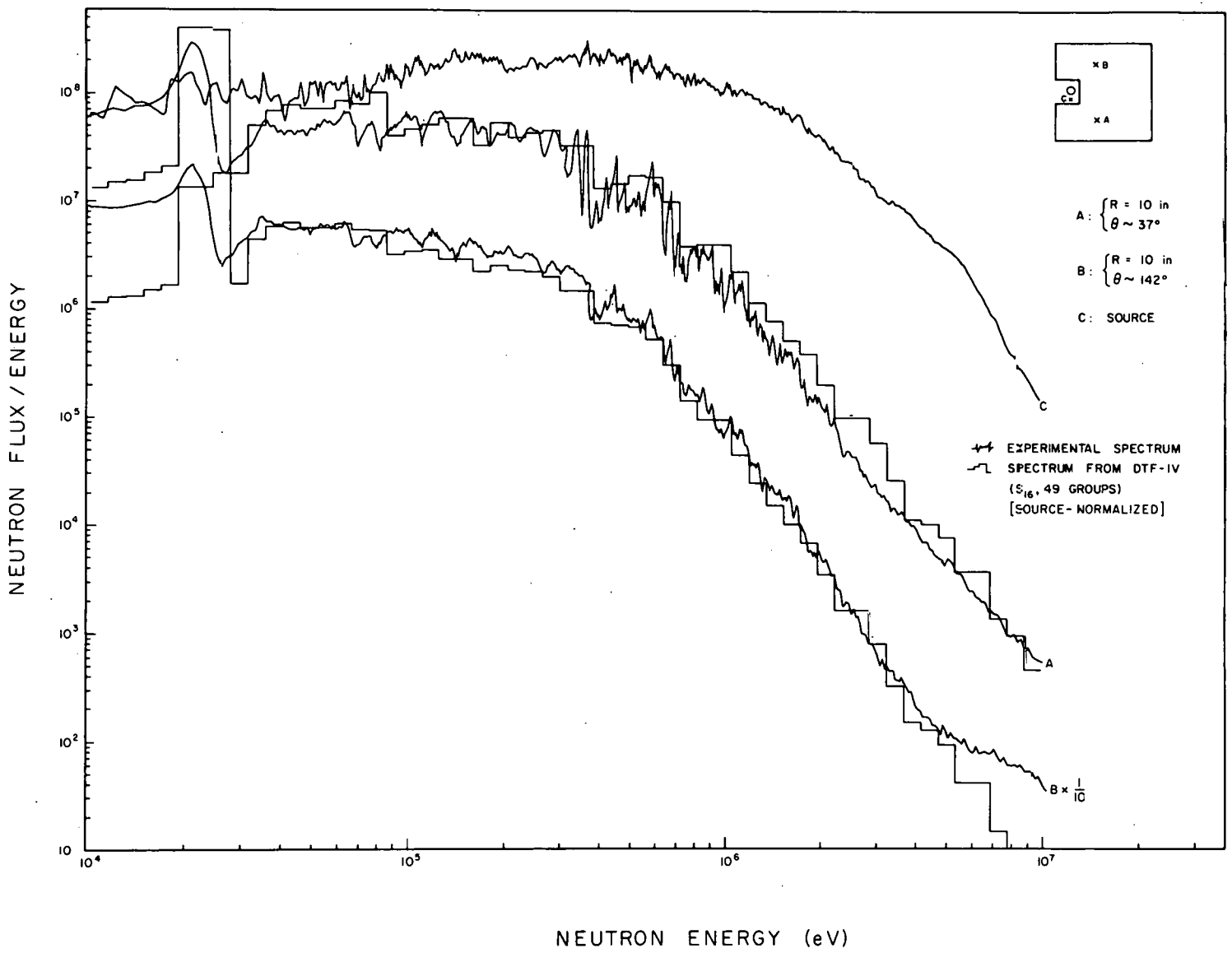
NEUTRON FLUX / ENERGY
NEUTRON ENERGY (eV)
× B
C
× A
A: R = 10 in, θ ~ 37°
B: R = 10 in, θ ~ 142°
C: SOURCE
EXPERIMENTAL SPECTRUM
SPECTRUM FROM DTF-IV
(S16, 49 GROUPS)
[SOURCE-NORMALIZED]
A
B × 1/10

Figure 3

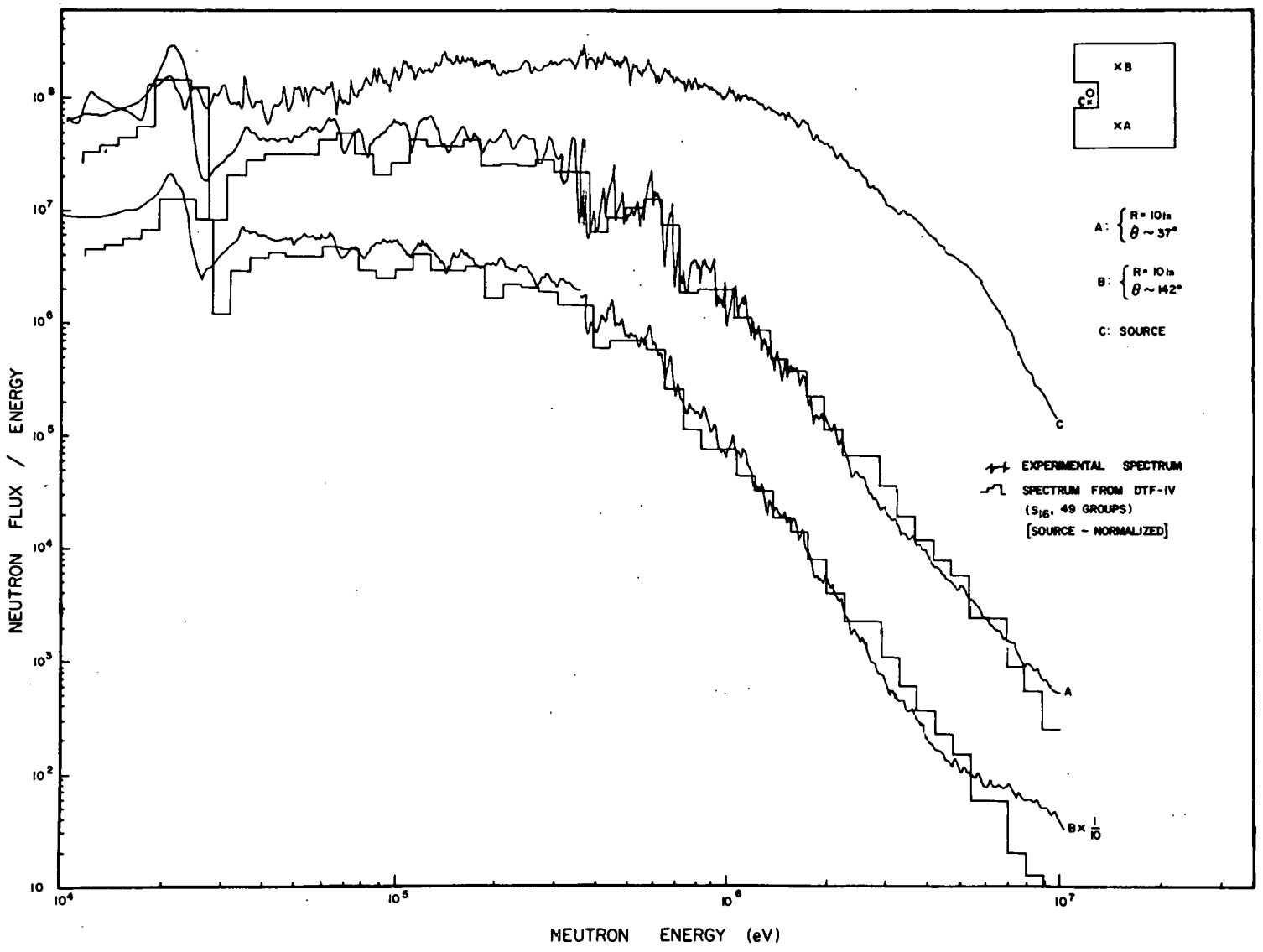
NEUTRON FLUX / ENERGY
MEUTRON ENERGY (eV)
×B
×A
A: R = 10in θ ~ 37°
B: R = 10in θ ~ 142°
C: SOURCE
EXPERIMENTAL SPECTRUM
SPECTRUM FROM DTF-IV
(S16, 49 GROUPS)
[SOURCE - NORMALIZED]
A
B × 1/10
C

Figure 4

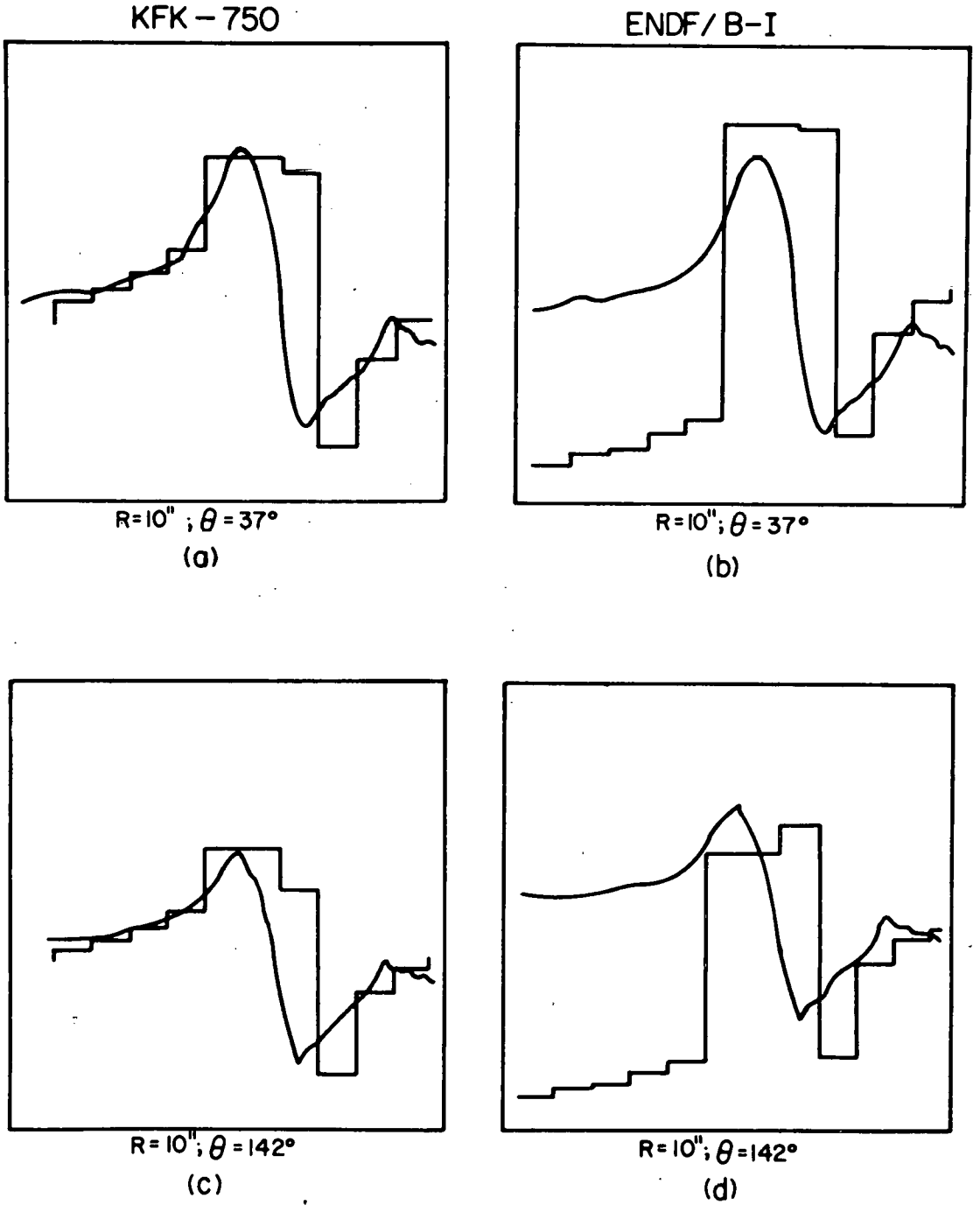

Figure 5

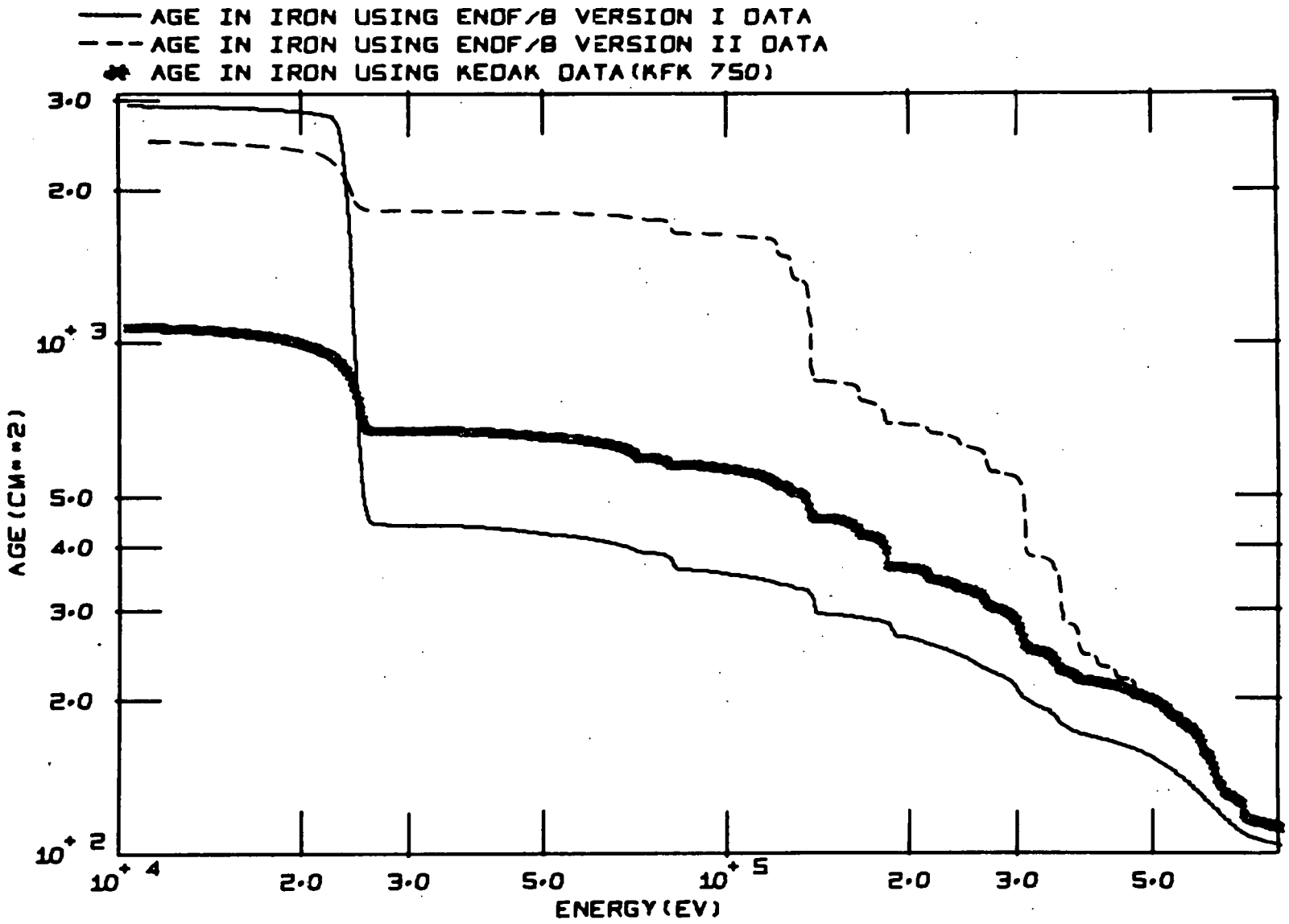
AGE IN IRON USING ENDF/B VERSION I DATA
AGE IN IRON USING ENDF/B VERSION II DATA
AGE IN IRON USING KEDAK DATA(KFK 750)
AGE(CM**2)
3.0
2.0
10+ 3
5.0
4.0
3.0
2.0
10+ 2
10+ 4
2.0
3.0
5.0
10+ 5
2.0
3.0
5.0
ENERGY(EV)

Figure 6

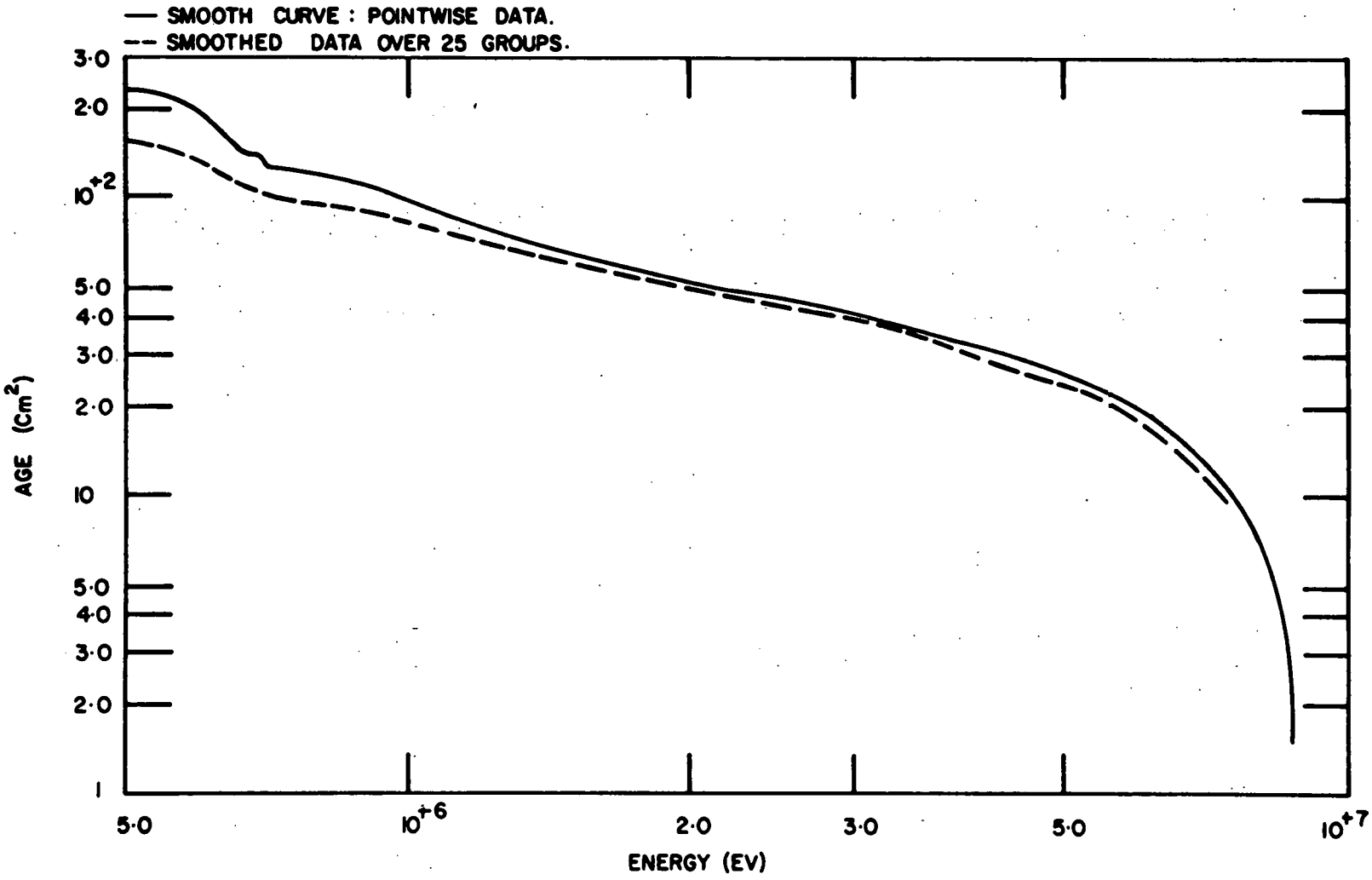
— SMOOTH CURVE : POINTWISE DATA.
-- SMOOTHED DATA OVER 25 GROUPS.
AGE (Cm²)
3·0
2·0
10+2
5·0
4·0
3·0
2·0
10
5·0
4·0
3·0
2·0
1
5·0
10+6
2·0
3·0
5·0
10+7
ENERGY (EV)

Figure 7

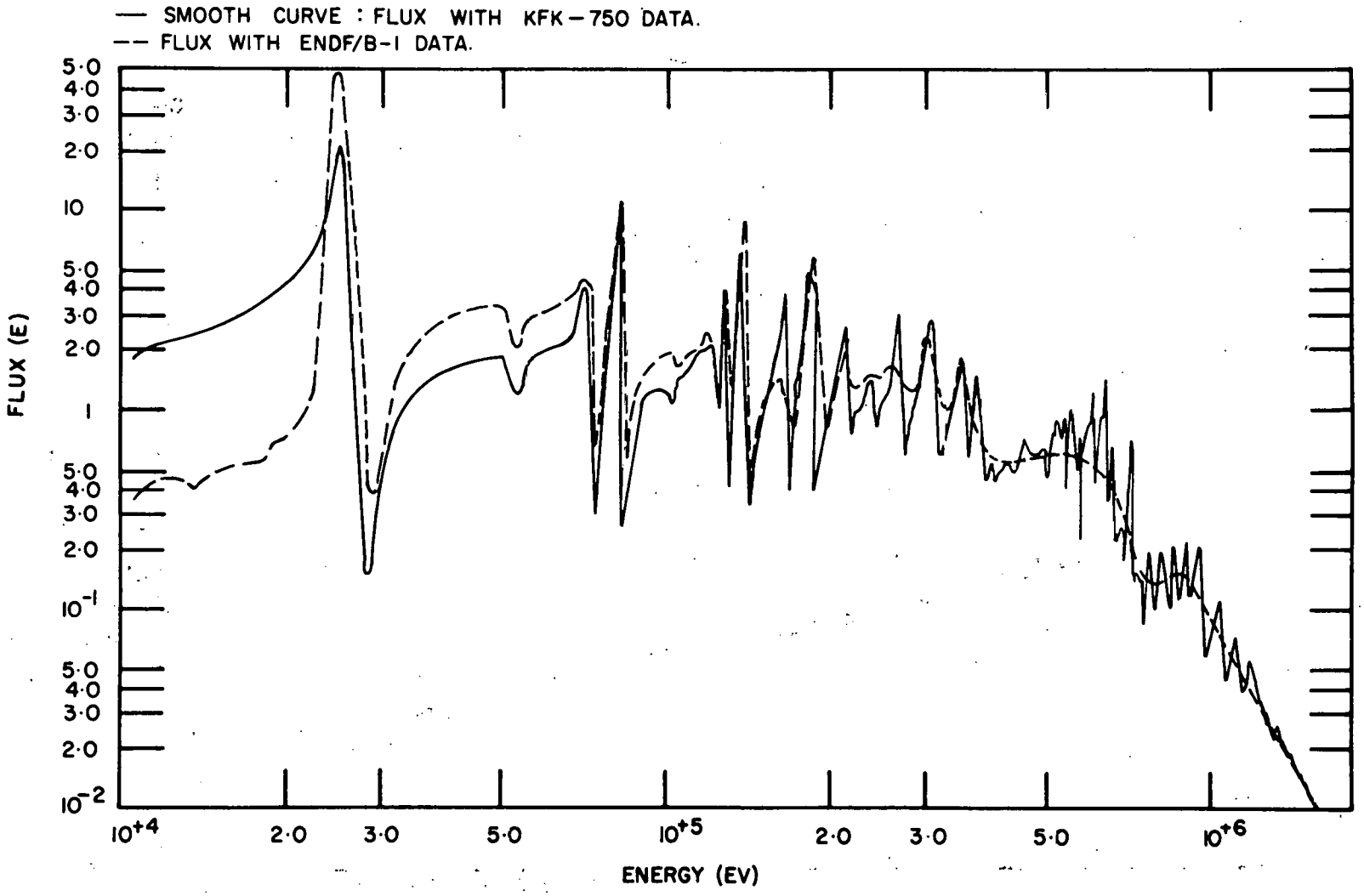
— SMOOTH CURVE : FLUX WITH KFK – 750 DATA.
-- FLUX WITH ENDF/B-I DATA.
FLUX (E)
5·0
4·0
3·0
2·0
10
5·0
4·0
3·0
2·0
1
5·0
4·0
3·0
2·0
10⁻¹
5·0
4·0
3·0
2·0
10⁻²
10⁺⁴
2·0
3·0
5·0
10⁺⁵
2·0
3·0
5·0
10⁺⁶
ENERGY (EV)

Figure 8

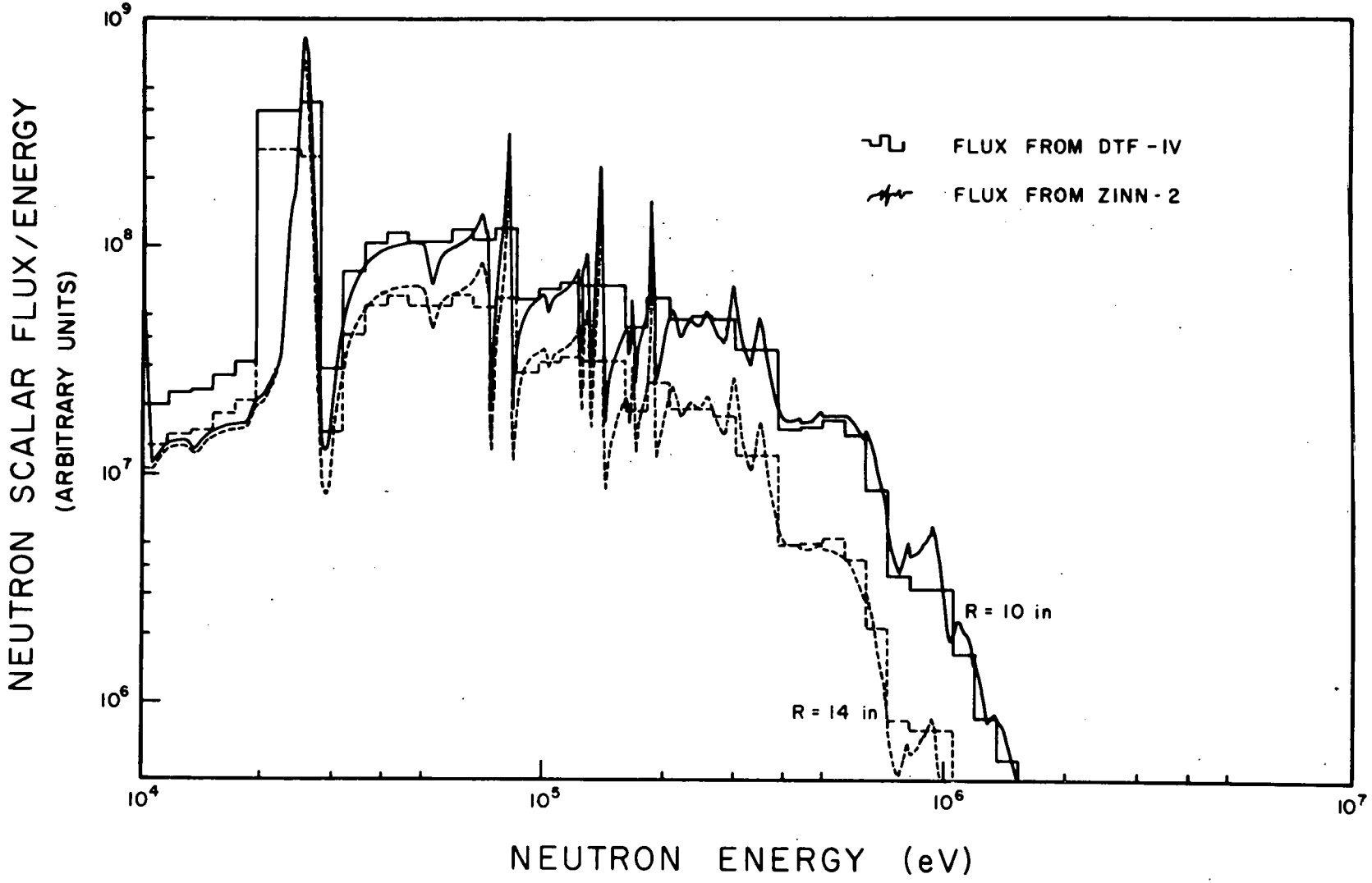
NEUTRON SCALAR FLUX/ENERGY
(ARBITRARY UNITS)
10^9
10^8
10^7
10^6
FLUX FROM DTF-IV
FLUX FROM ZINN-2
R = 10 in
R = 14 in
10^4
10^5
10^6
10^7
NEUTRON ENERGY (eV)

Figure 9

A STUDY OF NEUTRON TRANSPORT IN DEPLETED URANIUM WITH AN ASSESSMENT OF DATA FILES

N. N. Kaushal, B. K. Malaviya, M. Becker, E. T. Burns and E. R. Gaerttner

During the past year work was completed on the first phase of analysis and interpretation of fast neutron spectra in depleted uranium. Analysis was based on 49-group, P_o (with transport approximation) S_{16} calculations using one-dimensional transport theory code DTF-VI. In addition, extensive use was made of the continuous slowing down theory (CSDT) as extended at RPI to the case of fast neutron spectra, to facilitate sensitivity analysis and identification of diagreements between theory and experiment.

Several different data files were evaluated. These include ENDF/B (Versions I and II),[1] Karlsruhe data file and an old Argonne file. Definite conclusions have been reached on relative merits and adequacy of the data in these files. A detailed account of the work is being readied for journal publication. Following is a summary of a paper based on this material and presented at the Winter meeting of the American Nuclear Society held at Miami Beach, Florida, October 17-21, 1971.

Measurement of position and direction-dependent fast neutron spectra in large blocks of depleted uranium have been made at the RPI Linear Accelerator Laboratory, using the time-of-flight technique.[2] The primary motivation for these experiments is to provide integral checks on the cross-section data in various data files. Analysis is performed in two ways. Precise comparisons with experiment are made with multigroup transport calculations. Interpretation of theory-experiment discrepancies is aided by use of closed form continuous slowing down theory (CSDT).[3] The simple relationships between spectra, data, and the few basic CSDT parameters facilitate sensitivity analysis and identification of causes of theory-experiment discrepancies. In this paper we

present our evaluation of depleted uranium data in ENDF/B (Versions I and II), Karlsruhe,[4] and an old Argonne file.[5] The details of the experiment are given elsewhere.[2]

Several areas of strong sensitivities of measured neutron spectra to the basic cross-section data are seen. Below 40 keV, (i.e. in the unresolved resonance region) the resonance integral varies rapidly and the spectrum becomes increasingly sensitive to the effective absorption cross section, (i.e. accounting for self-shielding of unresolved resonances). We are therefore able to evaluate the accuracy of these data in various data files. Figure 1 shows a comparison of measured spectra with 49-group, S_{16}, DTF IV-calculations using the Argonne file. The shapes of the spectra below 40 keV are in fair agreement indicating that these data are essentially correct. The data in all data files agree at 40 keV. However, below 40 keV there is increasing divergence among various files. By 10 keV, the Argonne cross section is the lowest; the ENDF/B-I value is about 9% higher. The ENDF/B-II value is slightly above ENDF/B-I while Karlsruhe capture data is substantially higher. We find that multigroup transport calculations with ENDF/B and Karlsruhe files yield spectrum shapes with considerably steeper slopes than are measured experimentally, as expected from the CSDT resonance integral considerations.

Another area of sensitivity is the intermediate energy region (40-400 keV). In this region, the spectrum is very sensitive to the influence of the low-lying inelastic scattering levels, as measured by the collective slowing down parameter ξ in our models.[3] The Argonne data yield a value of ξ which is substantially lower than those for ENDF/B-I and Karlsruhe data. The ENDF/B-II data yield a value of ξ in between those for Argonne and ENDF/B-I. Figure 1 indicates that calculations with Argonne data predict well, the measured spectral shape at intermediate energies. Multigroup transport calculations with other files are in serious disagreement with experiment. For example, ENDF/B-I calculations overestimate spectra at 40 keV by about a factor of two.

At high energies (above 1 MeV), Argonne inelastic scattering

is also weaker than that of other files and gives better agreement with experiment. Calculations to date, however, have been based on the transport approximation. We prefer to withhold judgment on this energy range until explicit anisotropic scattering models[6] can be applied to the analysis of the measurements.

In summary, the single material spectrum measurement in depleted uranium is sensitive to important nuclear data; in particular inelastic scattering and low energy capture data. Results indicate that ENDF/B-I and ENDF/B-II low-energy capture and intermediate energy inelastic scattering data are too high.

REFERENCES:

1. (a) W. A. Wittkopf, D. H. Roy and A. Z. Livolsi, "U-238 Neutron Cross-Section Data for the ENDF/B," ENDF-103 (BAW-316), 1967.
   (b) T. A. Pitterle, "An Evaluation of ^{238}U Neutron Cross Sections for the ENDF/B File," CN26/83, Conf. on Nuclear Data for Reactors, Helsinki, Finland, June 1970.
2. Linear Accelerator Project Annual Technical Report, October 1, 1967 - September 30, 1968, RPI-328-142.
3. E. T. Burns and M. Becker, "Fast Neutron Spectrum Models and Their Application to Specific Materials," Trans. Am. Nucl. Soc., 13, 687 (1970).
4. I. Langner, J. J. Schmidt and D. Wall, "Tables of Evaluated Nuclear Cross Sections for Reactor Materials," KFK-750 (1968).
5. A. Travelli, Argonne National Laboratory, private communication, 1967.
6. A. Ginsberg and M. Becker, "Models for Anisotropic Weighting Spectra," Trans. Am. Nucl. Soc., 14, No. 1, in press (1971).

FIGURE CAPTION

Fig. 1 Comparison of 49-group, S_{16} Transport Theory Calculation Using Data from ANL Cross Section File[5] with Experimentally Measured Spectra in a Depleted Uranium Assembly. The experimental and calculated spectra are separately normalized for equal source intensity.

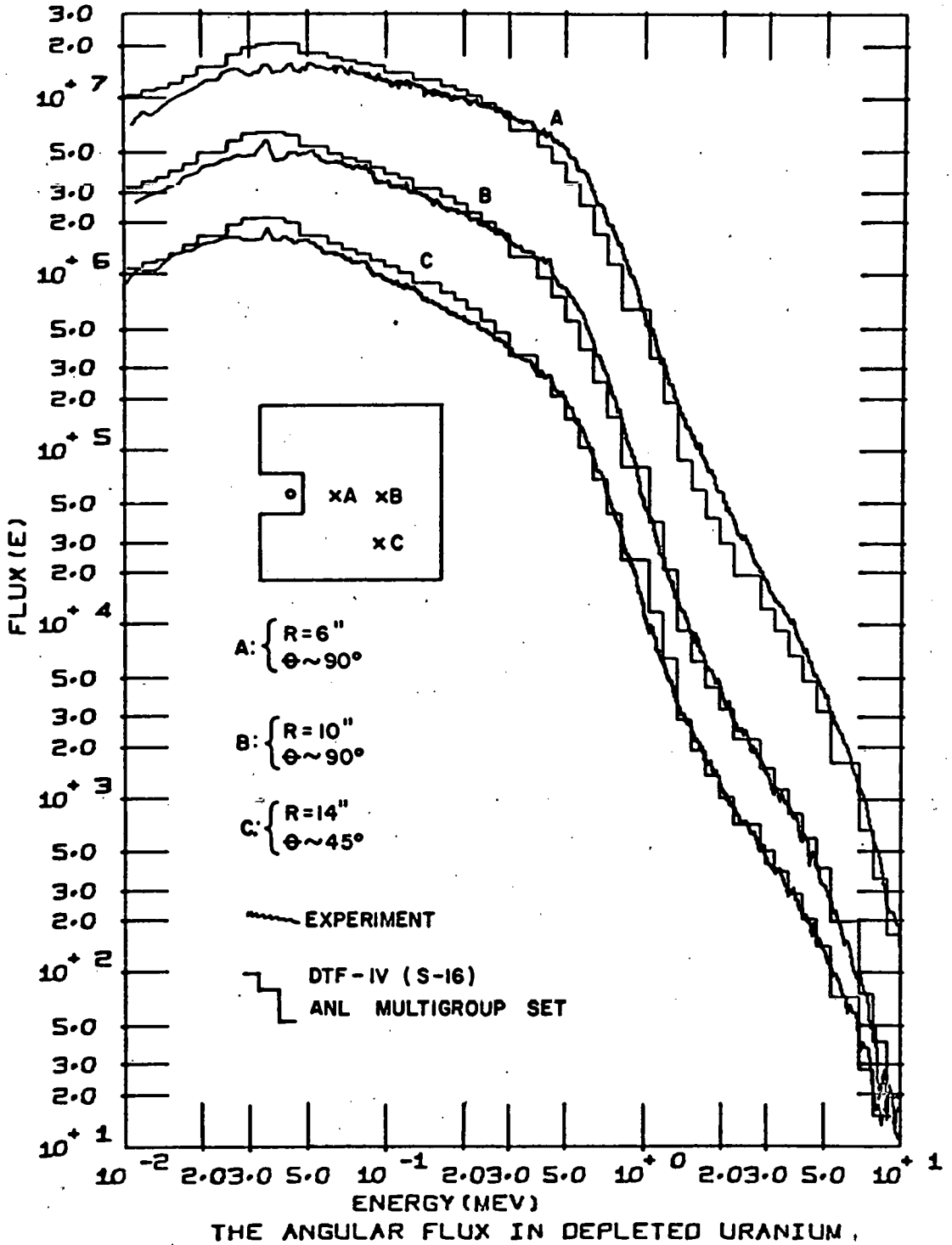

THE ANGULAR FLUX IN DEPLETED URANIUM.

Figure 1

FAST NEUTRON SPECTRA IN ALUMINUM

M. W. Golay, N. N. Kaushal and B. K. Malaviya

The fast neutron spectra measurements in an aluminum assembly were completed about a year ago. They have been described in detail elsewhere.[1] The past year has been spent refining the data and making preliminary evaluations.

One of the early aims of the experiments was achieved in providing reference data to guide the design of the new sodium experiment. It was found in the aluminum work that spatial effects were significant at low energies at some measurement points. As a consequence, the sodium assembly was chosen to be a six-foot cube, about eight times the volume of previous assemblies.

The experimental data in this case required some additional attention, due to certain problems with the proton-recoil detector during these measurements. All of the data have been reduced, including mean-emission-time corrections. A consistent data set has been culled from the total collection of measurements. These data consist of spectra from 10 MeV to 10 keV measured at each spatial point. The data from the proton-recoil detector (E>0.4 MeV) and the boron-vaselene detector (E<1 MeV) are consistently merged at an arbitrarily-chosen joining point within the energy range in which both detectors provide valid data. A program has been written to provide a "smooth" consistent merging of the data.* It has been found that disagreements in the overall spectra due to the arbitrariness of the merging point are less than 10%. The data are normalized using a solid state fission detector located outside the experimental assembly.[2]

The first iteration of calculations has been done comparing the measurements with spectra calculated using standard methods

*The procedure used involves taking ratios of point-wise data in the range of overlap. Average of these ratios was used as the normalization constant between the two spectra. After this normalization, the two spectra are joined at one point in the overlap region.

and available data sets. The calculations employed the code DTF-IV[3] in a 49-group spherical geometry model, using an asymmetric S_{18} quadrature set. The details of the calculation have been discussed earlier.[4] The group constant sets were calculated using the code MCC[5] for the ENDF/B-I data. The code SUPERTOG[6] employed the MCC-ENDF/B-I spectrum in generating additional group constant sets from both the ENDF/B-II and KEDAK data. The disagreements between the three cross-section sets are relatively small, and they predict very similar spectra. The principal differences are the following:

(a) for ENDF/B-II and KEDAK sets Σ_{inel} is approximately constant and greater than the value in the ENDF/B-I set for E>7.0 MeV,

(b) for the ENDF/B data the inelastic threshold comes at 0.9 MeV, while it is 1.07 MeV for the KEDAK set, and

(c) in the elastic scattering anti-resonance at 28 keV the KEDAK data specifies the same depth, but a much narrower width than the ENDF/B data.

Figure 1 shows the typical quality of the agreement which has been obtained consistently at different radii and streaming angles, in cases in which the neutrons have been scattered at least once. At high energies the slope of the measured spectra is less steep than that of the calculated spectra. At low energies (E<400 keV) the relative agreement is very good, except at energies below the 28 keV anti-resonance (see Fig. 2). In the range 800 keV>E>400 keV, there is substantial disagreement. Figure 3 shows spectra of neutrons streaming in the μ=1 direction. The neutrons observed in this case are mostly uncollided source neutrons, with a small component of scattered neutrons. With decreasing neutron energy the latter component becomes relatively larger. The good agreement observed at high energies is seen at other radii as well, and is thought to indicate that at high energies the values of Σ_{total} are reliable in all of the data sets cited.

The data have not yet been compared on an absolute normalized basis, and the tentative conclusions arrived at up to this point may be revised upon further analysis. However, a few preliminary results seem to be apparent. Because the assembly is relatively "leaky" (an "average" neutron collides on the order of four to eight times before escaping), the spectrum observed at a given measurement point depends mainly on the local energy dependence of the cross sections, and much less strongly upon the values of cross sections at higher energies. This observation is borne out in a variety of cross-section sensitivity calculations. Thus, observation of good shape agreement of spectra at a variety of measurement points over a significantly large energy interval would justify some faith in the validity of the data in that interval.

As has been cited from Fig. 2, the low energy agreement ($E<400$ keV) is good, except below the resonance minimum. The KEDAK calculation provides better agreement in the latter range than the ENDF/B prediction. It is also found that increasing the size of the calculated assembly improves the agreement somewhat; however, this effect is insufficient to explain the disagreement.

At high energies the calculated spectrum (see Fig. 1) is seen to be too soft. It is found that the ENDF/B-II and KEDAK calculations both predict even softer spectra above 7.0 MeV than the ENDF/B-I result. The sensitivity of the disagreement between the ENDF/B-I data and the experiment was tested by varying point-wise inelastic scattering cross-section data which was used in SUPERTOG to generate trial group constant sets. It was found that a reduction of the total inelastic scattering cross section of 40% over the entire energy range was required to provide agreement (see Fig. 4). At the time of the calculations, the recently-acquired anisotropic scattering capability was unavailable, so the influence of elastic slowing down on the high energy spectra was not investigated. It is reasonable to expect this effect to be

important, since the elastic scattering cross section is from ten to two times as large as the inelastic cross section depending upon the energy. High energy elastic scattering in aluminum is highly anisotropic. The calculation employed the transport approximation which should not be adequate for this energy range.

However, the initial work indicates that some reduction in the inelastic cross section would be in order for each cross-section data set. The early results of the two-region spectra experiments support this conclusion independently.[7]

The large disagreement in the range 800 keV>E>400 keV is thought to be due to use of a too soft source in the calculations. This source arises from approximations made in the source material description. It is currently being investigated.

In Fig. 2 is seen the effect of varying the calculational group structure. A finer group set was used in the interval 600 keV than was used in the standard 49-group set. This was done to investigate the poor theoretical prediction of the spectra in this energy range. It is found that the major disagreements are eliminated by use of group widths which are somewhat narrower than the measured spectral features.

REFERENCES:

1. Linear Accelerator Project Annual Technical Report, October 1, 1968 - September 30, 1969, 66-70, RPI-328-171.
2. Linear Accelerator Project Annual Technical Report, October 1, 1969 - September 30, 1970, 214, RPI-328-200.
3. DTF-IV, LA-3373, Los Alamos Scientific Laboratory (1965).
4. Linear Accelerator Project Annual Technical Report, October 1, 1969 - September 30, 1970, 110-124, RPI-328-200.
5. MCC, ANL-7318, Argonne National Laboratory (1967).
6. SUPERTOG, ORNL-TM-2679, Oak Ridge National Laboratory (1969).
7. D. C. Gibbs, private communication.

FIGURE CAPTIONS

Fig. 1 Measured and Calculated ENDF/B-I Spectra for 14-inch Radius, μ=0.89.

Fig. 2 Low Energy Shape-fit Agreement between Measured and Calculated ENDF/B-I Spectra at 14-inch Radius, μ=0.89. Dotted line histogram calculated using standard 49-group set. Solid line histogram calculated using modified fine-width group set.

Fig. 3 Measured and Calculated ENDF/B-I Spectra at 6-inch Radius, μ=1.0.

Fig. 4 Measured and Calculated Spectra at 10-inch Radius, μ=0.8. Dotted line histogram calculated using ENDF/B-I data. Solid line histogram calculated using ENDF/B-I data, with σ_{inel} reduced by 40% over entire energy range.

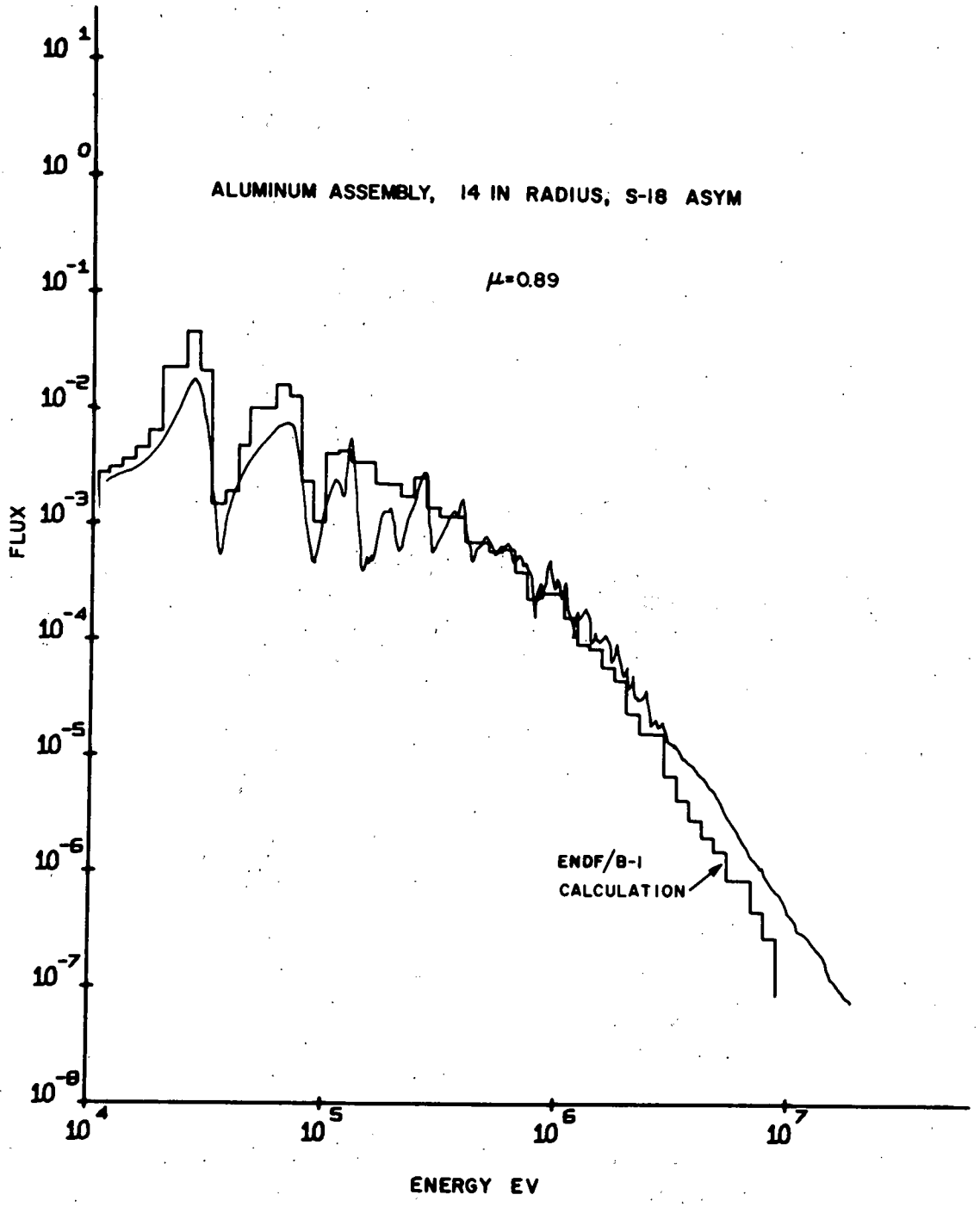
ALUMINUM ASSEMBLY, 14 IN RADIUS, S-18 ASYM
μ=0.89
FLUX
ENERGY EV
ENDF/B-I
CALCULATION
10 1
10 0
10 -1
10 -2
10 -3
10 -4
10 -5
10 -6
10 -7
10 -8
10 4
10 5
10 6
10 7

Figure 1

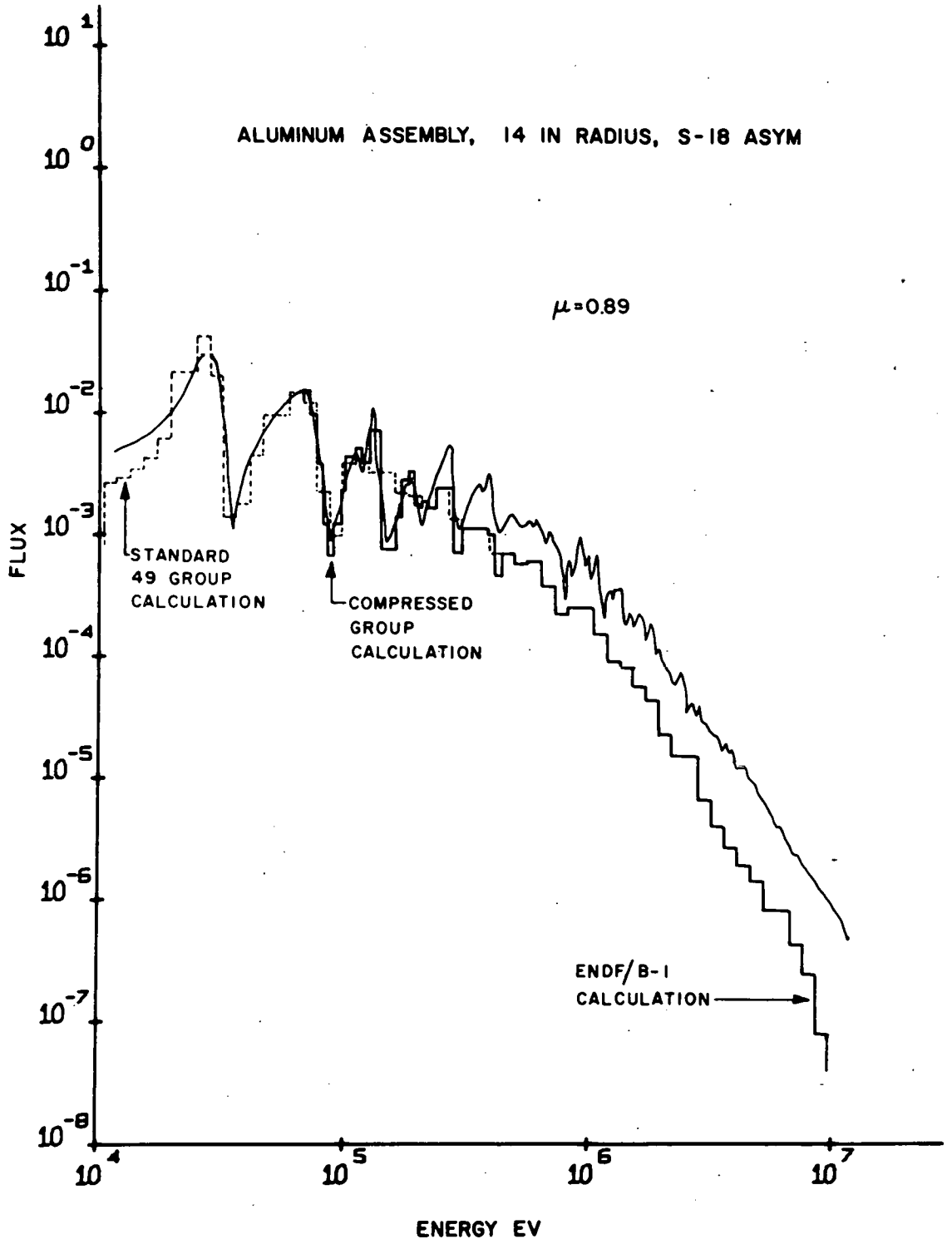
ALUMINUM ASSEMBLY, 14 IN RADIUS, S-18 ASYM
μ=0.89
FLUX
ENERGY EV
STANDARD 49 GROUP CALCULATION
COMPRESSED GROUP CALCULATION
ENDF/B-I CALCULATION
10^1
10^0
10^-1
10^-2
10^-3
10^-4
10^-5
10^-6
10^-7
10^-8
10^4
10^5
10^6
10^7

Figure 2

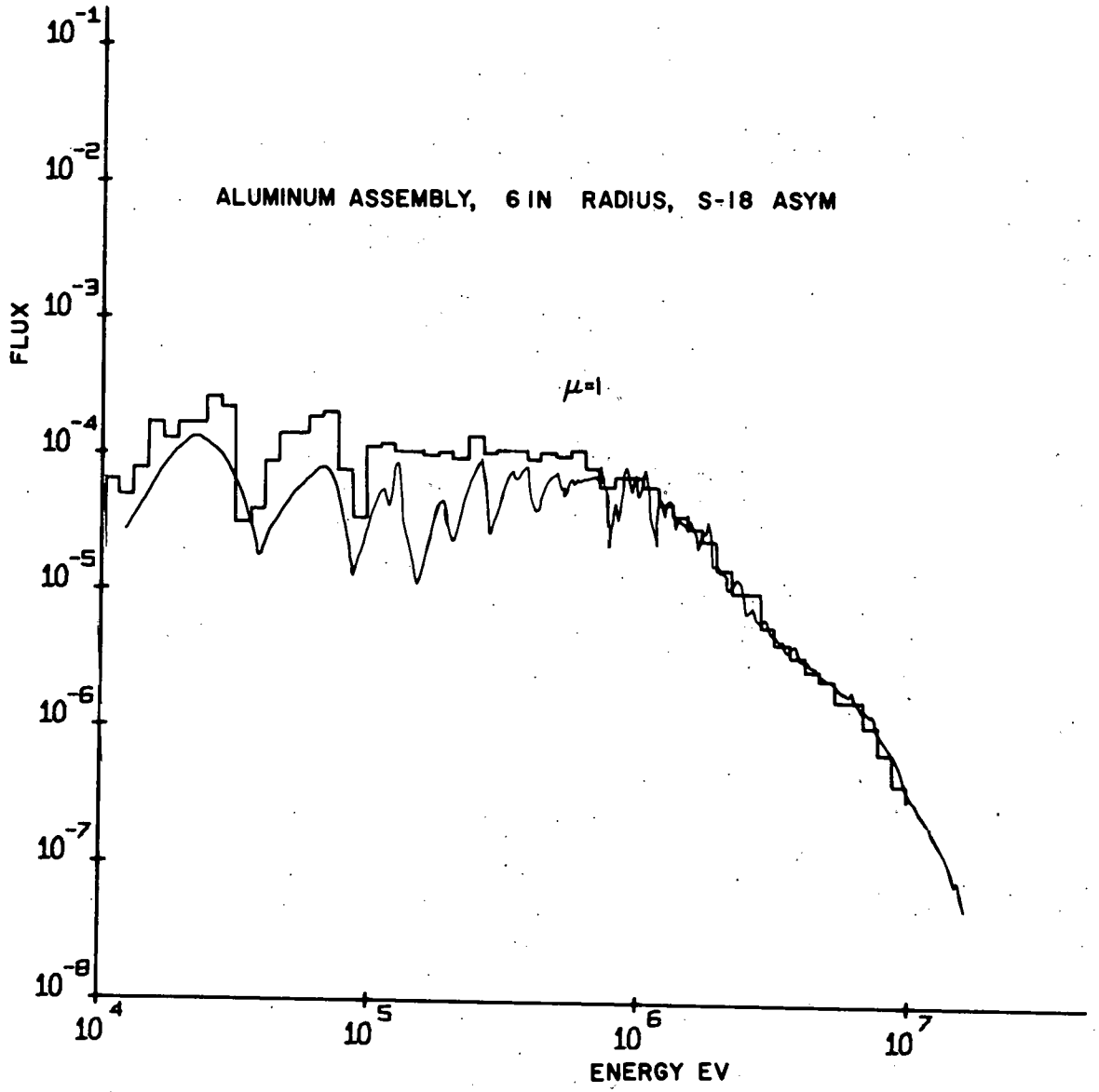
ALUMINUM ASSEMBLY, 6 IN RADIUS, S-18 ASYM
FLUX
10^{-1}
10^{-2}
10^{-3}
10^{-4}
10^{-5}
10^{-6}
10^{-7}
10^{-8}
μ=1
10^{4}
10^{5}
10^{6}
10^{7}
ENERGY EV

Figure 3

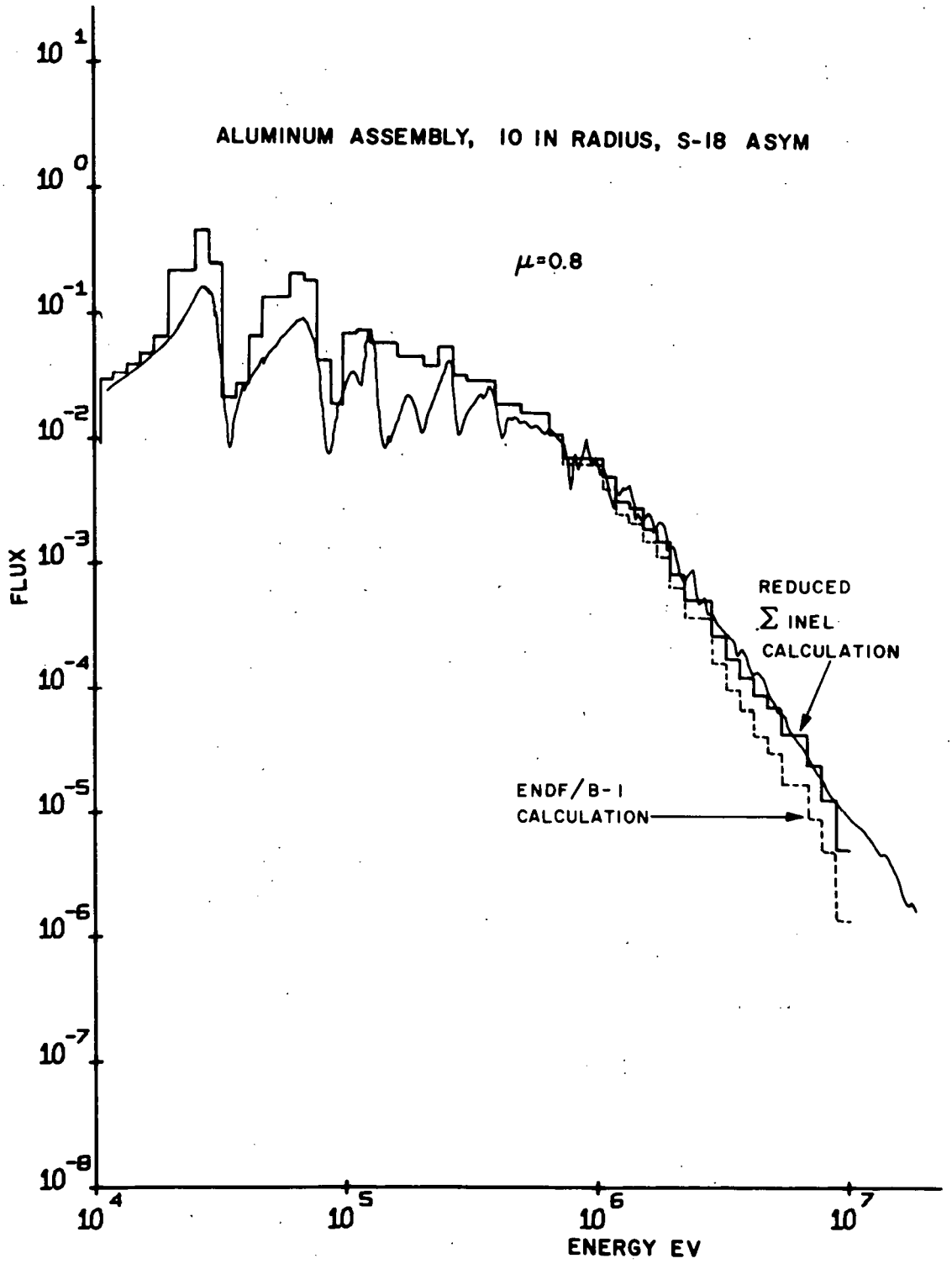
ALUMINUM ASSEMBLY, 10 IN RADIUS, S-18 ASYM
μ=0.8
REDUCED
Σ INEL
CALCULATION
ENDF/B-I
CALCULATION
FLUX
ENERGY EV
10^1
10^0
10^-1
10^-2
10^-3
10^-4
10^-5
10^-6
10^-7
10^-8
10^4
10^5
10^6
10^7

Figure 4

STUDIES OF FAST NEUTRON SPECTRA IN TWO-REGION SYSTEMS

D. C. Gibbs,* B. K. Malaviya, N. N. Kaushal
and E. R. Gaerttner

During the past year, preliminary feasibility studies were made to investigate fast neutron angular flux spectra across a material interface. The motivation for these studies and their significance from the point of view of fast-reactor applications and checks of cross-section data and analytical methods have been discussed in earlier progress reports.[1,2] The preliminary measurements were made on a two-region aluminum-iron assembly with a spherical source imbedded in the aluminum region. Two different geometrical arrangements were investigated; these are shown in Fig. 1. Fast neutron angular flux spectra for positions at different distances from the interface were measured by the time-of-flight technique. Some experimental results have been reported earlier.[3,4] The analysis of these measurements, using one- and two-dimensional transport theory codes is continuing. Here we summarize some features of the experimental results and present certain additional results of data reduction and analysis.

Figures 2, 3 and 4 show typical results of the measurements of fast neutron spectra in the vicinity of the interface for Assembly I and II. The rapid variation of angular flux with angle is clearly brought out by comparing Figs. 2 and 3 for Assembly II. Figure 3 represents a series of measurements which are the reflected image of those shown in Fig. 2. For an isotropic source the scalar flux for each of these sets of measurements will be identical, but it is immediately apparent that such is not the case for angular flux.

Figure 2 shows four spectra taken near the interface in Assembly II as indicated by the inset. The top curve, corresponding to position "A" in the inset is one inch from the interface in the aluminum region. The second curve is a measurement

---

*Based in part on the Ph.D. Thesis of C. D. Gibbs.

at the interface, and the third and fourth curves are 1 and 2 inches from the interface in the iron region. The bottom curve is a spectrum taken from a pure iron (one-region) assembly, in an earlier experiment,[5] at the same position relative to the source as point B. Curves A and B are essentially identical except for a very small difference in amplitude of about 5% from about 700 KeV to the highest energy plotted (20 MeV). As the interface is crossed, most of the essential features of the aluminum spectrum are preserved. The strong 28-KeV iron resonance is evident just 1-in. from the interface, but the remainder of the spectrum looks more like one typical of aluminum than the iron spectrum shown at the bottom. It is noted that the high-energy flux is considerably greater in the two region results than in the pure iron assembly . This is due to the greater inelastic scattering in iron which degrades the high energy component of the spectrum at a greater rate than in aluminum. The principal qualitative feature to be observed from this result is that a spectrum which is characteristic of aluminum is being supported by the iron region. Thus, coarse group constants weighted with an infinite-medium iron spectrum may be expected to yield erroneous results.

Figure 3 shows a series of measurements with the same geometric orientation relative to the source as the preceding figure. In this case, however, the angular flux being measured is of neutrons which are propagating from the iron into the aluminum region. These spectra are considerably different from the spectra presented in the Fig. 2 and are more typical of an iron spectrum. The top curve, one inch from the interface in the aluminum region, is more aluminum-like than iron-like, but it retains many of the features of an iron spectrum.

Figure 4 illustrates a typical result from assembly I. The positions being measured have the same geometric position with respect to the source and the interface as the two previous figures (2 and 3). In this case, the angular neutron flux propagating parallel to the interface is being measured. As opposed

to the angular fluxes shown in Figs. 2 and 3, it is seen in this case that the spectrum changes rapidly with position across the interface. Curves A and B were both obtained at positions just one inch from the interface.

The most significant qualitative result exhibited by Figs. 2,3 and 4 is that near the interface the angular flux is changing rapidly with both space and angle. This fact supports the greater sensitivity of this experiment to anisotropic scattering.

Two conclusions may be drawn from a comparison of these two sets of curves. First, in any group-collapsing scheme, it would not be correct to apply an infinite-medium weighting spectrum modified by a near-zero buckling (as is done in the MC^2 code) to the materials near the interface. Second, because of the rapid variation of angular flux with angle, any group-collapsing scheme should have a provision for including higher orders of the flux than simple φ_o, the scalar flux. The corollary to this statement is that a calculation using only Po cross sections may not be adequate near the interface for other than a fine energy spacing, even though anisotropic scattering may not be present, since Po cross sections are generated from scalar flux weighting spectra alone.

Some of these and other aspects of the data from two-region system measurements were discussed in detail in the last Progress Report.[3] Consider an additional aspect of the analysis of spatial dependence of the measured angular flux spectra, which the two-region results point up.

One of the principal uncertainties of spectrum measurements is the knowledge of detector efficiency versus energy. Any mechanism which could reduce or eliminate this uncertainty in spectrum experiments has the potential of considerably improving the accuracy of any critical evaluation of differential cross-section data. Such an opportunity is provided by considering the spatial variation of the angular flux across the media interface at a fixed energy and comparing the experimental result with a transport calculation. Since only a fixed energy is selected, the

data is independent of the detector efficiency and relies only on the accuracy of normalization between runs. Comparison of data obtained from identical points of measurement separated by several days running time indicates a normalization uncertainty of less than 4%.

This type of data is presented in Table 1. In this table, DTF 4 slab geometry P3 scattering, S16 quadrature, 99 region, 49-group data is compared against experimental measurements made at points along the line from the source normal to the interface in which the angular flux parallel to the interface plane was measured. A word of caution with respect to these data is in order. Since this was a preliminary experiment on a new concept, certain compromises were made in the experiment which would not have been made in typical fast spectrum measurements. In particular, the runs were foreshortened in order to gain the most data in the least time, and there were few repetitions of the individual measurements. Also, the electronics associated with the 28-meter detector suffered an unusually large timing uncertainty which has been removed in subsequent fast spectra measurements. Thus, these data, which are particularly sensitive to background and adequate timing resolution, may be subject to question. However, they are presented because they illustrate a potential for future two-region experiments which may be more specific in indicating where cross section errors might exist.

One might question the validity of replacing the actual point source by a plane source in this analysis. From Fermi age theory, the slowing down density from a plane source is given as

$$q(x,\tau) = \frac{S}{(4\pi\tau)^{\frac{1}{2}}} e^{-x^2/4\tau} \quad , \tag{1}$$

and from a point source

$$q(\gamma,\tau) = \frac{S}{(4\pi\tau)^{3/2}} e^{-r^2/4\tau} \quad . \tag{2}$$

These equations illustrate that for a specified age, the spatial relaxation of the slowing down density is independent of whether

the source is represented by a point or a plane. The slowing down density is related to the flux per unit energy by

$$\varphi(E) = \frac{q(\tau)}{E\xi\Sigma_s} \quad . \tag{3}$$

Table 1 was obtained by collapsing the experimental result into the same energy structure as the DTF 4 calculation. The quantity of interest is the ratio of the calculation to the experiment and how this quantity propagates as one crosses the media interface. If the input cross sections are satisfactory and there are no errors in the experiment, the ratio should remain constant in space. To illustrate the use of the Table, consider group 42. It is known that the actual cross section in the iron window is higher than the value used in the calculation which was obtained from ENDF/B-I file data. The Table indicates that the ratio of calculation to experiment is increasing as the interface is crossed. Thus, the experiment is relaxing faster than the calculation, implying that the cross section used in the iron region analysis is too low. Consider energy group 34 which includes an iron resonance at 84 KeV and a window at 82 KeV. The iron group constant is apparently too low since the calculated result increases while the experimental result decreases across the interface. This erroneous group constant does not specifically point to an error in the cross sections since it could be caused by an interface effect. The flux at the resonant energy at the interface will be higher than an infinite-medium iron spectrum since it is being supplied neutrons from the aluminum region. The supply is decreased somewhat by the fact that aluminum exhibits a resonance at 88 KeV and a minimum at about 66 KeV, causing the flux incident on the iron to be greatest at the lowest energy in the group. It is considered likely from this fact that the pointwise iron cross section is too low at the lower energy range of the group. A more conclusive result could be obtained by dividing the group into smaller groups which do not include both a resonance and a window as occurs in this case. In any case, the fact that a problem may exist in the pointwise data is suggested and the path for

further analysis indicated.

For this experiment, difficulties encountered in the timing resolution of the 28-m. detector discouraged further study along these lines. The sharp drop in the ratio values in group 41 was most probably caused by smearing of the data, which caused too much flux to be measured in the valleys of the spectra which occur at the resonant energies. It is nonetheless considered that an improved experimental arrangement would permit this type of analysis to be very fruitful in future two region-experiments.

For two-dimensional calculations using the computer code DOT,[6] it was necessary to collapse 49-group anisotropic matrices to 4 energy groups in the interest of reducing computer run time. In developing suitable recipes to perform this function, several interesting results have been obtained.

Collapse of the P_o matrix was achieved by using MC^2 generated finite-medium flux spectra. To collapse the anisotropic cross-section matrices, the respective flux moments must be provided for spectral weighting, for example

$$\sigma_{s\ell}^{I\to J} = \frac{\sum_{i\in I}\sum_{i\in J}\sigma_s^{i\to j}\varphi_{s\ell}^{i}}{\sum_{I}\varphi_{s\ell}^{i}} \tag{4}$$

Some scheme must therefore be devised to obtain the flux moments.

One starts with the P3 equations in multigroup form:

$$\frac{\partial\varphi_1^g}{\partial x} + \Sigma_T^g(o)\varphi_o^g = \sum_{g'}\Sigma_{so}^{g'\to g}(o)\varphi_o^{g'} \tag{5a}$$

$$\frac{2}{3}\frac{\partial\varphi_2^g}{\partial x} + \frac{1}{3}\frac{\partial\varphi_o^g}{\partial x} + \Sigma_T^g(1)\varphi_1^g = \sum_{g'}\Sigma_{s1}^{g'\to g}(1)\varphi_1^{g'} \tag{5b}$$

$$\frac{3}{6}\frac{\partial\varphi_3^g}{\partial x} + \frac{2}{5}\frac{\partial\varphi_1^g}{\partial x} + \Sigma_T^g(2)\varphi_2^g = \sum_{g'}\Sigma_{s2}^{g'\to g}(2)\varphi_2^{g'} \tag{5c}$$

$$\frac{3}{7}\frac{\partial\varphi_2^g}{\partial x} + \Sigma_T^g(3)\varphi_3^g = \sum_{g'}\Sigma_{s3}^{g'\to g}(3)\varphi_3^{g'} \tag{5d}$$

In these equations, energy dependence has been included through the group index g and the weighting of the cross sections with their appropriate flux moment is indicated by the numbers in parentheses. The approach usually taken is to first make the approximation in the last of the P3 equations that

$$\sum_{g'} \Sigma_{s3}^{g' \to g}(3)\varphi_3^{g'} \approx \Sigma_{s3}^{g}(3)\varphi_3^{g} \tag{6}$$

Having done this, one may define

$$\Sigma_T^g(3) - \Sigma_{s3}^g(3) \equiv \Sigma_{Tr}^g(3) \tag{7}$$

causing the last of the P3 equations to take the form,

$$\frac{3}{7}\frac{\partial \varphi_2^g}{\partial x} + \Sigma_{Tr}^g(3)\varphi_3^g = 0 \tag{8}$$

Over a sufficiently small spatial interval, one may always express any of the flux moments in the form

$$\varphi_\ell^g = \text{const.} \quad e^{iBx} \tag{9}$$

Doing this, the last of the P3 equations may be integrated giving

$$\varphi_3^g = - iB \frac{3}{7} \frac{\varphi_2^g}{\Sigma_{Tr}^g(3)} \tag{10}$$

If this value for φ_3 is then inserted into the third of the P3 equations, and one makes the further assumption that

$$\sum_{g',s2} \Sigma^{g' \to g}(2)\varphi_2^{g'} = \Sigma_{s2}^{g}(2)\varphi_2^{g} \tag{11}$$

whereby

$$\Sigma_{Tr}^g(2) \equiv \Sigma_T^g(2) - \Sigma_{s2}^g(2) \tag{12}$$

is obtained, a relation between φ_1, and φ_2 can be derived as

$$\varphi_2^g = \frac{-\,iB\,\frac{2}{5}\,\varphi_1^g}{\Sigma_{Tr}^g(2) + \frac{\frac{3}{7}\cdot\frac{3}{5}\,B^2}{\Sigma_{Tr}^g(3)}} \tag{13}$$

At this point, one may assert that large systems involve small values of buckling B^2 and that the second term in the denominator may be neglected. With this assumption, one may arrive at a general recursion relation between the flux moments as

$$\varphi_\ell^g \;\alpha\; \frac{\varphi_{\ell-1}^g}{\Sigma_{Tr}^g(\ell)} \tag{14}$$

The constant of proportionality is not needed here since the flux moments are to be used for weighting spectra only, so their amplitudes will be divided out.

On a pointwise basis, the transport cross sections are given simply as

$$\Sigma_{Tr}^g(\ell) \equiv \Sigma_T^g - \Sigma_{s\ell}^g \tag{15}$$

which is what is done in the RPI version of SUPERTOG.

There are two refinements which may be readily made to this recursion scheme. One may avoid the approximation implicit in the assumption

$$\sum_{g'} \Sigma_{s\ell}^{g'\to g}(\ell)\varphi_\ell^{g'} \;\approx\; \Sigma_{s\ell}^g(\ell)\varphi_\ell^g \tag{16}$$

by an iterative method. Specifically, assume we are interested in obtaining φ_1 from φ_o. Starting as before with

$$\varphi_1^g = \frac{\varphi_o^g}{\Sigma_T^g(1) - \Sigma_{s1}^g(1)} \tag{17}$$

one defines

$$\Sigma_{s1}^{g*}(1) = \frac{\sum_{g'} \Sigma_{s1}^{g' \to g} \varphi_1^{g'}}{\varphi_1^g} \tag{18}$$

This value for Σ_{s1} is inserted back into Eq. 17 to compute a new φ_1^g. The procedure is repeated until the iterated values of φ_1^g converge. The converged φ_1^g are then used to compute the φ_2^g and the procedure is continued.

Another refinement is to take a non-zero value for the buckling in Eq. 13. The recursion relationship from the P3 equations would then take the form:

$$\varphi_1^g = \frac{-iB \frac{1}{3} \varphi_o^g}{\Sigma_{Tr}^g(1) + \dfrac{\frac{2}{3} \cdot \frac{2}{5} B^2}{\Sigma_{Tr}^g(2) + \dfrac{\frac{3}{5} \cdot \frac{3}{7} B^2}{\Sigma_{Tr}^g(3)}}} \tag{19}$$

$$\varphi_2^g = \frac{-iB \frac{2}{5} \varphi_1^g}{\Sigma_{Tr}^g(2) + \dfrac{\frac{3}{5} \cdot \frac{3}{7} B^2}{\Sigma_{Tr}^g(3)}} \tag{20}$$

$$\varphi_1^g = \frac{-iB \frac{3}{7} \varphi_2^g}{\Sigma_{Tr}^g(3)} \tag{21}$$

The use of these equations permits testing the sensitivity of the group constants to buckling.

A locally prepared computer program COLAPS has been written for operation on the CDC-6600 computing system to perform all the above functions. Tables 2 and 3 show the effects of using straight recursion versus iterated recursion on the four group aluminum and iron cross sections, collapsed from ENDF/B-I data. The tables show the cross sections weighted with their respective flux moments. It is noted that the introduction of an iteration scheme to obtain the flux moments has little effect on the group constants. Since

the scalar flux guess is the same in both schemes, PO cross sections are not shown in these tables. Each of these tables may be compared with Table 4 which shows the effect of introducing a non-zero buckling into the recursion formulae. Since a buckling of 0.003 was used as input to the MC^2 code to obtain the scalar flux guess, the same value for buckling was used to prepare Table 4 for both aluminum and iron. Comparison of Table 4 with Tables 2 and 3 shows that the inclusion of a non-zero buckling introduces little change to the group constants.

The analysis of the two-region experiments is continuing and is nearing completion. Further results will be reported in the next quarter.

REFERENCES:

1. Linear Accelerator Project Annual Technical Report, October 1, 1968 - September 30, 1969, RPI-328-171.
2. Linear Accelerator Project Annual Technical Report, October 1, 1969 - September 30, 1970, RPI-328-200.
3. Linear Accelerator Project Progress Report, April - June 1971, 56, RPI-328-226.
4. D. C. Gibbs, B. K. Malaviya, N. N. Kaushal and E. R. Gaerttner, "Studies of Fast-Neutron Spectra Across a Material Interface," Trans. Am. Nucl. Soc., 14, 383 (1970).
5. B. K. Malaviya, N. N. Kaushal, M. Becker, E. Burns and E. R. Gaerttner, "Experimental and Analytical Studies of Fast Neutron Transport in Iron," to be published in Nuclear Science and Engineering.
6. F. G. Soltesz and R. K. Disney, "Users Manual for the DOTII-W Discrete Ordinates Computer Code," WANL-TME-1982, 59 (1969).

FIGURE CAPTIONS

Fig. 1 Geometrical Arrangements Employed for the study of Fast Neutron Spectra in Two-Region Systems.

Fig. 2 Neutron Angular Flux at a Region near the Interface. Neutrons propagating from aluminum to iron.

Fig. 3 Neutron Angular Flux at a Region near the Interface. Neutrons propagating from iron to aluminum.

Fig. 4 Neutron Angular Flux at a Region near the Interface. Neutrons propagating parallel to the interface.

FIGURE I

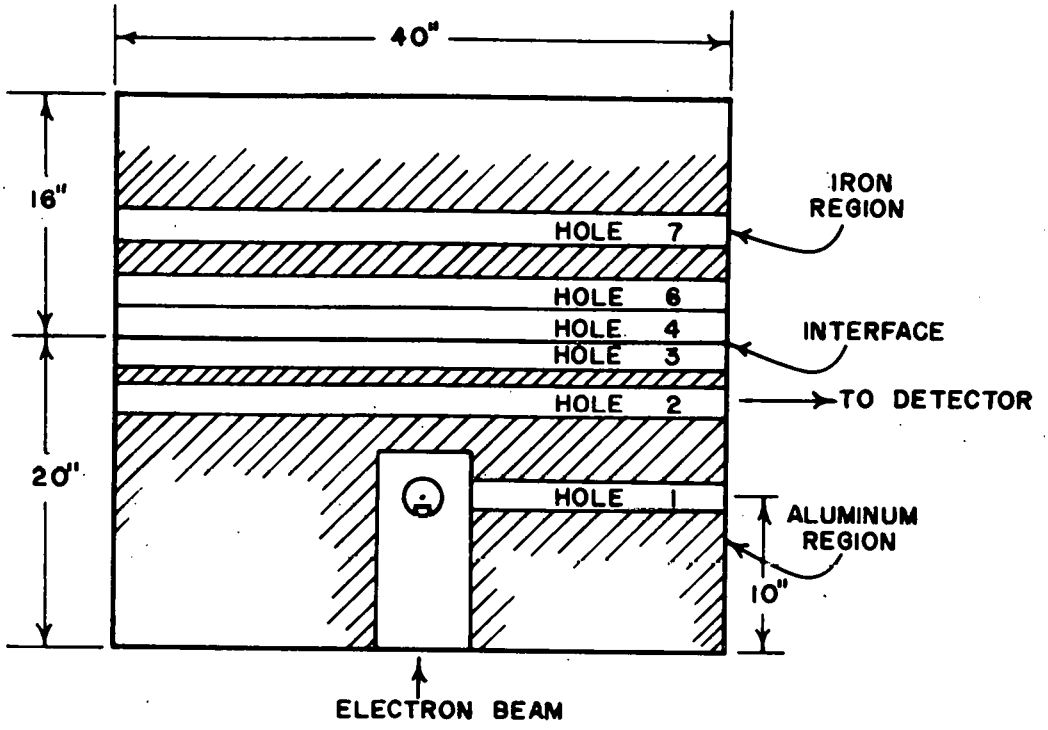

ASSEMBLY I

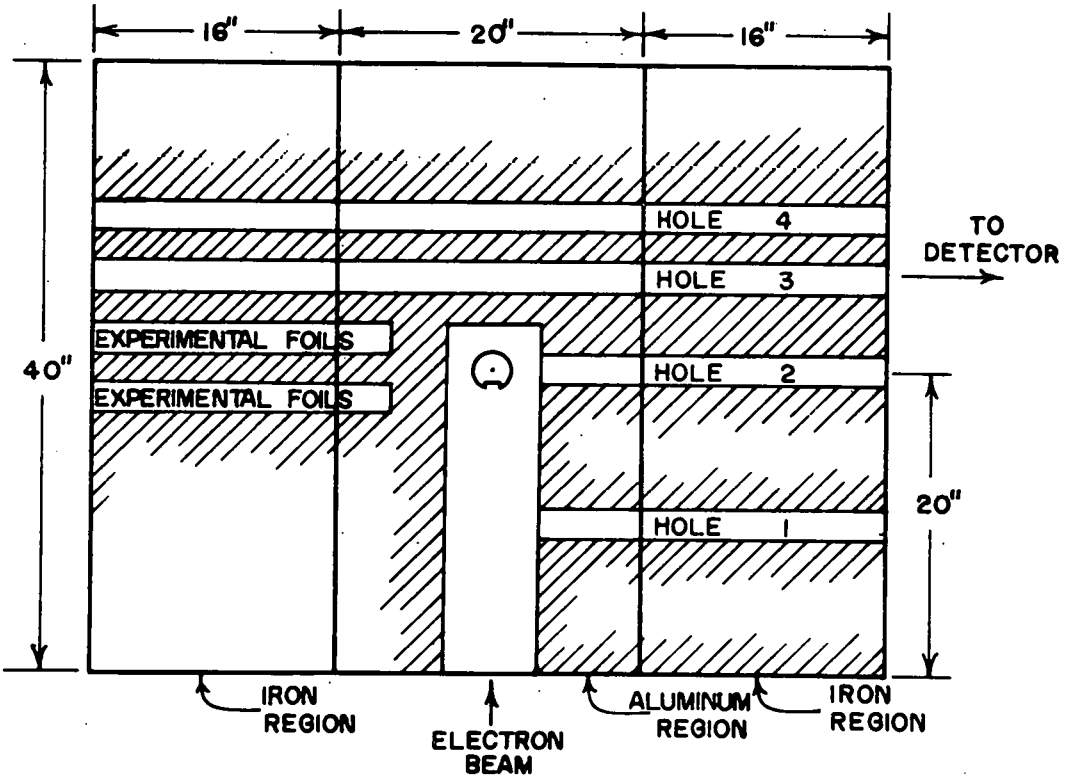

ASSEMBLY 2

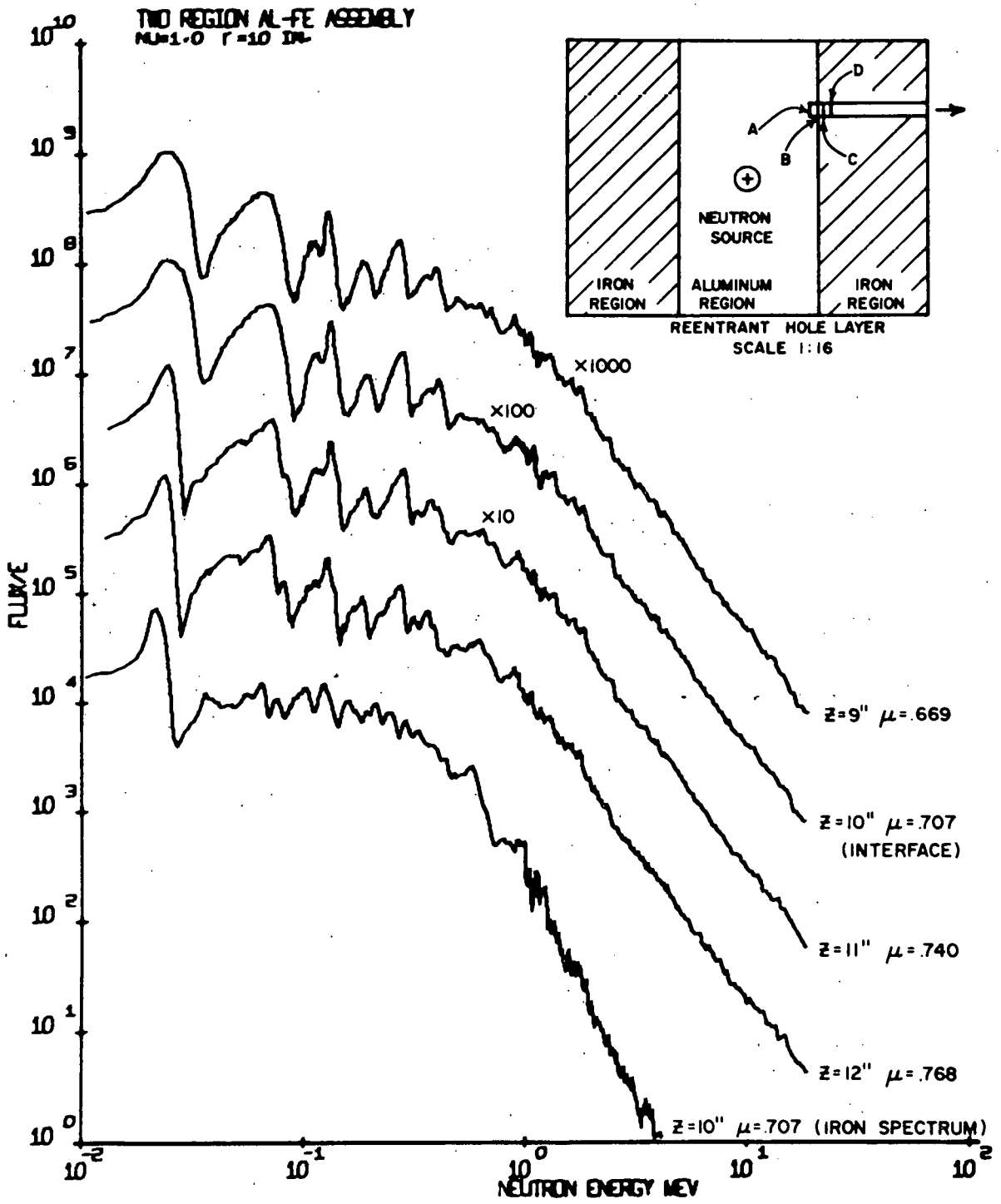
TWO REGION AL-FE ASSEMBLY
NU=1.0 r=10 IN.
FLUENCE
NEUTRON ENERGY MEV
×1000
×100
×10
z=9" μ=.669
z=10" μ=.707
(INTERFACE)
z=11" μ=.740
z=12" μ=.768
z=10" μ=.707 (IRON SPECTRUM)
A
B
C
D
NEUTRON SOURCE
IRON REGION
ALUMINUM REGION
IRON REGION
REENTRANT HOLE LAYER
SCALE 1:16

Figure 2

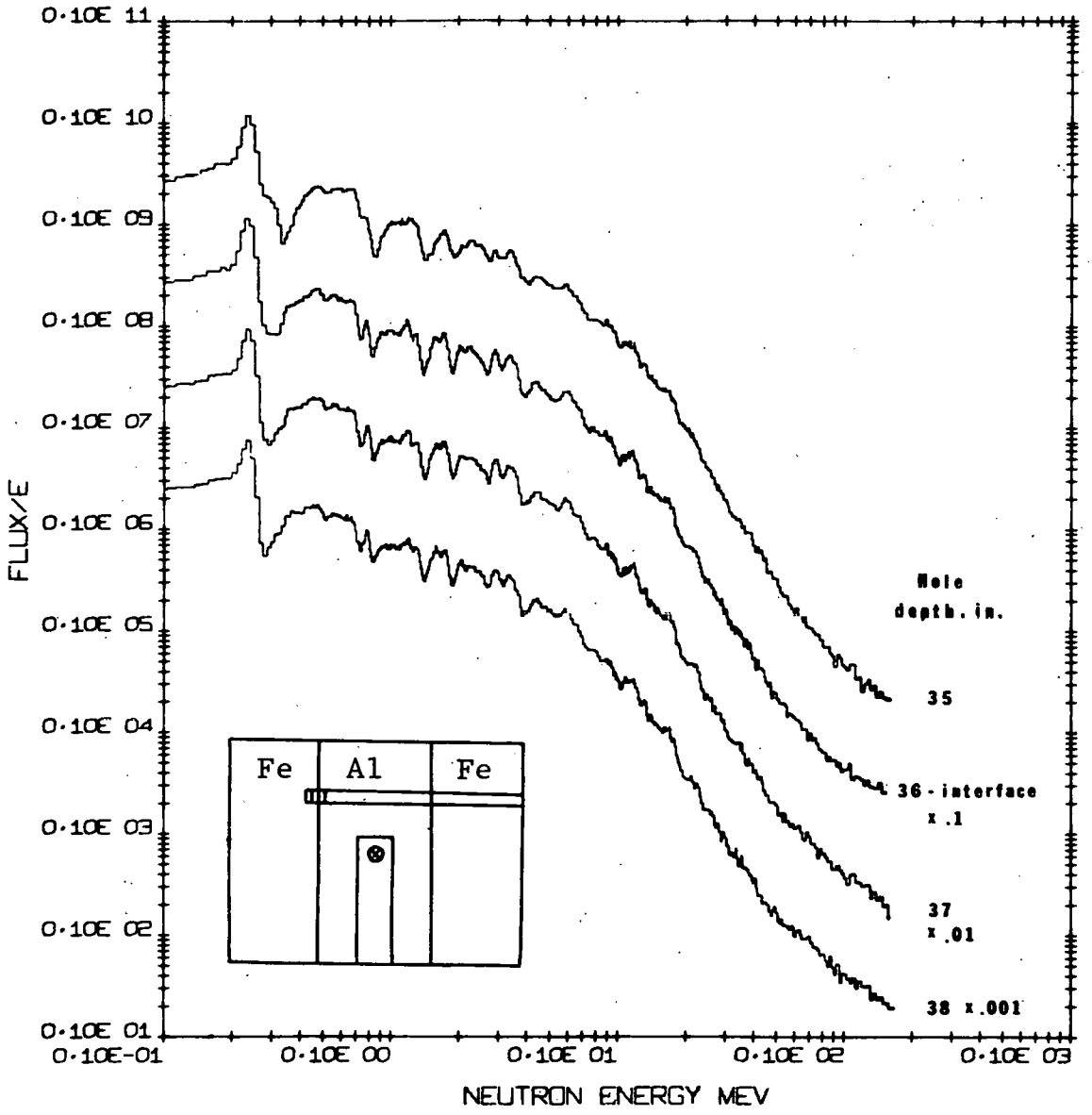
0·10E 11
0·10E 10
0·10E 09
0·10E 08
0·10E 07
0·10E 06
0·10E 05
0·10E 04
0·10E 03
0·10E 02
0·10E 01
FLUX/E
0·10E-01
0·10E 00
0·10E 01
0·10E 02
0·10E 03
NEUTRON ENERGY MEV
Hole depth, in.
35
36 - interface x .1
37 x .01
38 x .001
Fe
Al
Fe

Figure 3

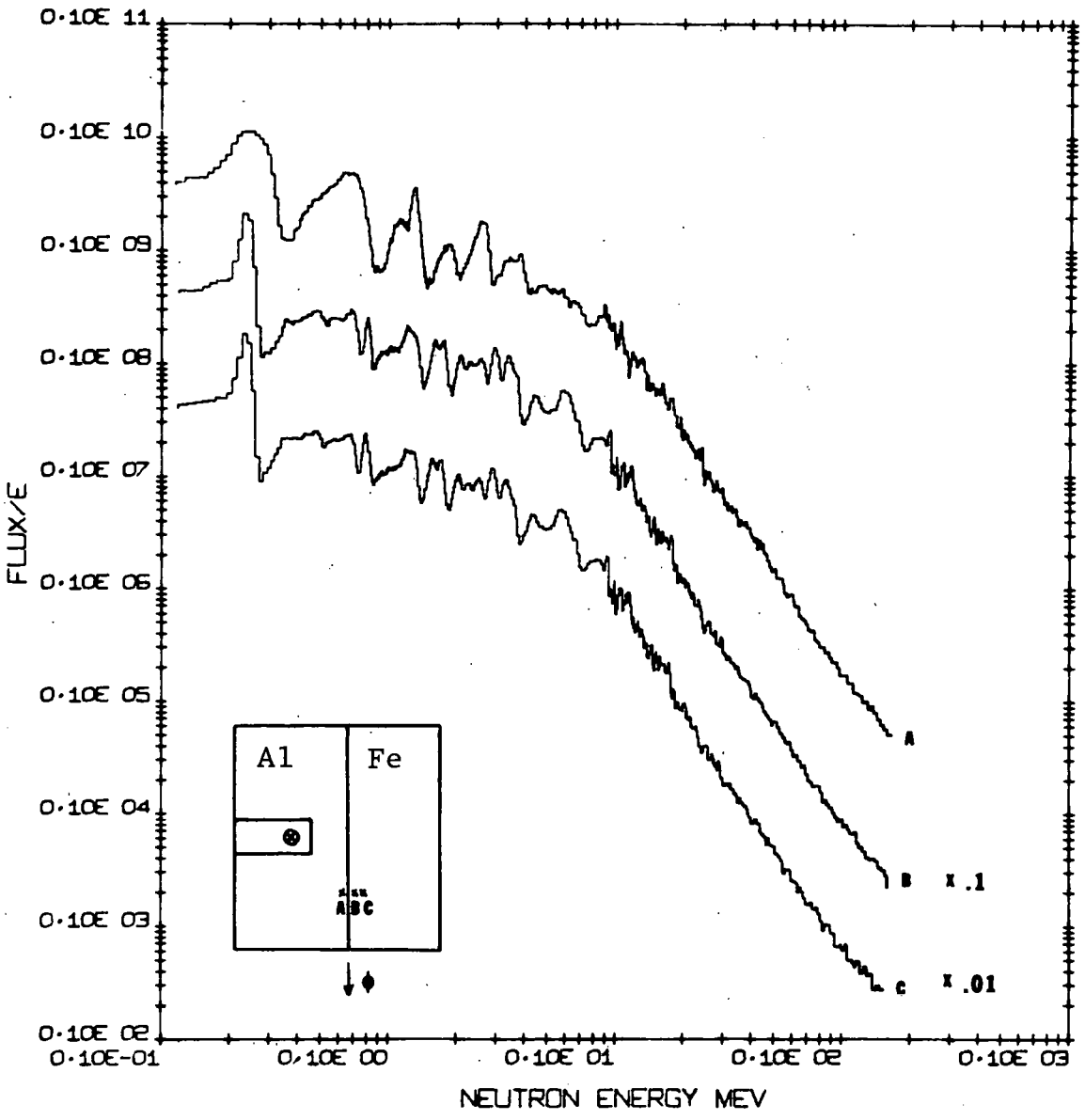
0·10E 11
0·10E 10
0·10E 09
0·10E 08
0·10E 07
0·10E 06
0·10E 05
0·10E 04
0·10E 03
0·10E 02
FLUX/E
0·10E-01
0·10E 00
0·10E 01
0·10E 02
0·10E 03
NEUTRON ENERGY MEV
Al
Fe
A
B
C
A
B x .1
C x .01

Figure 4

TABLE I

DTF 4 SLAB CALCULATION AND GROUP-COLLAPSED EXPERIMENTAL RESULT

DISTANCE FROM SOURCE		6"	9"	Interface	11"	12"	13"	17"
Group 47	Calc.	8.31	7.56		6.98	5.50	4.46	2.59
11.7-13.3	Expt.	.448	.464		.526	.511	.513	.406
keV	Ratio	18.6	16.3		13.2	10.8	8.69	6.39
Group 43	Calc.	57.2	55.1		74.9	66.8	60.3	38.9
Below 25 keV Fe	Expt.	.923	.975		1.33	1.11	1.01	.619
Window 19.3-24.8	Ratio	61.9	56.5		56.1	60.4	59.7	62.8
Group 42	Calc.	92.7	82.3		62.0	54.6	48.2	24.0
25 keV Fe Window	Expt.	1.22	1.13		.684	.486	.514	.293
24.8-28.1	Ratio	76.0	72.5		90.7	112.2	93.9	82.1
Group 41	Calc.	52.3	54.3		3.56	3.25	3.00	1.51
28.1-31.8	Expt.	.833	.878		.190	.167	.159	.097
keV	Ratio	62.8	61.8		18.8	19.5	18.9	15.5
Group 40	Calc.	5.52	5.54		9.91	9.67	8.57	4.27
31.8-36.1	Expt.	.264	.261		.291	.282	.262	.144
keV	Ratio	20.9	21.2		34.05	34.29	32.7	29.7
Group 39	Calc.	7.05	6.74		14.27	13.46	11.65	5.61
36.1-40.9	Expt.	.261	.214		.349	.319	.286	.147
keV	Ratio	27.01	31.5		40.9	42.2	40.7	38.2
Group 38	Calc.	15.35	14.13		18.07	15.39	12.70	5.93
40.9-46.3	Expt.	.409	.356		.402	.348	.302	.146
keV	Ratio	37.5	39.7		44.9	44.2	42.1	40.6
Group 37	Calc.	27.99	23.46		17.82	14.08	11.21	5.13
46.3-59.5	Expt.	.573	.475		.388	.308	.256	.127
keV	Ratio	48.8	49.4		45.9	45.7	43.8	40.4
Group 36	Calc.	38.85	30.81		10.00	13.62	10.72	5.16
59.5-67.4	Expt.	.771	.623		.383	.301	.259	.129
keV	Ratio	50.4	49.5		47.0	45.2	41.4	40.0
Group 35	Calc.	33.85	27.81		11.87	9.66	8.10	4.42
67.4-76.4	Expt.	.745	.585		.277	.213	.189	.113
keV	Ratio	45.4	47.5		42.9	45.4	42.9	39.1
Group 34	Calc.	9.11	7.35		11.65	10.45	8.98	4.78
76.4-86.5	Expt.	.330	.276		.201	.185	.181	.102
keV	Ratio	27.6	26.6		58.0	56.5	49.6	46.9
Group 33	Calc.	4.61	3.48		5.95	5.25	4.48	2.34
86.5-98.0	Expt.	.193	.137		.184	.150	.136	.0785
keV	Ratio	23.9	25.4		32.3	35.0	32.9	29.8
Group 32	Calc.	14.04	10.32		6.88	5.58	4.63	2.43
98.0-111.0	Expt.	.356	.274		.197	.168	.146	.0823
keV	Ratio	39.4	37.7		34.9	33.2	31.7	29.5

Table 2

Effects of Using Iterated Recursion Formula on
Aluminum Four Group Cross-Section Set

		Straight Recursion			Iterated Recursion		
	Energy Group						
P1	1	2.78046	.09207	0.0	2.77988	.90151	0.0
	2	3.39533	.78806	- .01393	3.39712	.78838	- .01382
	3	2.71547	.21854	- .03928	2.67424	.22198	- .03851
	4	1.17714	.02968	- .06094	1.22090	.03082	- .06715
P2	1	2.70433	.40675	0.0	2.70617	.40614	0.0
	2	3.25558	.17458	- .00814	3.26127	.17635	- .00804
	3	2.21824	.02939	.00192	2.19228	.03023	.00181
	4	.83261	.00072	- .01317	.88769	.00079	- .01447
P3	1	2.62521	.14182	0.0	2.62710	.14141	0.0
	2	3.14204	.01813	- .00760	3.15196	.01796	- .00761
	3	1.9.832	.00209	.00029	1.89879	.00213	.00028
	4	.66338	-.00027	- .00068	.70553	-.00013	- .00076

Table 3

Effects of Using Iterated Recursion Formula on
Iron Four Group Cross-Section Set

		Straight Recursion			Iterated Recursion		
	Energy Group						
P1	1	3.07813	.82948	0.0	3.07649	.82717	0.0
	2	2.75110	.47692	- .03089	2.75354	.47634	- .03096
	3	2.21856	.18476	- .02496	2.20984	.18372	- .02479
	4	1.03662	.01402	- .01643	1.28411	.01747	- .01631
P2	1	3.05870	.67998	0.0	3.05769	.67907	0.0
	2	2.61787	.30135	.01256	2.61984	.30135	.01253
	3	1.05551	.02610	- .00551	1.05048	.02576	- .00551
	4	.32142	.00035	.00011	.41253	.00073	.00011
P3	1	3.03932	.36600	0.0	3.03707	.36430	
	2	2.51514	.04614	- .00836	2.51605	.04590	- .00841
	3	.58605	.00397	- .00296	.58700	.00396	- .00297
	4	.23464	-.00005	.00005	.27225	.00024	.00005

Table 4

Test of Aluminum and Iron Cross Sections for Buckling Sensitivity - B^2=0.003

		Aluminum			Iron		
	Energy Group						
P1	1	2.78530	.90378	0.0	3.07829	.82939	0.0
	2	3.39740	.78739	- .01409	2.75417	.47684	- .03085
	3	2.73101	.21851	- .03946	2.25491	.18837	- .02504
	4	1.26320	.03185	- .05942	1.27620	.17603	- .01713
P2	1	2.71581	.40467	0.0	3.05926	.68016	0.0
	2	3.25829	.17380	- .00837	2.62227	.30046	.01253
	3	2.24953	.02922	- .00193	1.18610	.02705	- .00555
	4	.99094	.00094	- .01247	.50423	.00086	.00014
P3	1	2.63886	.13901	0.0	3.03984	.36606	0.0
	2	3.14583	.01797	- .00786	2.51844	.04584	- .00833
	3	1.94251	.00211	.00029	.62760	.00387	- .00298
	4	.75286	-.00027	- .00073	.28025	.00026	.00007

MEASUREMENT OF NEUTRON SPECTRA IN A SODIUM ASSEMBLY

N. N. Kaushal, B. K. Malaviya, J. F. Lewis,
A. N. Mallen and E. R. Gaerttner

During the past year, work was completed on the design, fabrication, filling and testing of a sodium assembly suitable for fast neutron spectrum measurements.[1]

The assembly consists of a steel vessel filled with metallic sodium. The vessel is a double-walled hollow cube with inside dimensions of 6 feet (nominal). The inner walls are made of ¼-inch stainless steel, the outer walls of 3/16-inch carbon steel. The two walls are separated by 4 inches and structurally tied together by means of several steel channels welded to the walls in the annular space. This annular space is used for circulation of hot or cold oil as needed during the filling operation (or for possible emptying of the vessel at some later date).

There is a 6-inch diameter 30-inches deep cylindrical recess extending from the center of one face of the assembly and in a direction perpendicular to that face. This recess is used to house a neutron target and electron beam stripper assembly.

In a direction perpendicular to the target recess and in a horizontal plane there are five 2½-inch I.D. reentrant channels constructed out of 1/16-inch thick brass tubing. Four of these channels extend the total length of the assembly and the fifth one terminates at the target housing recess. Relative geometry of the double-walled vessel, the target recess and the reentrant channels is shown in Fig. 1.

The procedure adopted for filling the vessel was as follows.[2] The vessel was heated to about 100°C by circulating hot oil through the jacket of the double-walled sodium vessel. The vessel was "baked" at this temperature for almost two hours in order to drive out any moisture from the inner chamber. Towards the end of this period, the inner chamber was purged with dry nitrogen. The vessel was then cooled by circulating cold oil through the jacket and liquid sodium at a temperature of about 120°C was poured into

the inner chamber which was maintained at a positive nitrogen pressure. Pouring was done in batches of approximately 600 lbs. each. After each pouring, sodium was allowed to solidify. This was ascertained by inserting a dipstick through an inspection port at the top. As the level of sodium approached the bottom of the reentrant tubes and the target recess provided in the vessel, extra cooling time was allowed to permit shrinkage of sodium due to cooling.

Sodium was poured from the top through a specially designed manifold which distributed sodium equally into four corners of the assembly, in order to achieve even filling. Sodium was filled up to about 2 inches from the top of the inner chamber. The top surface of sodium was ascertained to be level within a quarter of an inch. The remaining volume of the inner chamber is used to maintain a gas cover of dry nitrogen. The vessel was transported on a truck trailer to the RPI LINAC Laboratory and unloaded onto a specially designed platform fitted with air cushion bearings. These air cushion bearings by application of suitable air supply, allow the assembly to be lifted by a film of air. The assembly can then be very easily moved over level floors.

A special set of "slugs" and "plugs" of sodium was prepared (on site) for filling up the reentrant channels. The "plugs" are 2½-inch O.D. 12-inch long thin-walled cylinders of brass filled with sodium and capped on both ends. The "slugs" (of different lengths) are similar except that the cylinder ends are open and covered only with a thin foil of aluminum. The "slugs" are to be used for filling up to the desired depth the reentrant hole under study.

A new neutron source-target was fabricated for use with the sodium assembly. The target essentially consists of a set of plates of tantalum cooled by air and embedded in a 3.2-inch diameter lead sphere. Associated with the target is a new electron-beam "stripper" necessary to limit the size and position of the electron beam before it impinges on the target. The stripper consists of a series of graphite discs with a ½-inch hole at the center. There

is sufficient space between successive discs to allow for air cooling of the stripper.

Some difficulty was encountered in directing a sufficiently large fraction of the electron beam on the target because of the air path that the electrons travel from the LINAC output window to the target in the present experimental setup. It is believed that the main reason for this beam divergence is the water-cooled end window which produces some electron scattering. We have made some tests that show that a thin air-cooled titanium window will help in reducing the scattering. Such a window has been tested and will be used in the near future.

Attention has been given to the problem of aligning the assembly accurately with the neutron flight path collimation. The method adopted is to move the assembly on air cushion on a smooth floor (aluminum plates) and bring it to rest against a well-anchored stop on the floor. This stop is adjusted so that one of the re-entrant holes is accurately in line with the neutron collimation. Alignment of any other reentrant hole is then achieved simply by placing "shims" of proper length next to the end stop and moving the assembly against these "shims".

A new end section for the linac electron drift tube is being fabricated. As before, this section terminates in a stainless steel bellows section to provide for movement of the linac end window along with the assembly as is necessary for alignment of the assembly with the reentrant holes. The new device will provide for a maximum of 18 inches of travel. Positions requiring greater than 18 inches of travel will be achieved by insertion of a separate fixed 18-inch drift tube section.

Preliminary measurements of neutron spectra in the assembly were carried out for the purpose of checking out the whole system and to assess the data accumulation rates and the radioactivity buildup problems. For this purpose, no particular attention was paid to proper filling up of the reentrant channels with slugs and plugs.

On the basis of these experiments, we believe that the buildup

of radioactivity will not be a serious problem. After a 72-hour irradiation of the assembly at an average electron beam power of 300 watts, an activity of 20 mr/hr was observed at a distance of about 4 feet from the side of the assembly facing the electron beam. However, this activity died out after about 3 hours and after a week of cooling, no measurable long-life activity was observed. The "slugs" and "plugs" were scanned on a sensitive gamma-ray spectrometer and little long-lived activity in sodium was observed above background.

Preliminary neutron spectrum data show that even with the present arrangement, significant neutron data can be collected down to neutron energies of 1 KeV although the signal to background ratio may be somewhat poor (1 to 1 at 1 KeV) and the time required to accumulate sufficient data may be quite large (several days per spatial point). Several alternative targets are being considered to improve the neutron count rate at low energies.

Figure 2 shows neutron spectra at two angles symmetrical with respect to 90^{o} direction. A strong variation of the structure in the spectrum can be seen. Thus we expect large anisotropic effects in the treatment of the sodium assembly.

Measurements have also been carried out on the mean-emission-time effects in the assembly[3] and studies of the effect of the assembly on the surface leakage spectrum from the neutron source[4] have also been made. These are described elsewhere in this report.

REFERENCES:

1. Linear Accelerator Project Annual Technical Report, October 1, 1969 - September 30, 1970, 134, RPI-328-200.

2. Linear Accelerator Project Progress Report, October - December 1970, 21, RPI-328-209.

3. This report, p. 117.

4. This report, p. 113.

FIGURE CAPTIONS

Fig. 1 Sectional View of a Horizontal Plane through the Center of the Sodium Assembly.

Fig. 2 Fast Neutron Spectra in a Sodium Assembly at $r \cong 35$ cm, and $\mu \cong +0.75$. These are preliminary data shown for demonstration only and may not be quoted.

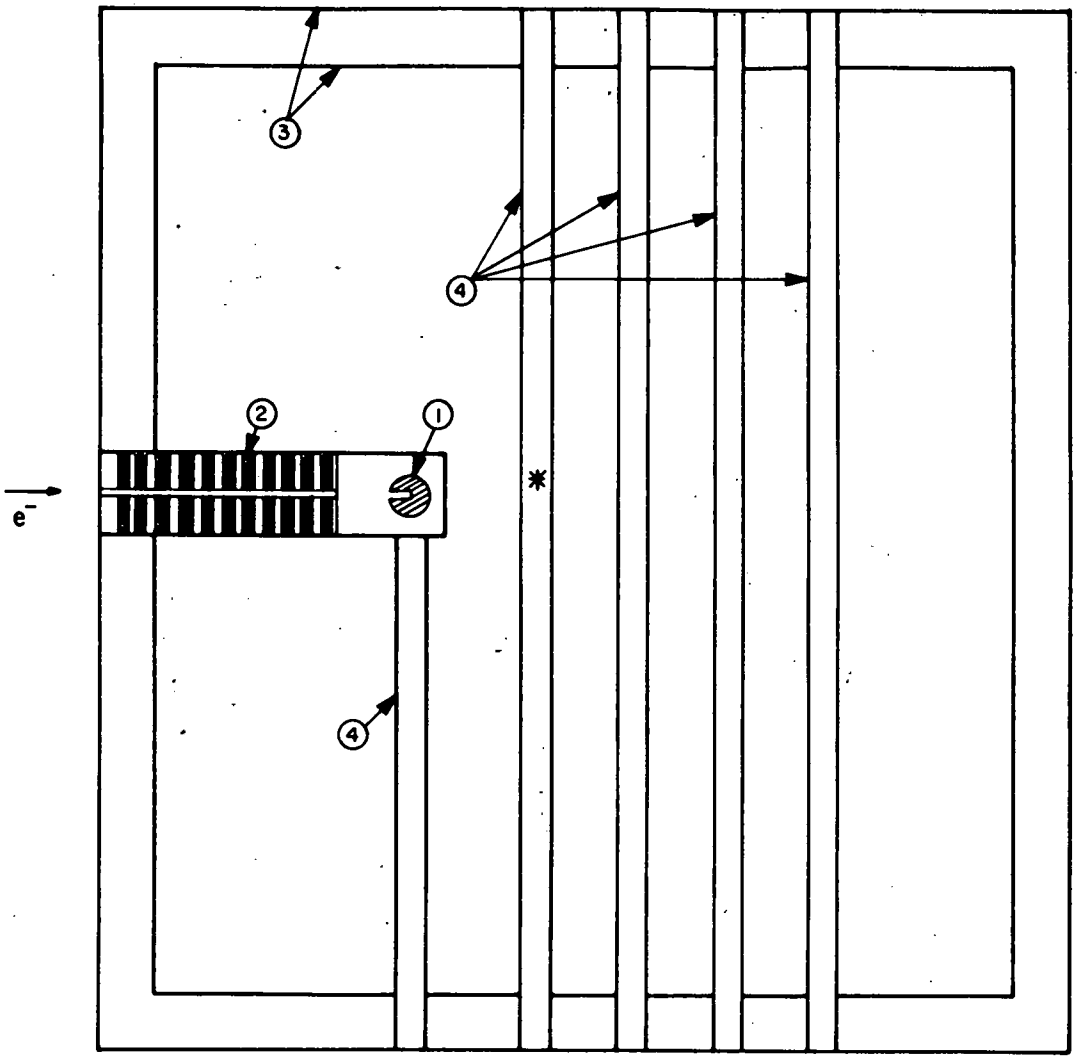

1 · AIR COOLED TARGET
2 · ELECTRON BEAM STRIPPER
3 · DOUBLE WALLED VESSEL
4 · REENTRANT HOLES
* FLUX MEASUREMENT POINT

Figure 1

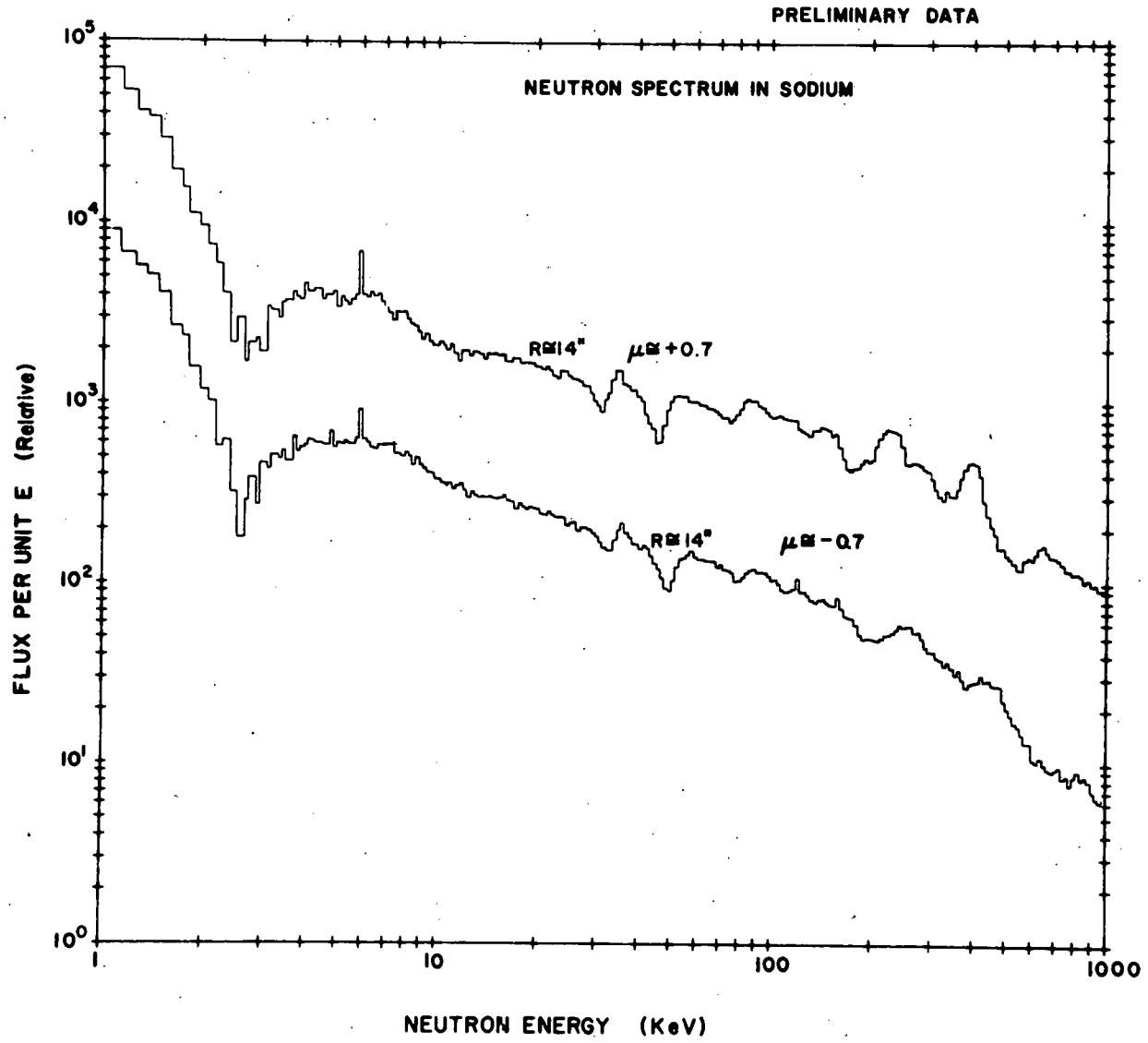
PRELIMINARY DATA
NEUTRON SPECTRUM IN SODIUM
R≅14"
μ≅+0.7
R≅14"
μ≅-0.7
FLUX PER UNIT E (Relative)
NEUTRON ENERGY (KeV)
10^5
10^4
10^3
10^2
10^1
10^0
1
10
100
1000

Figure 2

PERFORMANCE OF THE NEUTRON TARGET FOR THE SODIUM ASSEMBLY

N. N. Kaushal, B. K. Malaviya, A. N. Mallen
and E. R. Gaerttner

A new Ta-Pb target and associated electron-beam stripper assembly have been constructed for use with the sodium assembly. Details of construction of the target and the beam stripper are shown in Fig. 1. The target, basically similar to the earlier versions used with other assemblies,[1] consists of a series of 1/16-inch and 1/8-inch plates of tantalum separated by 1/32-inch gap for circulation of air for target cooling. The plates are contained in a double-walled cylindrical aluminum container and this container is then embedded in a cylindrical recess in a 3.3-inch diameter lead sphere. The electron beam stripper, constructed out of graphite to minimize the photoneutron production, consists of a series of ¼-inch plates of graphite with a ½-inch hole for the beam, arranged concentrically and spaced about ¼-inch apart -- the space being used for circulation of cooling air.

Inasmuch as it is a new target-stripper arrangement, it was considered desirable to run several tests as to its power-handling capabilities, alignment of the electron beam stripper and the target, the neutron spectrum characteristics, etc. The target performed satisfactorily. Up to 300 watts of electron beam power were employed in the course of these tests without exceeding 150° C on the target temperature at an air flow rate estimated at 5 cfm. The target is expected to handle approximately 800 watts of power with increased air flow.

Approximately 50% of the beam is dissipated in the stripper due to beam divergence over the length of the stripper. We hope to improve on this performance by using a titanium air-cooled end window on the LINAC.

Neutron spectrum measurements were made both on the bare target and stripper assembly and also with the target embedded in the

sodium assembly but directly visible to the detector through a completely open reentrant channel.[2] These spectra are shown in Fig. 2. Considerable difference between the two spectra is observed especially at low energies. This is expected because in the latter case there is a significant contribution of neutrons due to scattering from the assembly. This effect is particularly apparent at low energies because of very small neutron flux directly from the source at these energies.

A determination of the neutron spectra under these two different conditions is important from the point of view of analysis of our spectrum measurements. The calculations of neutron spectra for comparison with our experiments have been carried out to date, assuming a shell source surrounding a perfectly absorbing sphere. For this purpose the input required is the experimentally determined surface leakage spectrum from the source with the source in position in the assembly. However, if one intends to use a point source or a volume distributed source in the calculations, one needs to use the spectrum from the source in vacuo. For the case of the sodium assembly, we expect to use both calculational approaches for purposes of comparison.

REFERENCES:

1. B. K. Malaviya, E. Greenspan and E. R. Gaerttner, "Development of Special Targets for Fast Neutron Spectrum Studies," Trans. Am. Nucl. Soc., 11, 211 (1968).

2. This report, p. 106.

FIGURE CAPTIONS

Fig. 1 Details of Construction of the Neutron Target Intended for Use with the Sodium Assembly.

Fig. 2 Comparison of Neutron Spectra from the Surface of the Target-Source (a) with the Target in Air and (b) with the Target Embedded in the Sodium Assembly but Directly Visible to the Detector.

Figure 1

NEUTRON TARGET AND ELECTRON BEAM STRIPPER FOR SODIUM ASSEMBLY

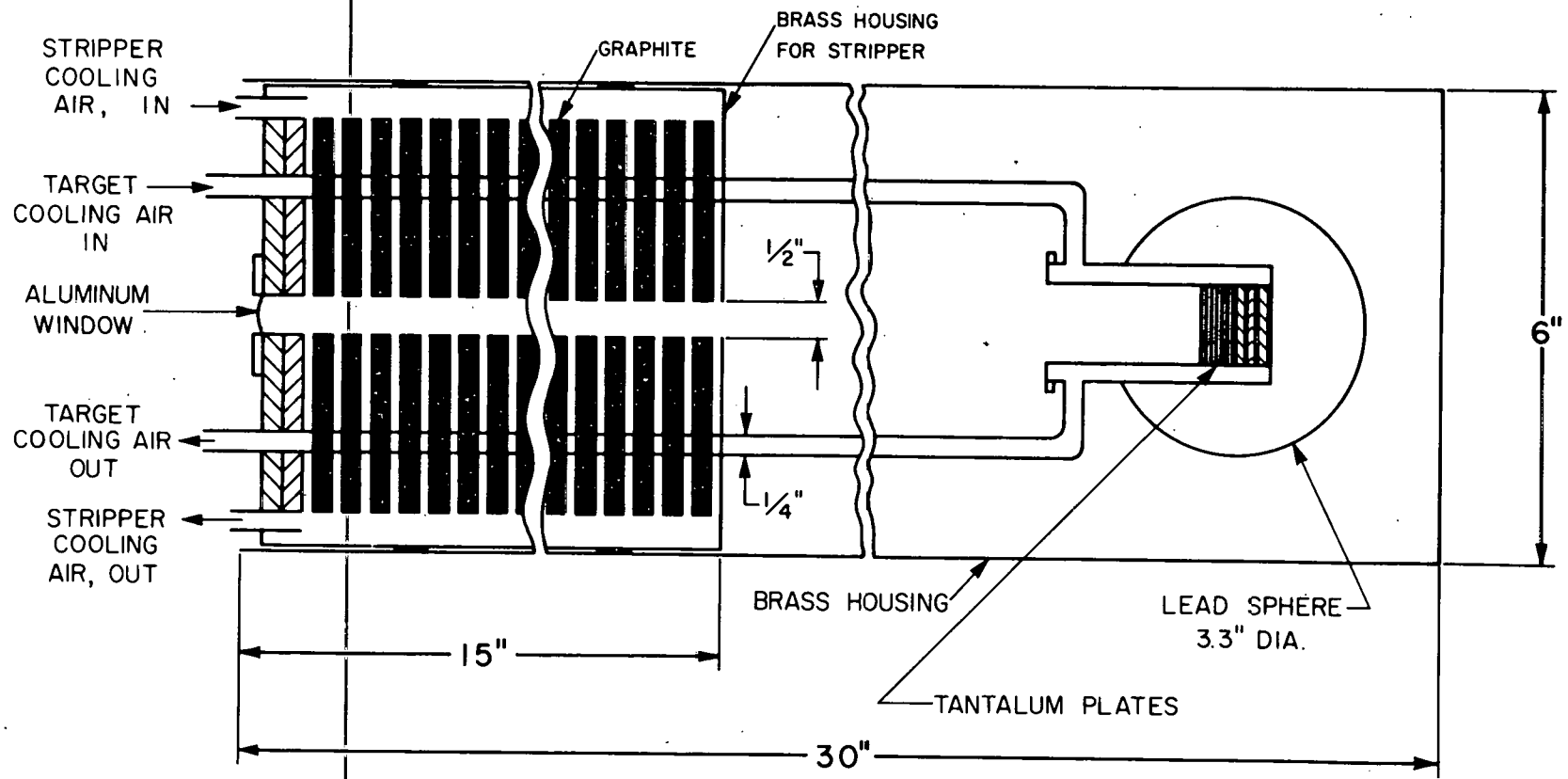

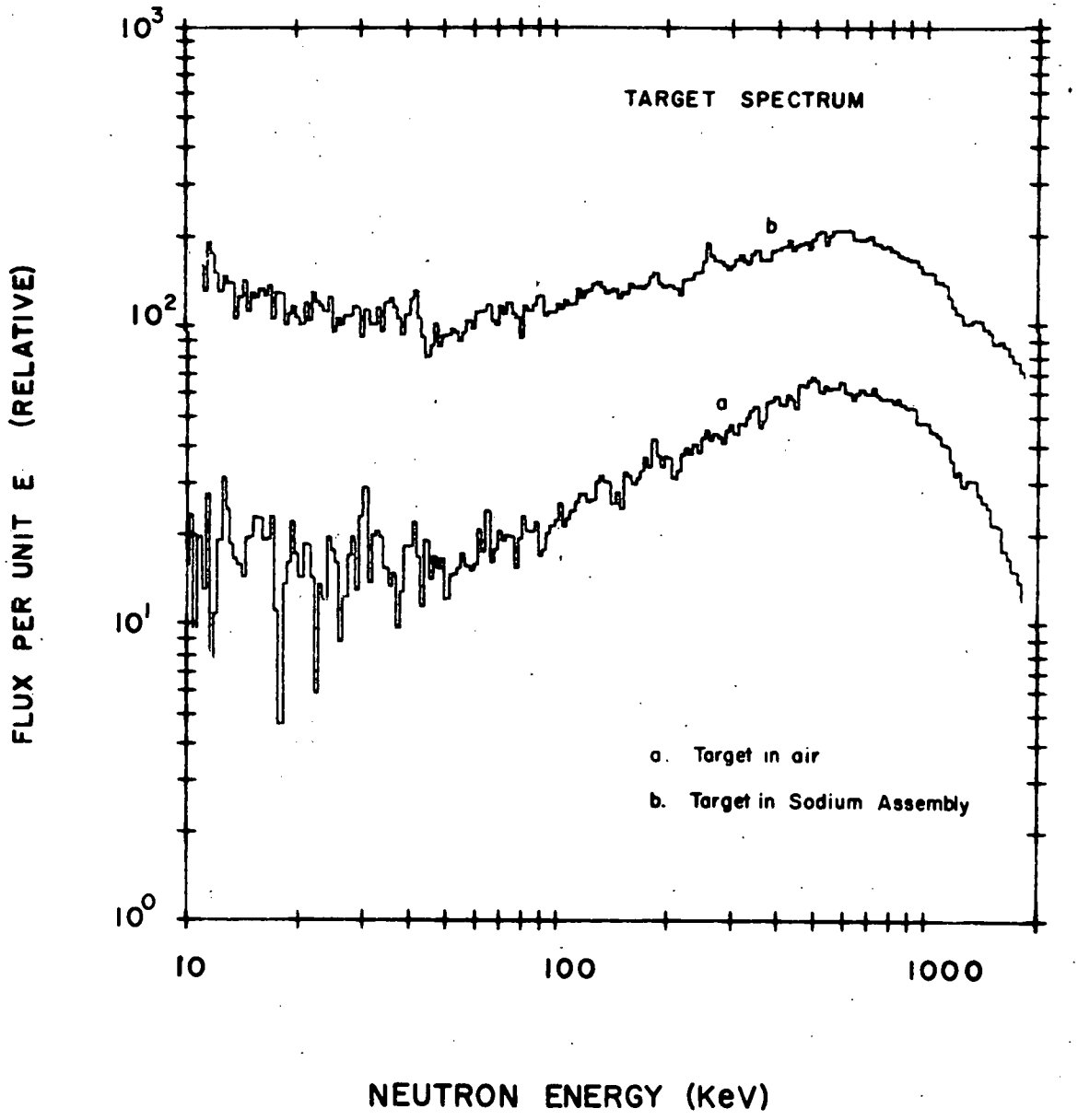
TARGET SPECTRUM
b
a
a. Target in air
b. Target in Sodium Assembly
10^3
10^2
10^1
10^0
10
100
1000
FLUX PER UNIT E (RELATIVE)
NEUTRON ENERGY (KeV)

Figure 2

MEASUREMENT OF EMISSION-TIME EFFECTS IN A SODIUM ASSEMBLY

N. N. Kaushal, B. K. Malaviya, A. N. Mallen
and E. R. Gaerttner

A knowledge of the emission-time effects is desirable for a correct interpretation of the neutron spectra measured by time-of-flight techniques.[1] This is important for two reasons. Firstly, the first time moment or the mean emission time is included in the time of flight and hence must be subtracted to obtain the correct neutron energy. Secondly, the higher time moments have the effect of "time smearing" resulting in a deterioration of the energy resolution of the system. This effect should be taken account of in interpreting highly structured spectra.

A simple experiment was performed to obtain information on both counts. Neutron spectrum from the Ta-Pb target was filtered through a 10-inch thick iron stack (placed in the neutron path 10 meters away from the source) and the filtered spectrum recorded by time of flight. The same neutron target was then embedded in the sodium assembly.[2] The neutron spectrum from the sodium assembly ($r \cong 14"$, $\theta \cong 135^{o}$), filtered through the same iron filter was then recorded by means of the same time-of-flight system.

The two time-of-flight spectra are shown in Fig. 1. A comparison of the two spectra shows up some interesting features. The gamma flash occuring around channel 161 falls essentially in one time channel thus verifying that the resolution and timing of the system were identical in both cases. Features corresponding to structure in the neutron spectrum, however, are both broadened and shifted to higher times in the spectrum from the assembly. The shift and broadening get progressively larger with decreasing neutron energies. Table 1 lists the time shifts which correspond to mean emission times as a function of neutron energy.

We also intend to extract quantitative information on the resolution broadening effect as a function of neutron energy. However, we have not completed our data reduction in that respect.

REFERENCES:

1. Linear Accelerator Project Annual Technical Report, October 1, 1969 - September 30, 1970, 71, RPI-328-200.

2. This report, p. 106.

FIGURE CAPTION

Fig. 1 Comparison of Neutron Spectra Filtered through a 10-inch Iron Filter from (a) Bare Neutron Target, (b) with Target Embedded in the Sodium Assembly and the Neutron Spectrum from $r \cong 14"$ and $\theta \cong 135^{o}$.

Figure 1

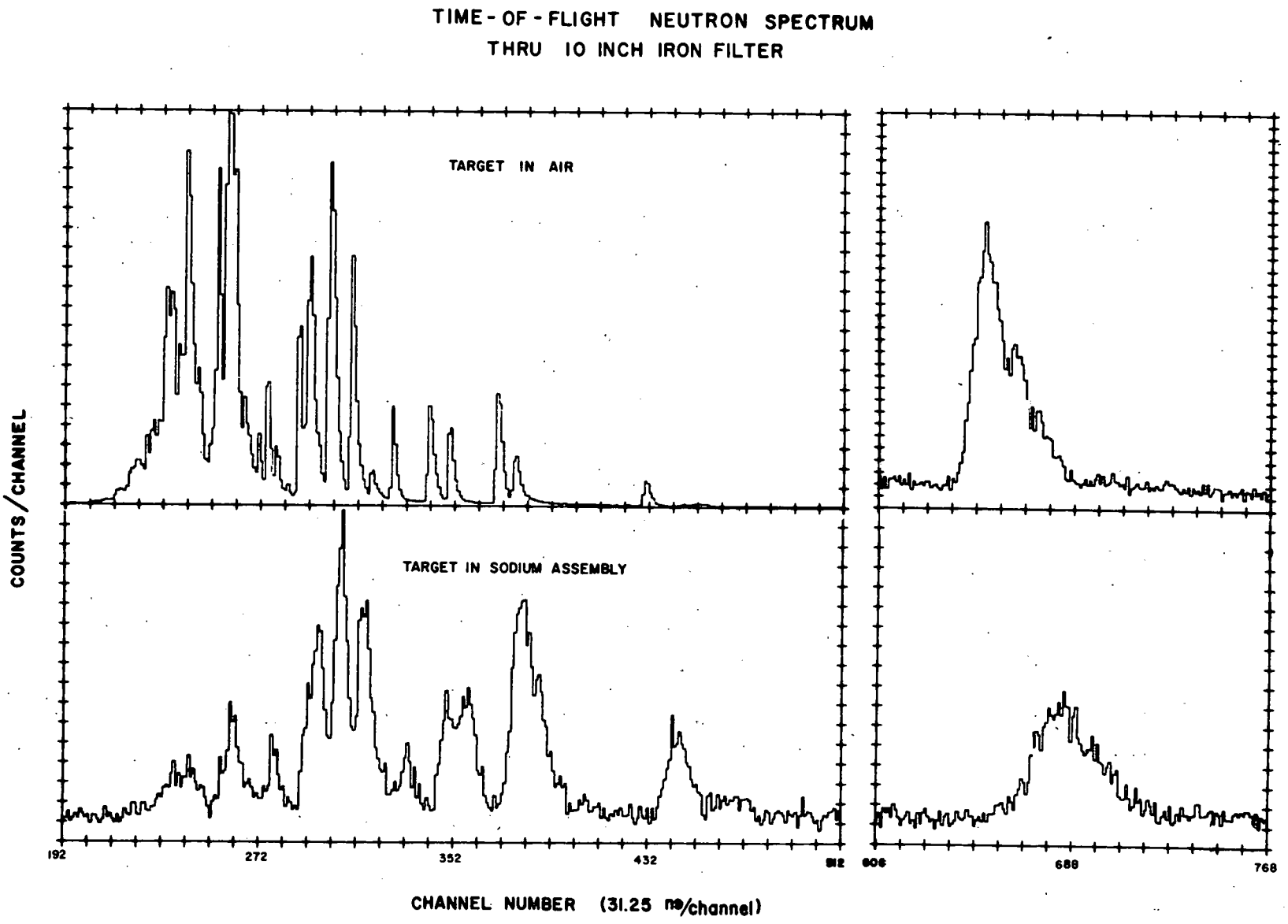
TIME-OF-FLIGHT NEUTRON SPECTRUM
THRU 10 INCH IRON FILTER
TARGET IN AIR
TARGET IN SODIUM ASSEMBLY
COUNTS/CHANNEL
192
272
352
432
512
608
688
768
CHANNEL NUMBER (31.25 nsec/channel)

Table 1*

Neutron Emission Times in a Sodium Assembly

Energy keV	Channel No. Target in Air	Channel No. Target in Sodium	Δ(Ch)	Emission Time
650	256	260	4	125
350	292	296	4	125
310	300	306	6	187
270	309	315	6	187
220	326	333	7	218
180	341	349	8	250
165	350	358	8	250
130	373	382	9	281
80	430	442	12	375
25	651	684	33	1031

*Preliminary Data

REACTOR PHYSICS AND ENGINEERING - THEORETICAL

REACTOR PHYSICS AND ENGINEERING - THEORETICAL

The theoretical effort is concerned with problems of theory and analysis important in our experimental program in particular, and in fast reactor development in general.

Our ability to analyze, understand and interpret fast neutron spectra has been improved by both refinement of existing practice and implementation of basically new capability.

The principal new capability is the development of the RPI version of SUPERTOG to the point where anisotropic group constants can be generated with reasonable anisotropic weighting spectra to use in transport calculations. To the best of our knowledge, the RPI anisotropic scattering capability is the most sophisticated treatment available in the field. The RPI version of SUPERTOG has been transmitted to the Radiation Shielding Information Center.

A second milestone is the completion of a set of in-house programs (RPI Package) for generating group constants. These codes have permitted us to generate group constants from Karlsruhe data. They also have provided us with a vehicle for assessing assumptions made in standard codes. In some cases, we have found where increased accuracy would be desirable. In others, we have found that adequate results could be obtained with substantially simpler and less expensive procedures.

We have continued to take measures to upgrade our existing capabilities. These include improved difference approximations and anisotropic scattering treatments in DTF-IV and an improved interpolation treatment in SUPERTOG. We continue to strive to ensure that the procedures we use include recent important developments. Our continuous slowing down procedures have been coupled to transport calculations by exploiting the separable kernel analogy we discovered.

Additional developments have been made with the interface model, time-dependent spectra and re-entrant hole effects. These areas should lead to applications in our experimental program in the near future.

This year has seen a marked increase in theoretical effort oriented toward nuclear structure and refined differential cross-section analysis.

In cross-section data analysis, the experimental resolution function must be determined to transform raw data into useful cross-section information. An improved time-dependent fast neutron leakage spectra calculational method has been developed for employment in determining the experimental resolution function. Calculations of the total neutron cross section from transmission experiments with the refined resolution function are being conducted.

Attention has also been focused on fitting and prediction capabilities of energy averaged neutron cross sections. The JUPITØR code that RPI had, which performs coupled channel calculations, has been modified to calculate, in addition, S and P-wave strength functions, potential scattering length, channel cross sections and phase shifts. With interest centered on the KeV energy region, JUPITØR has been used to perform spherical optical model calculations. The deep minima that has been experimentally observed in the P-wave strength function in the mass 55 region has been locally fitted but at the expense of either the S-wave strength function or potential scattering length. Considerably smaller than normal real central and imaginary surface diffuseness parameters were required, attributed to magic number effects. As would be expected, adequate global fits with these same optical model parameters are poor. Efforts are underway to refine the calculations by incorporating information on single-particle states in the formalism.

TRANSPORT THEORY

A. Ginsberg,* M. Becker, D. C. Gibbs* and B. K. Malaviya

The RPI version of SUPERTOG[1] has been developed to the point where it is believed that anisotropic group constants can be generated reliably for use in transport calculations. Several basic improvements and extensions have been made. Most important, the sequential transport approximation[2] has been incorporated into the program so as to yield properly weighted anisotropic group constants. Additional options which have been developed have been the ability to generate more Legendre moments (up to P_{16} instead of the P_8 in the original SUPERTOG) and the ability to use more integration points in evaluating group constants.

We have found that group constants do depend on the anisotropic weighting spectrum used. Generally speaking, the total cross section will decrease as the order of weighting spectrum increases. This is because each order spectrum involves additional inverse dependence on total cross section. Thus high-order spectra de-emphasize large cross sections and emphasize small cross sections to a greater degree than do low-order spectra. This observation has significant implications for the method of incorporating anisotropic scattering into transport calculations. In order to obtain angle-independent total cross sections, it is necessary to modify the in-group scattering for each moment. The extended K-table transport approximation[3] leads to an in-group cross section

$$\Sigma^{gg}_{m,eff} = \Sigma^{gg}_{m}(m) + \Sigma_t(K) - \Sigma_{SK}(K) - \Sigma_t(0) \qquad (1)$$

for the mth moment. The letter in parenthesis indicates the order of moment spectrum used for weighting. In view of our observations above, the modification introduced in Eq. (1) generally will be negative. Situations have been observed (even with only

*Based in part on the Ph.D. Theses of A. Ginsberg and D. C. Gibbs.

P_3-scattering) particularly in few-group results where the resulting in-group cross section is negative. Negative sources can lead to difficulty in S_N codes. The consistent P_{K-1} approach,[3] on the other hand, involves

$$\Sigma^{gg}_{m,eff} = \Sigma^{gg}_{m}(m) + \Sigma_t(0) - \Sigma_t(m) \qquad (2)$$

which generally is a positive correction. Thus, the preference cited in the literature[3] for the extended transport approximation may be questionable when properly weighted group constants are used except for low orders of anisotropy.

Another observation we have made is that the number of angular moments required to describe group constants can exceed what might be expected from the cross section itself, particularly for light materials. This is because the angular distribution is correlated with final energy. For example, there is a tendency for the in-group cross section to drop sharply for negative angles, because most backward scattered neutrons may be scattered out of the group. In general, we find that as more moments are added to the in-group cross section, the forward directions converge first and the backward directions last.

The adequacy of the number of integration points depends on the number of angular moments desired in the final cross section set. We have modified SUPERTOG to permit use of more integration points. The reference SUPERTOG integration appears to be adequate up to about P_8, the maximum order permitted in the original SUPERTOG, based on comparisons in which we have doubled the number of integration points. For higher orders, more points are needed to integrate the resulting rapidly fluctuating functions. Going to higher orders and increased numbers of integration points leads to very long running times, particularly for materials with many CM moments on the data file. Calculations to date indicate that the P_8-49 integration point reference method should be adequate for most purposes.

Our experience to date indicates a real need for increased attention and effort to be applied to cross-section processing

and group constant generating codes, because of the time, and therefore cost, involved. As of now, performance of multi-group one-dimensional transport calculations tends to be substantially less expensive than the generation of the multi-group constants from the ENDF/B file, particularly for a material such as iron. There are three areas where some hard thinking would be in order. First, with regard to the data files themselves, is all the information really necessary for most purposes? It appears that there are several areas in which the cross-section detail provides for more of an increase in processing costs than can be justified by increases in accuracy. It may be worthwhile to have basic and supplementary data sections on the files, with the supplementary data used only if desired. Second, the efficiency with which data is being handled should be reviewed. Third, the use of simpler and less expensive calculations of adequate accuracy, analogous to those discussed elsewhere in this report,[4] should be explored.

By the above, we do not mean to cast aspersions at the codes in use, such as SUPERTOG and the ETOE-MC^2 system. On the contrary, those code systems represent substantial improvements over previous capability. In addition, these codes must deal with the data files as they exist. We offer these comments for those involved in creating newer versions of these codes and of data files. We do find one particular advantage for SUPERTOG. Since it is a single code, it may prove simpler to maintain and upgrade than a sequence of codes leading to a similar output.

We also have considered the sensitivity of our results to various factors. In slab geometry, the sequential transport approximation by which the anisotropic weighting spectra are calculated can include a buckling term. We have not found results to date to be very sensitive to the buckling used. This is fortunate because in curvilinear geometries, a buckling term cannot be introduced in a space-independent fashion. We therefore are using the sequential transport approximation in the limit of zero buckling.

As a second sensitivity study, we have assessed the desirability of upgrading the sequential transport approximation. In

the sequential transport equation,[2] we assume

$$\int dE' \, \Sigma_{sk}(E' \to E)\varphi_k(E') = \Sigma_{sk}(E)\varphi_k(E) \tag{3}$$

so that we may use the recursion formula

$$\varphi_k(E) = \frac{1}{\Sigma_t(E) - \Sigma_{sk}(E)} \varphi_{k-1}(E) \tag{4}$$

As an alternative, we consider

$$\begin{aligned} \int dE' \Sigma_{sk}(E' \to E)\varphi_k(E') &= \int dE' \Sigma_{sk}(E' \to E)\varphi_k(E) \frac{\Psi_k(E')}{\Psi_k(E)} \\ &= \Sigma'_{sk}(E)\varphi_k(E) \end{aligned} \tag{5}$$

$$\Sigma'_{sk}(E) = \int dE' \Sigma_{sk}(E' \to E) \frac{\Psi_k(E')}{\Psi_k(E)} \tag{6}$$

where $\Psi_k(E)$ is an initial estimate of $\varphi_k(E)$. We have previously studied this type of approximation at thermal energies.[5] As a further improvement, we have applied an iterative upgrading of the spectra as follows:

$$\Psi_{ko}(E) = \frac{1}{\Sigma_t - \Sigma_{sk}} \varphi_{k-1} \tag{7}$$

$$\Sigma'_{sko} = \int dE' \Sigma_{sk}(E' \to E) \frac{\Psi_{ko}(E')}{\Psi_{ko}(E)} \tag{8}$$

$$\Psi_{kj}(E) = \frac{1}{\Sigma_t - \Sigma'_{sk,j-1}} \varphi_{k-1} \qquad j \geq 1 \tag{9}$$

$$\Sigma'_{skj} = \int dE' \Sigma_{sk}(E' \to E) \frac{\Psi_{kj}(E')}{\Psi_{kj}(E)} \qquad j \geq 1 \tag{10}$$

While some small differences between the upgraded method and the basic method of Eqs. (3) and (4), we believe that the basic method is adequate for our needs.

One deficiency observed in SUPERTOG is the neglect of Doppler broadening of resonances. This neglect implies an error of roughly a factor of two in the unresolved resonance capture cross section at 10 keV in uranium.

We have incorporated improved difference procedures of the type developed by Reed and Lathrop[6] into DTF-IV. We also have improved the anisotropic scattering treatment by replacing "mean values" of Legendre polynomials by integration over the interval. We observed that the interpolation used by SUPERTOG was not always compatible with that on the ENDF/B file and corrected the problem.

REFERENCES:

1. R. Q. Wright et al., ORNL-TM-2679, Oak Ridge National Laboratory (1969).
2. A. Ginsberg and M. Becker, Trans. Am. Nucl. Soc., 14, 368 (1971).
3. G. Hansen, G. I. Bell, H. Sandneier, Nucl. Sci. Eng., 28, 376 (1967).
4. E. T. Burns and M. Becker, this report, p.
5. F. McGirt and M. Becker, Nucl. Sci. Eng., 42, 104 (1970).
6. W. H. Reed and K. D. Lathrop, Nucl. Sci. Eng., 41, 237 (1970).

SLOWING DOWN THEORY

E. T. Burns* and M. Becker

This area of activity has been concerned with the development and use of a capability for analyzing and interpreting slowing down phenomena in fast neutron spectra.

Activity was required to obtain and make operational new versions of the various cross-section processing and group constant generating codes so as to be able to deal with ENDF/B-II data. Simple procedures for generating group-constants for both elastic and inelastic transfer and average cross sections were developed. These have been used together as an RPI package for generating group constants from Karlsruhe data for use in transport calculations. The elastic scattering capability has been used alone to study the sensitivity of group constants to different types of weighting spectra and to generate group constants for use with heavy elements where the MC^2 treatment[1] breaks down.

The elastic group constants are based on the simple kernel[2]

$$\Sigma(u'\to u) = \frac{\Sigma_s(u')e^{u'-u}}{1-\alpha}\left[1+3\bar{\mu}' - \frac{6}{1-\alpha}\bar{\mu}'(1-e^{u'-u})\right] \qquad (1)$$

except for highly forward anisotropy when we use

$$\Sigma_{g\to g+1} = \frac{q(u_{g+1})}{\varphi_g} = \frac{(\xi_{el}\Sigma_{sel} + \gamma_u\Sigma_a)\varphi_w(u_{g+1})}{\int_{u_{g-1}}^{u_{g+1}}\varphi_w(u)du} \qquad (2)$$

where φ_w is the weighting spectrum. Excellent agreement is

*Based in part on the Ph.D. Thesis of E. T. Burns.

obtained with SUPERTOG results, which are based on many Legendre moments in CM coordinates and are consequently much more time-consuming.[a] An example is shown in Fig. 1.

The inelastic procedure eliminates approximations made in both MC^2 and SUPERTOG.[3] The treatments in ETOE-MC^2 do not account properly for motion of the center of mass (though Version II has an improvement over Version I). The treatment in SUPERTOG involves an assumption of separability of cross section and secondary energy distribution. The magnitudes of the effects involved are illustrated in Table 1.

The significance of the success of the elastic group constant procedure should be considered in connection with routine design methods. Much attention to date (as in MC^2 and SUPERTOG) has been oriented toward accuracy, rather than computer costs, because of the need for standards. Such standard procedures, however, can prove too costly in routine use. Our results indicate the possibility of approaching the accuracy of the standards at far less cost. In our view, a stage has been reached where more attention could usefully be paid to procedures suitable for routine use.

A paper on the group constant work, "The Generation of Fast Neutron Group Constants," has been accepted for presentation at the October 1971 American Nuclear Society Meeting.

---

[a] Equation (2) generates elastic transfer to only one group. For intermediate and heavy elements, this is satisfactory given the group structures we use. For lighter materials such as aluminum, and sodium, scattering to more than one group is possible. However, for highly forward peaked anisotropy, almost all scattering is in-group and to the next group, so this procedure introduces little error in resulting spectra.

Further use of continuous slowing down theory has been accomplished through the separable kernel analogy.[4] The slowing down parameter $\xi(E)$ can be adjusted to obtain a measure of the changes required in inelastic scattering to obtain agreement with experiment. A separable kernel can be generated based on the new $\xi(E)$ from which a new set of group constants can be obtained for use in transport calculations. This procedure has been particularly useful in studying uranium.

REFERENCES:

1. B. J. Toppel, et al. ANL-7318, Argonne National Laboratory (1967).
2. M. M. R. Williams, The Slowing Down and Thermalization of Neutrons, Wiley, New York, 1966, p. 330.
3. R. Q. Wright, et al, ORNL-TM-2679, Oak Ridge National Laboratory (1969).
4. M. Becker and E. T. Burns, Nucl. Sci. Eng., 42, 100 (1971).

FIGURE CAPTION

Fig. 1 49-Group Elastic Removal for Iron (ENDF/B-1).

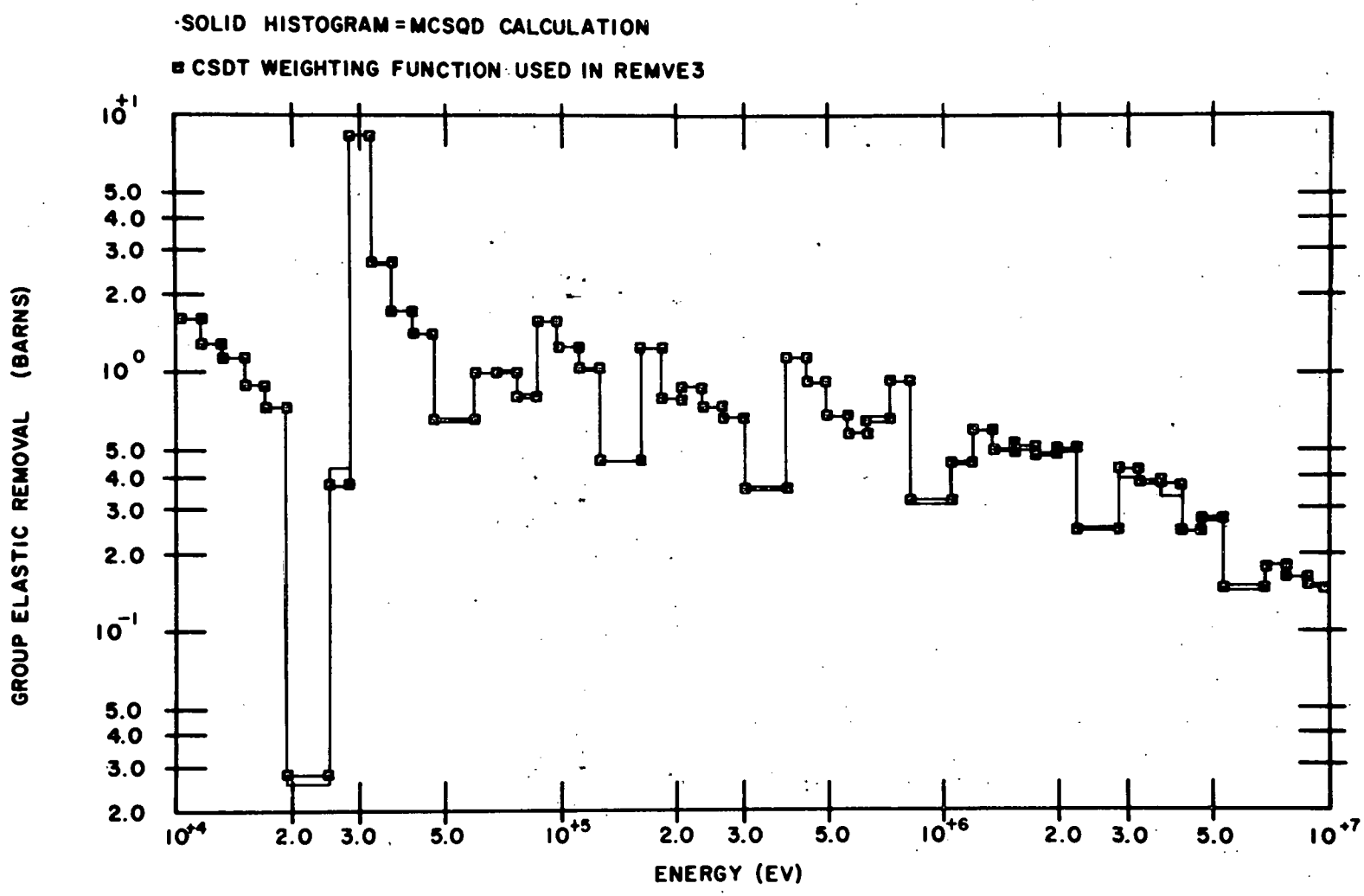

FIG. 1 49-GROUP ELASTIC REMOVAL FOR IRON (ENDF/B 1)

Table 1

Comparison of the Inelastic Matrix Elements for U238 as Generated by SUPERTOG & MC^2

Group Transfers	SUPERTOG	MC^2	$\Delta\sigma/\sigma$
32-36	.2707	.3117	-0.141
32-37	.3007	.2621	+0.135
33-37	.2526	.2829	-0.110
33-38	.1988	.1705	+1.150
35-41	.0898	.1089	-0.190
35-42	.0951	.0937	+0.010
35-43	.07178	.05584	+0.240
29-30	.5051	.5578	-0.100
29-31	.4580	.4067	+0.120
25-30	.09936	.1042	-0.010
25-31	.0313	.0262	+0.180
34-38	.0141	.03486	-0.800
34-39	.1657	.1696	-0.020
34-40	.1464	.1390	+0.040
34-41	.0216	.0056	+1.200

LOW ENERGY SPECTRA

M. Becker and A. Ginsberg*

Analysis of experiments on depleted uranium assemblies has indicated a strong sensitivity to capture in the unresolved resonance region. This sensitivity has made it possible to draw conclusions regarding data files having moderately different capture cross sections. The unresolved capture cross section, however, involves a self-shielding correction of the order of thirty percent at 10 keV. As a result it was deemed worthwhile to review the assumptions made in the MC^2 and SUPERTOG codes.[1,2] A second reason for this review was the interest in extending the range of measurement and analysis to lower energies, particularly in uranium. The strong sensitivity of the experiments to low energy capture implies that lower energy spectra could span the energy range most important for the Doppler effect in a fast reactor and lead to an unambiguous assessment of the nuclear data needed to calculate the Doppler effect.

Review of the MC^2 and SUPERTOG treatments indicate that the following assumptions have been involved:

(1) There is no interference between adjacent resonances. For uranium at 10 keV the average width is about a tenth of the average spacing, so that this assumption should be reasonable.

---

*Based in part on the Ph.D. Thesis of A. Ginsberg.

(2) There is no interference among resonances of different sequences. This is generally considered a small effect, particularly for fertile material.[3]

(3) Interference between resonance and potential scattering can be neglected. According to Dresner,[4] this is a good assumption if

$$\beta >> \frac{\theta^2}{6} \qquad (1)$$

where β is the self-shielding factor and θ is the ratio of nuclear to Doppler widths. For the average width in uranium at 10 keV, θ is about .1 (at room temperature) and β is about .05. For lower energies, however, the assumption might have to be modified.

(4) In SUPERTOG, Doppler broadening is neglected. For θ of .1 an average width at 10 keV of 200 mV, and a β of .05, we find

$$\frac{J(\theta,\beta)}{J(\infty,\beta)} \approx 2 \qquad (2)$$

where J is the Doppler broadened resonance integral function.[4] This implies a substantial error in the self-shielded cross sections obtained from SUPERTOG.

A simple approach was taken to attempt to resolve the Doppler broadening problem. Dresner cites a simple rapidly converging series

$$J(\theta,\beta) = \frac{\pi}{2\beta} \sum_{\nu=0}^{\infty} B_\nu \left(\frac{x}{1+x}\right)^\nu , \quad x = \frac{\sqrt{\pi}}{2}\frac{\theta}{\beta} \tag{3}$$

We have improved the accuracy of this approach considerably by

$$x = \frac{\sqrt{\pi}}{2}\frac{\theta'}{\beta} \qquad \theta' = \theta e^{\frac{1}{4}\theta^2} \operatorname{erfc}\left(\frac{\theta}{2}\right) \tag{4}$$

This substitution is motivated as follows. Equation 3 is based on the approximation

$$\Psi(\theta,x) \approx \frac{\theta\sqrt{\pi}}{2} e^{-\frac{1}{4}\theta^2 x^2} \tag{5}$$

Use of θ' in Eq. 5 leads to the correct value at x equal to zero and produces a change in the exponential in the right direction. While this approximation has proved to be accurate for individual resonances for a wide range of parameters, it did not resolve the problem when inserted into SUPERTOG unresolved treatment. In the future, we plan to look into alternate simple treatments, such as the table interpolation approach used in the Idaho Nuclear PHROG code.

Equations (3) and (4) have been used for individual resonances in uranium to verify that indeed the sensitivity to uranium capture would persist into the resolved resonance region.

REFERENCES:

1. B. J. Toppel, et al., ANL-7318, Argonne National Laboratory (1967).
2. R. Q. Wright et al., ORNL-TM-2679, Oak Ridge National Laboratory (1969)
3. R. Nicholson and E. Fischer, in Advances in Nuclear Science and Technology, Vol. 5.
4. L. Dresner, Resonance Absorption in Nuclear Reactors, Pergamon Press, New York, 1960.

TIME-DEPENDENT SPECTRA

S. Kang* and M. Becker

The TDA code, a time-dependent one-dimensional discrete ordinate code, has been made operational. We thus now have a procedure for precise analysis of time-dependent spectrum experiments. To date, the code has been used for a moderate number of test calculations. It is a time-consuming code.

Our analytical work on time-dependent spectra has evolved away from continuous slowing down theory to the following approach. Consider an infinite-medium problem with a source in the top group. The time-dependent flux is governed by the equation

$$\frac{1}{V_1}\frac{\partial\varphi_1}{\partial t} = S_1(t) - \Sigma_{r1}\varphi_1 \tag{1}$$

If the source is a delta-function at time zero, Eq. (1) yields

$$\varphi_1(t) = \varphi_{10}e^{-V_1\Sigma_{r1}t} \tag{2}$$

for the second group,

$$\frac{1}{V_2}\frac{\partial\varphi_2}{\partial t} = S_2(t) + \Sigma_{1\to2}\,\varphi_1(t) - \Sigma_{r2}\varphi_2 \tag{3}$$

For a purely down-scattering problem, $\varphi_1(t)$ is a known function (from Eq. (2), so Eq. (3) can be solved analytically. This approach has been found to be reliable numerically for about thirty groups in our 49-group structure.

This approach provides several benefits. First, being a sequence of analytic solutions, it is relatively easy to generate. Second, since explicit expressions exist for the coefficients, it is possible to determine the influence of the solution component characteristic of one group G on another group G'. Third, the technique can handle simply substantially different time constants.

---

*Based in part on the Ph.D. Thesis of S. Kang.

(Finite difference procedures can have difficulty treating high energy groups with time-step sizes that are appropriate to lower energy groups).

To handle space and time dependence, a Fourier expansion is used. The removal cross sections for each component are augmented by a buckling term. The external source is expanded in Fourier series. Equations such as Eq. (3) are then obtained for each component and solved separately. The results of each solution are combined to obtain the total solution. Initial numerical calculations have been performed for space-dependent problems.

The space-dependent model tends to converge most rapidly at low energies. Thus, we have the capability of extending our time-dependent spectrum interests to the use of slowing-down spectrometers, for example, for safeguards purposes. Such a possibility is enhanced by the presence at the LINAC laboratory of a large lead assembly to which there is a possibility of access.

Reasons for numerical difficulty with the basic analytical procedure beyond thirty groups have been postulated and remedies have been proposed. We hope to test them in the near future.

INTERFACE MODEL

G. Epstein* and M. Becker

This study is an attempt to utilize continuous slowing down theory to generate space-dependent spectra in the vicinity of an interface between dissimilar media. As in our single region work, we expect the continuous slowing down approach will be useful in providing weighting spectra and in facilitating understanding of the transition in spectral characteristics near the interface.

The basic idea of the model is as follows. A single region age solution is performed for the medium containing the source. This calculation is on an infinite-medium basis, implicitly assuming that the second region is identical to the first. The flux at the interface location is then used as the basis for a second age calculation for the second region taken as an infinite medium. This step provides a spectrum for the second region which is influenced by the presence of the first. The second age calculation leads to a new flux at the interface location. The change in the partial current is used as the basis for a third age calculation, this one for the first region. This step provides a spectrum for the first region which has been influenced by the presence of the second region.

In this approach, it is desirable that the age calculations not be limited by neglect or poor treatment of first and last collision effects. As a result, we have developed an accurate analytical treatment for including these effects. A paper describing this treatment[1] was presented at the June 1971 American Nuclear Society Meeting.

The spectral variation in the vicinity of the interface turns out to depend strongly on the assumed angular dependence of the source used at the interface. To perform the second age calculation; i.e., to get the spectrum in the second region, we assume the source to have the angular dependence

---

*Based in part on the Ph.D. Thesis of G. Epstein.

$$S(E) = \frac{a(E)}{1-\beta(E)\mu} \qquad (1)$$

The parameter β is chosen to match the ratio of forward and backward partial currents at the interface location in the first age calculation. Equation 1 has been found to give good agreement with the transport calculations. Current effort is being directed at testing the sensitivity to angular distribution in the source for the third age calculation.

REFERENCE:

1. G. Epstein and M. Becker, Trans. Am. Nucl. Soc., 14, 366 (1971).

RE-ENTRANT HOLE PERTURBATIONS

M. Danchak* and M. Becker

A model has been formulated for extending earlier RPI work on re-entrant hole models to handle spherical geometry configurations. The approach consists of determining the unperturbed fluxes along the hole surfaces based on an unperturbed spherical geometry DTF-IV problem, using these unperturbed fluxes to determine the partial currents at hole bases, and using the difference between perturbed and unperturbed partial currents to generate the perturbation in the fluxes emitted from the holes on the basis of slab-geometry DTF-IV calculations. The entire sequence of operations has been programmed. Initial results, however, indicate that some problems still exist. Current status is that the coding and logic are being reviewed to check for possible errors.

A key assumption in our re-entrant hole work has been that the detailed angular flux incident upon the hole base can be replaced by an isotropic source introducing the same partial current into the medium.[1] The reason for this is that using a detailed angular flux boundary condition in DTF-IV led to severe convergence problems. We undertook to study the basis behind the observed insensitivity of emergent forward flux to incident angular distribution by means of analytic solutions to monoenergetic slab albedo problems.[2] We found that the insensitivity is not rigorously obtained. Insensitivity is most nearly satisfied for high ratios of scattering-to-total cross sections. It seems that the approach is reasonable in general, but that validity should be verified in dealing with highly absorbing media.

REFERENCES:

1. F. McGirt and M. Becker, Nucl. Sci. Eng., 39, 56 (1970); see also F. McGirt, Ph.D. Thesis, RPI, 1969.
2. K. M. Case and P. F. Zweifel, Linear Transport Theory, Addison-Wesley, Reading, Massachusetts (1968).

*Based in part on the Master's Engineering Project of M. Danchak.

VARIATIONAL AND SYNTHESIS METHODS

M. Becker

A low level of activity has been maintained over the past several years in the area of variational methods. We hope in this way to maintain previously developed expertise in this area and to make contributions which are of potential benefit to the fast reactor program. In particular, we have been concerned with discontinuous trial function methods (DM). Previous work has been oriented toward understanding the gains provided by DM in space-time kinetics,[1,2] particularly in regard to Green's function modes, and toward alleviating the well-known problem of ambiguity caused by overdetermined interface conditions.[3,4]

Our previous effort regarding interface conditions dealt with initial-value[3] and boundary-value[4] problems. Our approach to initial-value problems, based on the use of "asymmetric discontinuities," appears to have become accepted as a standard method of treating time-discontinuities.[5,6] Our previous effort in connection with boundary-value problems was restricted to the special case of trial functions based on asymptotic solutions far from an interface (as in the case of overlapping spectra). While that result stimulated further applications,[7] it was restricted to a special category of trial function expansion.

Others concerned with applications of spatial synthesis,[8] space-energy synthesis[9] and space-time synthesis[5,8] to fast reactor problems, attempted to apply the type of approach we used in Ref. 3 to boundary-value problems. While substantial progress was made, some ambiguity and arbitrariness remained in the specification of interface conditions.

We have formulated what we call a Principle of Information Flow to guide the extension of the asymmetric discontinuity concept to boundary-value problems. The essence of the approach is to work in terms of variables which transmit information separately in separate directions (such as partial currents in diffusion

theory). The approach appears to be successful in alleviating ambiguity in assigning interface conditions to boundary-value problems. Details of the approach are to be published in Nuclear Science and Engineering.

REFERENCES:

1. P. C. Rohr and M. Becker, Trans. Am. Nucl. Soc., 11, 169 (1968).
2. P. C. Rohr and M. Becker, Trans. Am. Nucl. Soc., 12, 619 (1969).
3. M. Becker, Nucl. Sci. Eng., 34, 343 (1968).
4. M. Becker, Nucl. Sci. Eng., 34, 339 (1968).
5. E. L. Fuller, D. A. Meneley, D. L. Hetrick, Nucl. Sci. Eng., 40, 206 (1970).
6. G. Kessler, Nucl. Sci. Eng., 41, 115 (1970).
7. E. L. Wachspress, Nucl. Sci. Eng., 34, 342 (1968).
8. W. L. Woodruff and V. Luco, ANL-7710, Argonne National Laboratory, p. 410 et seq. (1971).
9. M. J. Lancefield, Nucl. Sci. Eng., 37, 423 (1969).

LEAKAGE PROBABILITY APPROACH TO APPROXIMATELY DETERMINING FAST NEUTRON LEAKAGE SPECTRA FOR PULSED MODERATORS

P. J. Turinsky

Crucial to an accurate analysis of cross sections obtained from neutron time-of-flight experiments is a knowledge of the neutron spectral-time distribution for small, pulsed moderators. Such moderators are employed to soften the initial neutron spectrum to energies of experimental interest. The leakage probability approach is a calculational method enabling approximate solutions for the spectral-time neutron leakage distribution required in the analysis of experimental data. It offers higher accuracy than a diffusion theory approach for comparable calculational effort.

The basic approximation introduced in the method is that of estimating the time-dependent neutron leakage probability function, $P_e(E,t'\rightarrow t)$, defined as the probability of a neutron born at time t' with energy E of escaping at time t without suffering an interaction. The neutron conservation equation for all neutrons in the moderator system is then given by

$$\frac{1}{v}\frac{\partial\langle\varphi(E,t)\rangle}{\partial t} = \int_{-\infty}^{t} dt'\left[\delta(t-t') - P_e(E,t'\rightarrow t)\right] \quad (x)\ \left[\int_0^{\infty}\Sigma_S(E'\rightarrow E)\langle\varphi(E',t')\rangle dE' + \langle Q(E,t')\rangle\right] \quad (1)$$

$$-\Sigma_t(E)\langle\varphi(E,t)\rangle \ .$$

Introducing the total leakage spectra function, $\langle L_T(E,t)\rangle$, characterizing the energy distribution and rate of neutrons leaking out at time t, we note that

$$\langle L_T(E,t)\rangle = \int_{-\infty}^{t} dt' P_e(E,t'\rightarrow t)\ \left[\int_0^{\infty}\Sigma_S(E'\rightarrow E)\langle\varphi(E',t')\rangle dE' + \langle Q(E,t')\rangle\right] \ . \quad (2)$$

Hence, if Eq. (1) can be solved for the total neutron flux, $\langle\varphi(E,t)\rangle$, from Eq. (2) the leakage spectra can be obtained. It is exactly $\langle L_T(E,t)\rangle$ which must be determined to accurately convert raw experimental results into useful cross-section information.

The leakage probability approach has the advantage over diffusion calculations of providing more accurate results with equivalent labor. In particular, a more accurate treatment of neutron migration can be achieved by the present method. This is of considerable importance for the small moderators we must consider. Since the leakage probability function must be estimated, the method is less accurate than a direct numerical solution of the transport equation. But such accuracy is not required in our particular work, so we have chosen to avoid the high computational costs associated with obtaining a transport equation solution.

Recognizing Eq. (1) to be a Volterra integral equation for neutron slowing down, this equation and subsequently Eq. (2) was solved by standard numerical methods on the NYU CDC-6600. P_e was estimated by assuming both an isotropic and spatially independent flux and source distribution exist, allowing direct extension of the results of Case et al.[1] Considering a spherical (radius $\cong$ 1.9 cm) hydrogenous moderator and photoneutron energy spectra and ramp-on-off time distribution for the source, which is representative of the RPI experimental setup, $\langle\varphi(E,t)\rangle$ and $\langle L_T(E,t)\rangle$ were computed. Figure 1 illustrates the anticipated pulse broadening for lower energy neutrons due to increased slowing-down times. The change of spectrum with time from initially a source spectrum to near a $1/E^{\alpha}$ spectrum is shown in Fig. 2.

Work is currently progressing to imbed the leakage probability approach in the calculation of resolution functions employed in the analysis of cross-section measurements. This should increase the accuracy of our analysis over the presently employed method based on an infinite moderator calculation.[2]

REFERENCES:

1. K. M. Case, F. DeHoffmann and G. Placzek, Introduction to the Theory of Neutron Diffusion, Vol. 1, U. S. Government Printing Office, Washington 25, D. C. (1953).

2. Linear Accelerator Project Progress Report, January - March 1969, 11, RPI-328-160.

FIGURE CAPTIONS

Fig. 1 Flux and Leakage Spectra vs. Time for Hydrogenous Sphere of Radius ≅ 1.9 cm.

Fig. 2 Flux and Leakage Spectra vs. Energy for Hydrogenous Sphere of Radius ≅ 1.9 cm.

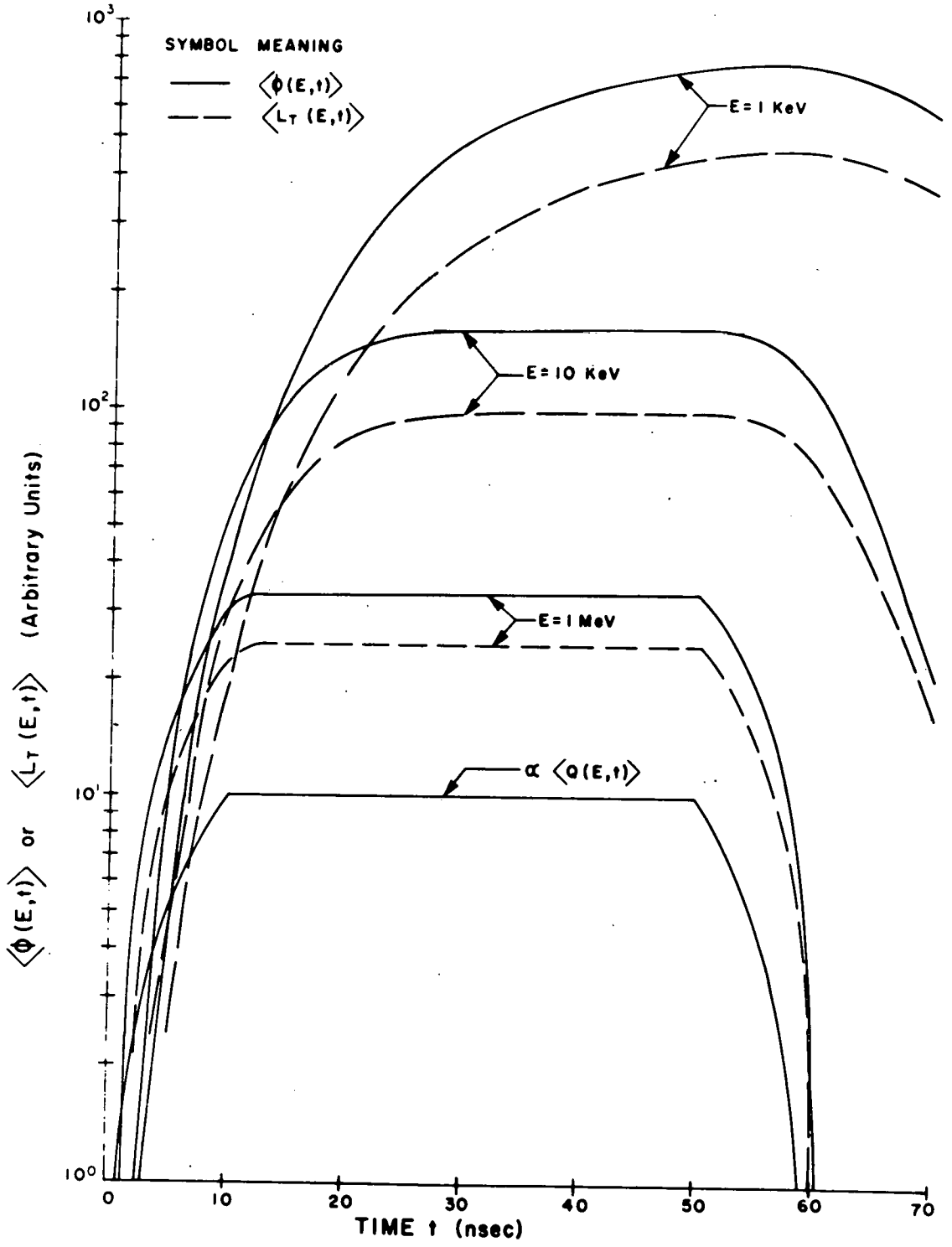
SYMBOL MEANING
⟨φ(E,t)⟩
⟨L_T (E,t)⟩
E = 1 KeV
E = 10 KeV
E = 1 MeV
∝ ⟨Q(E,t)⟩
10^3
10^2
10^1
10^0
⟨φ(E,t)⟩ or ⟨L_T (E,t)⟩ (Arbitrary Units)
0
10
20
30
40
50
60
70
TIME t (nsec)

Figure 1

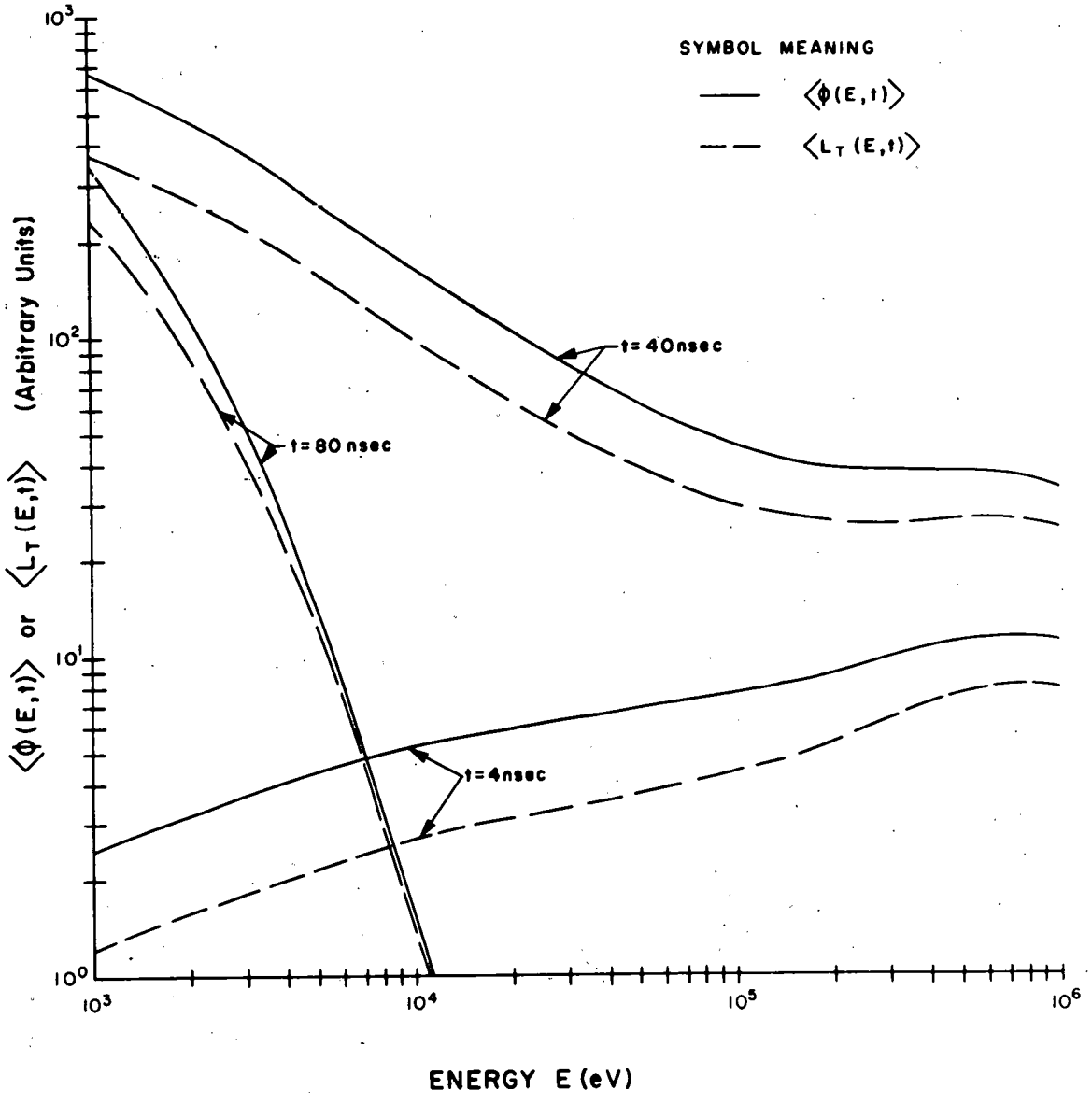
SYMBOL MEANING
⟨φ(E,t)⟩
⟨L_T(E,t)⟩
t = 40nsec
t = 80 nsec
t = 4nsec
⟨φ(E,t)⟩ or ⟨L_T(E,t)⟩ (Arbitrary Units)
ENERGY E (eV)
10^3
10^2
10^1
10^0
10^3
10^4
10^5
10^6

Figure 2

OPTICAL MODEL FIT TO THE P-WAVE NEUTRON STRENGTH FUNCTION

P. J. Turinsky

As reported previously[1] and indicated in Fig. 1, recent measurements conducted at RPI and elsewhere have indicated a strong minima in the P-wave neutron strength function, S_1, for the atomic mass number ranges about 60 and 160. A modified set of optical model parameters has been determined to fit these new data

The JUPITØR program was employed as the basic computational tool to perform standard spherical optical model calculations using the optical model complex potential

$$V(r) = -Vg(r,a_V) - 4iWa_W p(r,a_W) - V_{SO}(\sigma \cdot \ell)\, \lambda_\pi^2 \frac{1}{r} p(r,a_{V_{SO}})$$

where

$$g(r,a) = \frac{1}{1 + \exp[(r-R)/a]}$$

$$p(r,a) = \frac{dg(r,a)}{dr}$$

and the nuclear radius, R, given as a function of the mass number A by

$$R = r_o A^{1/3} .$$

The diffuseness parameter associated with the real central potential term, a_V, can be interpreted as a measure of the diffuseness of the nuclear surface. That is, small a_V indicates a sharp nuclear surface, while large a_V indicates a gradual change in nuclear density about R. For the diffuseness parameter connected with the imaginary surface potential, a_W, it may be interpreted as a measure of the spread in radial position about R where incident channel neutron removal can occur; that is, a large a_W implies a large spread.

In Figs. 1 through 3 are presented respectively S_1, the S-wave neutron strength function S_0 and potential scattering radius R', versus mass number A. Table 1 summarizes the optical model parameters employed in obtaining the results presented in

the figures. The figure curve labeled "Desirable Fit" signifies a smooth visual curve fit through a great amount of experimental data; hence, it should not be interpreted as the absolute best fit due to the spread in experimental data.

The historic results of Perey and Buck[2] clearly fail to predict the minima in either S_0 or S_1. Moldauer's fit,[3] which employed an imaginary surface potential term

$$-iW_M \exp\left[-\left(\frac{r-R-c}{b}\right)^2\right]$$

and nuclear radius formula

$$R = r_o A^{1/3} + r_1 ,$$

considerably improves both the S_0 and S_1 fits in the range $A\epsilon[30,120]$. It does, however, overestimate the S_1 minima about A=60. Considering that no experimental data on this minima was known at the time of Moldauer's work, his prediction is quite remarkable. Jain[4] also predicted a strong S_1 minima at A=60 and also A=160, but not of sufficient depth.

We have fitted simultaneously S_0 and S_1 in the range $A\epsilon[50,60]$. It was found possible to preserve only these two properties by introducing rapid oscillations in our calculated values of R'. Having obtained an optical model parameter set for this restricted mass number range, this set was employed in the extended mass range calculations presented in the figures. As illustrated in Fig. 1, a satisfactory fit to the S_1 experimental data has been obtained for the range $A\epsilon[50,200]$ where there is appreciable data. The 3P resonance peak does appear somewhat narrow on the high A side. Figure 2 indicates that as the minima of S_1 becomes deeper, a similar effect occurs in S_0. As a result, the predicted minima in S_0 do appear deeper than presently available data indicates. This same effect causes the 3S and 4S resonances to be narrower than desired. The poor agreement for all parameter sets for $A \geq 140$ is due to deformed nuclei effects which the spherical optical model ignores. Lastly, the results for the potential scattering radius are presented in Fig. 3, indicating the increased oscillatory behavior of R' about R as we attempt to fit to the deep S_1 minima.

Comparing our optical model parameters with those of Perey and Buck as presented in Table 1, it has been found necessary to increase V from 48 to 52 and decrease a_V from 0.65 to 0.45. This implies that a slightly denser central nucleus with a sharper nuclear surface was required to obtain a satisfactory fit to S_1. It was also necessary to decrease both W and a_W from respectively 11 to 4 and 0.47 to 0.25, implying a reduced strength and narrower radial region for transitions out of the neutron entrance channels. Moldauer's concept of shifting the r dependence of the imaginary surface potential term from (r-R) to (r-R-c) appears to have some desirable fitting properties and also is physically acceptable.

Studies are presently underway to interpret these results more fundamentally and obtain an improved simultaneous fit to S_0, S_1 and R'.

REFERENCES:

1. Linear Accelerator Project Progress Report, April - June 1971, 31, RPI-328-226.
2. B. Buck and F. Perey, Phys. Rev. Letters, 8, 444 (1962).
3. P. A. Moldauer, Nucl. Phys., 47, 65 (1963).
4. A. P. Jain, Nucl. Phys., 50, 157 (1964).

FIGURE CAPTIONS

Fig. 1 P-wave Neutron Strength Function Versus Atomic Mass Number.
Fig. 2 S-wave Neutron Strength Function Versus Atomic Mass Number.
Fig. 3 Potential Scattering Radius Versus Atomic Mass Number.

FIG. 1

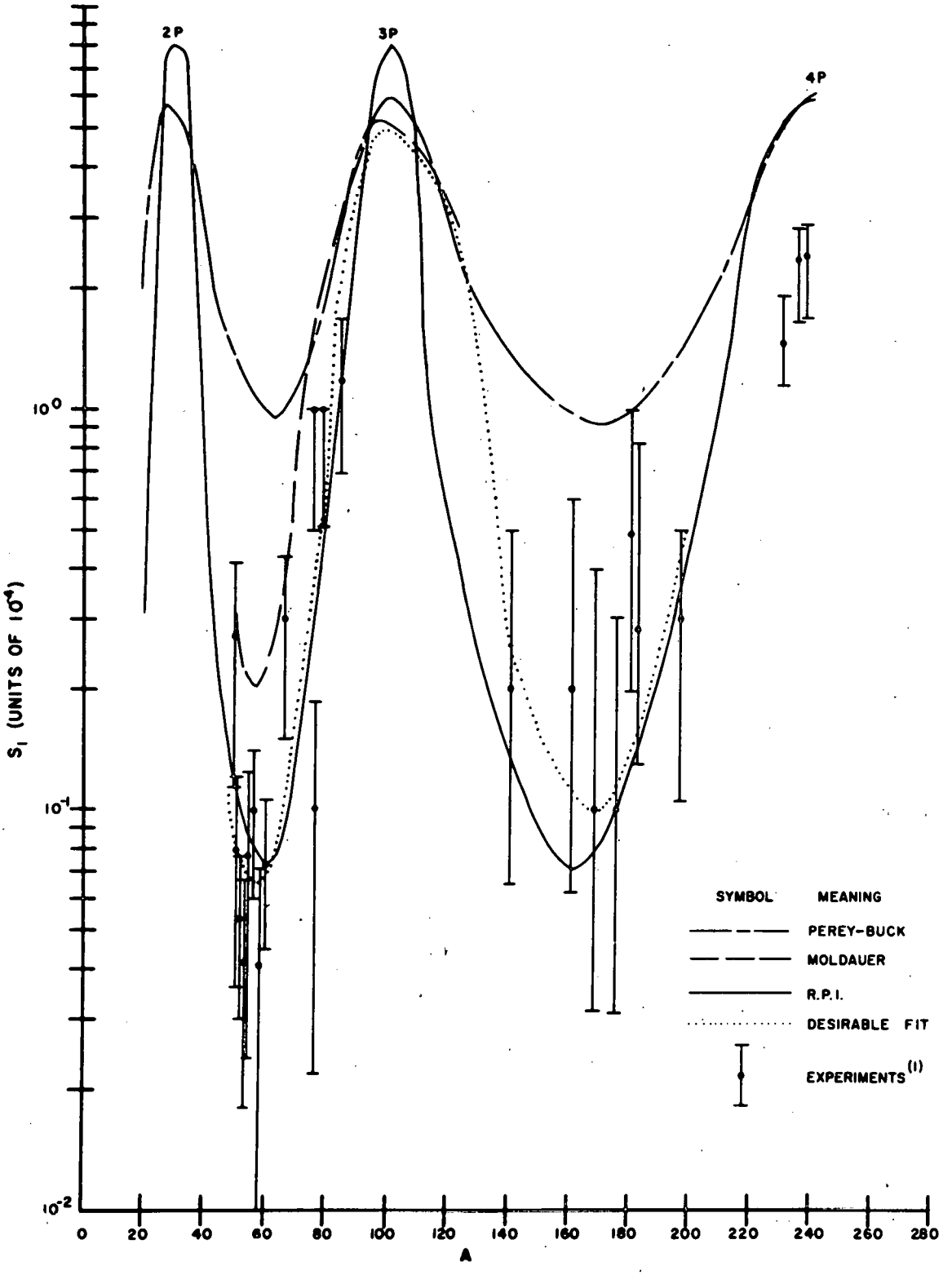
2P
3P
4P
10^0
10^{-1}
10^{-2}
S_l (UNITS OF 10^{-4})
0
20
40
60
80
100
120
140
160
180
200
220
240
260
280
A
SYMBOL
MEANING
PEREY-BUCK
MOLDAUER
R.P.I.
DESIRABLE FIT
EXPERIMENTS(1)

FIG. 2

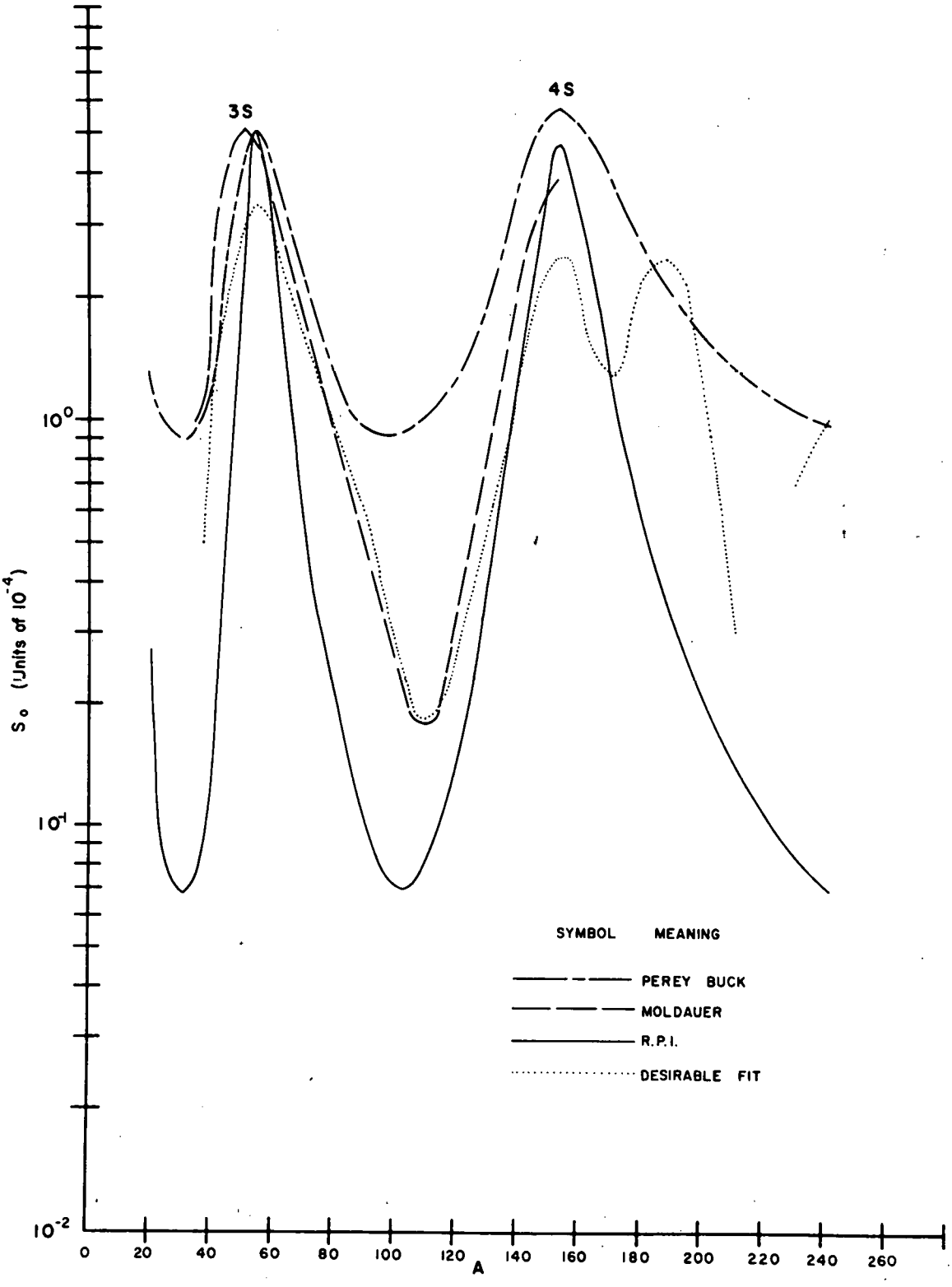
3S
4S
10^0
10^{-1}
10^{-2}
S_o (Units of 10^{-4})
0
20
40
60
80
100
120
A
140
160
180
200
220
240
260
SYMBOL MEANING
PEREY BUCK
MOLDAUER
R.P.I.
DESIRABLE FIT

FIG. 3

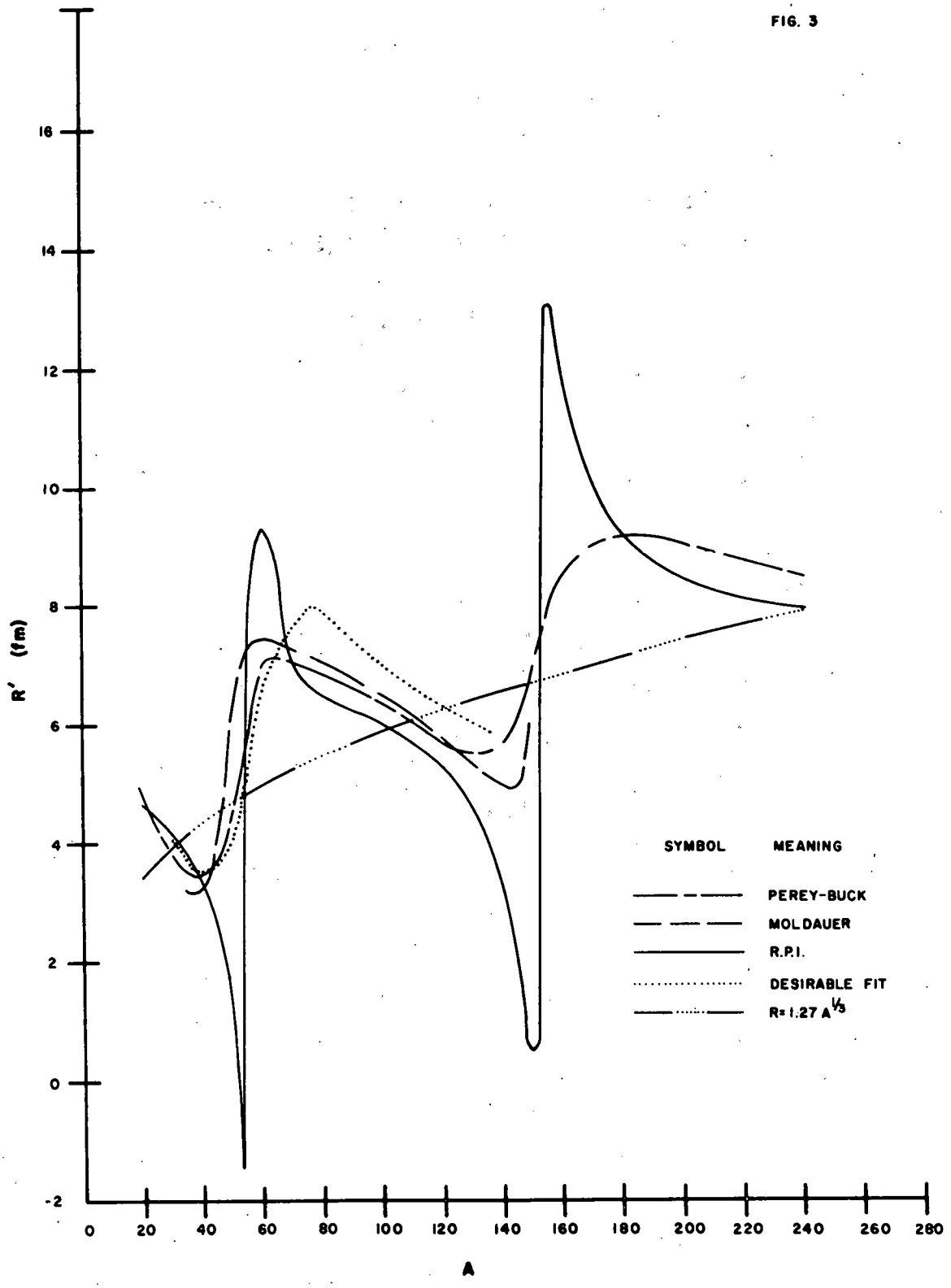
R' (fm)
16
14
12
10
8
6
4
2
0
-2
0
20
40
60
80
100
120
140
160
180
200
220
240
260
280
A
SYMBOL
MEANING
PEREY-BUCK
MOLDAUER
R.P.I.
DESIRABLE FIT
R= 1.27 A^1/3

Table 1

Optical Model Parameter Sets Employed
Units: Potential-MeV, Length-fm

Perey-Buck Parameters

$V = 48$, $a_V = 0.65$

$W = 11$ $a_W = 0.47$

$V_{SO} = 6$ $a_{V_{SO}} = 0.65$

$r_o = 1.27$

Moldauer Parameters

$V = 46$, $a_V = 0.62$

$W_M = 14$, $b = 0.5$, $c = 0.5$

$V_{SO} = 7$, $a_{V_{SO}} = 0.62$

$r_o = 1.16$, $r_1 = 0.6$

RPI Parameters

$V = 52$, $a_V = 0.40$

$W = 4$, $a_W = 0.25$

$V_{SO} = 6$, $a_{V_{SO}} = 0.65$

$r_o = 1.27$

*PH.D. DEGREES IN NUCLEAR ENGINEERING GRANTED BY DEPARTMENT OF NUCLEAR SCIENCE

NAME	TITLE OF THESIS
Burns, Edward T.	"Continuous Slowing Down Theory with Applications to Fast Neutron Spectra in Single Materials"
Esch, Louis J.	"The Temperature Dependence of Neutron Inelastic Scattering from Water"
Young, Rosa C.	"Photoconductivity Studies of Radiation Induced Defects in Silicon"

*October 1, 1970 - September 30, 1971

PUBLICATIONS DURING THE PERIOD 1970-1971

"Analytical Age Models with First and Last Collision Effect," M. Becker and G. Epstein, Trans. Am. Nucl. Soc., 14, 366 (1971).

"An Assessment of the ENDF/B-II File for Iron Based on Integral Transport Experiments," B. K. Malaviya, M. Becker, E. T. Burns, N. N. Kaushal and E. R. Gaerttner, Trans. Am. Nucl. Soc., 14, 350 (1971).

"The Average Angle of Scattering in Energy-Dependent Problems," M. Becker and F. McGirt, Nucl. Sci. Eng., 42, 104 (1970).

"Capture Cross Section of ^{240}Pu from 4 to 60 KeV," R. W. Hockenbury, J. D. Boice, W. R. Moyer and R. C. Block, Trans. Am. Nucl. Soc., 13, 299 (1970).

"A Central Compilation of the Results for Integral Tests of Microscopic Data," B. K. Malaviya and E. R. Gaerttner, Proceedings of the Third Conference Neutron Cross Sections and Technology, Knoxville, Tennessee, March 1971, Vol. 1, 456 (1971).

"Cross-Section Data Analysis Utilizing an Interactive Graphics Display," M. Lubert and R. C. Block," Proceedings of the Third Conference Neutron Cross Sections and Technology, Knoxville, Tennessee, March 1971, Vol. 1, 373 (1971).

"Experimental and Analytical Studies of Fast Neutron Transport in Iron," M. Becker, B. K. Malaviya, N. N. Kaushal, E. T. Burns, A. Ginsberg and E. R. Gaerttner, to be published in Nucl. Sci. Eng. (1971).

"Fast Neutron Spectrum Models and Their Application to Specific Materials," M. Becker and E. T. Burns, Trans. Am. Nucl. Soc., 13, 688 (1970).

"Fast Reactor Spectrum Measurements and Their Interpretation," B. K. Malaviya and V. V. Verbinski, International Atomic Energy Agency Meeting of the Specialists, Argonne National Laboratory, U.S.A., A Conference Summary, IAEA Report (1971).

"The Formulation and Application of Analytic Representations of Fast Reactor Flux and Importance Spectra," M. Becker and F. E. Dunn, Nucl. Sci. Eng., in press. (1971)

"The Formulation of Continuous Slowing Down Theory for General Processes in Terms of Separable Kernels," M. Becker and E. T. Burns, Nucl. Sci. Eng., 42, 100 (1970).

"The Generation of Fast Neutron Group Constants," M. Becker and E. T. Burns, Trans. Am. Nucl. Soc., 14, No. 2 (1971).

"Improvements to Slowing Down Theory for Fast Reactors," M. Becker and F. E. Dunn, to be published in Nucl. Sci. Eng. (1971).

"Integral Tests and Evaluation of Cross-Section Data from Studies of Fast Neutron Transport in Bulk Media," B. K. Malaviya, N. N. Kaushal, M. Becker, E. T. Burns, A. Ginsberg and E. R. Gaerttner, Proceedings of the Third Conference Neutron Cross Sections and Technology, Knoxville, Tennessee, March 1971, Vol. 1, 91 (1971).

"KeV Neutron Capture and Transmission Measurements on ^{50}Cr, ^{52}Cr, ^{53}Cr, ^{54}Cr, ^{60}Ni and V," R. G. Stieglitz, R. W. Hockenbury and R. C. Block, Nucl. Phys., A163, 592-624 (1971).

"Models for Anisotropic Weighting Spectra," M. Becker and A. Ginsberg, Trans. Am. Nucl. Soc., 14, 368 (1971).

"Monte Carlo Evaluation of Multiple Scattering and Resolution Effects in Double-Differential Neutron Scattering Cross-Section Measurements," F. G. Bischoff, W. E. Moore and M. L. Yeater, to be published in Nucl. Sci. Eng. (1971).

"Neutron Fission and Capture Cross-Section Measurements for ^{233}U in the Energy Region 0.02 to 1 eV," L. W. Weston, R. Gwin, G. de Saussure, R. W. Ingle, J. H. Todd, C. W. Craven, R. W. Hockenbury and R. C. Block, Nucl. Sci. Eng., 42, 143 (1970).

"Neutron Scattering and Capture Cross-Section Measurements," Chapter by E. R. Rae and R. C. Block in Experimental Neutron Resonance Spectroscopy, J. A. Harvey, ed., Academic Press, New York (1970).

"Neutron Scattering Cross Sections of ^{233}U, ^{235}U and ^{239}Pu," F. B. Simpson, L. G. Miller, M. S. Moore, R. W. Hockenbury and T. J. King, Nucl. Phys., A164, 34 (1971).

"The Observations of Correlation Between Γ_n^o and Γ_γ in the Mass Range 50 to 60," R. C. Block, R. G. Stieglitz and R. W. Hockenbury, Proceedings of the Third Conference Neutron Cross Sections and Technology, Knoxville, Tennessee, March 1971, Vol. 2, 889 (1971).

"Resonance Parameters of ^{240}Pu from 20 to 500 eV," R. W. Hockenbury, J. D. Boice, W. R. Moyer and R. C. Block, Proceedings of the Third Conference Neutron Cross Sections and Technology, Knoxville, Tennessee, March 1971, Vol. 2, 721 (1971).

"Spin Determination of Resonances in $^{165}Ho(n,\gamma)$ from Low Level Occupation Probability Ratios," W. P. Poenitz and J. R. Tatarczuk, Nucl. Phys., A151, 569 (1970).

"Studies of Fast Neutron Spectra Across a Material Interface," B. K. Malaviya, D. C. Gibbs, N. N. Kaushal, M. W. Golay and E. R. Gaerttner, Trans. Am. Nucl. Soc., 14 (1971).

"A Study of Neutron Transport in Depleted Uranium with an Assessment of Data Files," M. Becker, N. N. Kaushal, B. K. Malaviya, E. T. Burns and E. R. Gaerttner, Trans. Am. Nucl. Soc., 14, No. 2 (1971).

"A Study of Neutron Transport in Iron with an Assessment of Data Files," B. K. Malaviya, M. Becker, N. N. Kaushal, E. T. Burns, A. Ginsberg and E. R. Gaerttner, Trans. Am. Nucl. Soc., 13, 757 (1970).

"The Temperature Dependence of Neutron Inelastic Scattering from Water," L. J. Esch and M. L. Yeater, to be published in Nucl. Sci. Eng. (1971).

"Temperature-Dependent Transmission and Self-Indication Measurements upon Ta in the Unresolved Region," T. Y. Byoun, R. C. Block and T. Semler, Proceedings of the Third Conference Neutron Cross Sections and Technology, Knoxville, Tennessee, March 1971, Vol. 2, 895 (1971).

"Thick-Sample Neutron Transmission Measurements of the ^{229}eV Resonances in ^{65}Cu," N. Yamamuro and R. C. Block, J. Physical Soc. of Japan, 29, 1378 (1971).

"Time Dependent Neutron Spectra Measurements in H_2O," J. H. Menzel, R. E. Slovacek and E. R. Gaerttner, Nucl. Sci. Eng., 42, 119-136 (1970).